

Dissertation zur Erlangung des Doktorgrades  
der Fakultät für Chemie und Pharmazie  
der Ludwig-Maximilians-Universität München

**Atg11 initiates selective autophagy in yeast by  
tethering Atg9 vesicles**

Peter Mayrhofer

aus

Zell am See, Österreich

2019



## Erklärung

Diese Dissertation wurde im Sinne von § 7 der Promotionsordnung vom 28. November 2011 von Herrn Dr. Thomas Wollert betreut.

## Eidesstattliche Versicherung

Diese Dissertation wurde eigenständig und ohne unerlaubte Hilfe erarbeitet.

Peter Mayrhofer

Paris, 25.04.2019

Dissertation eingereicht am 04.02.2019

1. Gutachter: Dr. Thomas Wollert
2. Gutachter: Prof. Dr. Franz-Ulrich Hartl

Mündliche Prüfung am 17.04.2019



# Table of Contents

Summary .....	9
1 Introduction .....	11
1.1 Vesicular trafficking.....	11
1.1.1 The role of Rab GTPases.....	11
1.1.2 SNARE proteins.....	12
1.1.3 Tethering factors .....	13
1.2 Autophagosome biogenesis.....	14
1.2.1 Initiation.....	15
1.2.2 Expansion.....	18
1.2.3 Completion of autophagy.....	20
1.3 Selective autophagy .....	20
1.3.1 The Cvt pathway .....	21
1.3.2 Mitophagy .....	21
1.3.3 Pexophagy.....	22
1.3.4 Aggrephagy .....	22
1.3.5 Atg11.....	22
1.4 Human homologues of the yeast system.....	24
1.5 Aim of the thesis .....	25
2 Materials and methods.....	27
2.1 Materials .....	27
2.1.1 Bacterial strains .....	27
2.1.2 Plasmids .....	27
2.1.3 Yeast strains.....	28
2.1.4 Antibodies.....	29
2.1.5 Insect cell lines .....	29
2.2 Molecular biology methods .....	30
2.2.1 Competent bacteria .....	30
2.2.2 Cloning and plasmid preparation.....	30
2.2.3 Genomic manipulation of yeast.....	31
2.2.4 Plasmid transformation into yeast cells .....	32
2.3 Biochemical methods .....	32

2.3.1	SDS-PAGE and Western blotting.....	32
2.3.2	Crosslinking .....	33
2.4	Protein purification .....	33
2.4.1	Purification of Atg11 .....	33
2.4.2	Purification of Atg11 variants.....	34
2.4.3	Purification of other Atg proteins .....	35
2.5	Biophysical methods.....	39
2.5.1	Preparation of small unilamellar vesicles (SUVs) .....	39
2.5.2	Reconstitution of Atg9 into proteoliposomes .....	39
2.5.3	Floatation assays .....	39
2.5.4	Cryo-electron microscopy .....	40
2.6	<i>In vivo</i> methods .....	40
2.6.1	Growth of yeast cultures .....	40
2.6.2	Preparation of whole cell lysates.....	41
2.6.3	Immunoprecipitation experiments .....	41
2.6.4	Proteasomal block assay .....	41
2.7	Mass spectrometry .....	42
3	Results .....	43
3.1	Protein purifications.....	43
3.1.1	Purification of Atg11 .....	43
3.1.2	Purification of other Atg proteins .....	46
3.2	<i>In vitro</i> analysis of Atg11-Atg32 interaction.....	53
3.2.1	Requirement of Atg9 for interaction of Atg11 with Atg32.....	53
3.2.2	Atg32-dependent dimerization of Atg11 .....	54
3.2.3	Atg11 dimerization leads to tethering of Atg9 proteoliposomes.....	59
3.3	Atg11 and Atg17 compete for liposome binding.....	62
3.4	The role of Atg29 phosphorylation in autophagy initiation .....	64
3.4.1	Differences in the stability of the Atg17 <sup>TC</sup> and Atg17 <sup>TC,SD</sup> complex.....	64
3.4.2	Atg29 phosphorylation has no effect on interaction with Atg9 or Atg11.....	67
3.4.3	Atg29 phosphorylation does not alter Atg17 binding to Atg9 proteoliposomes	68
3.4.4	Atg11 might increase recruitment of the Atg1 kinase complex <i>in vitro</i> .....	69

3.4.5	Atg13 phosphorylation influences protein-protein interactions .....	70
3.5	Competition between Atg11 and Atg17 in vivo .....	72
3.5.1	Atg11 is degraded upon starvation .....	72
3.5.2	Proteasomal degradation of Atg11 during starvation.....	75
4	Discussion .....	79
4.1	Atg11 directly interacts with Atg9 vesicles .....	79
4.2	Atg11 dimerizes upon complex formation with Atg32 .....	81
4.3	Atg11 is a cargo-activated membrane tether .....	82
4.4	Atg11 and Atg17 are mutually exclusive Atg9 vesicle tethers .....	84
4.5	A possible effect of protein phosphorylation on Atg11-Atg17 competition .....	85
4.6	Atg11 degradation could aid in Atg17 recruitment .....	87
4.7	Outlook .....	90
	References .....	93
	Appendix.....	99
	List of Figures .....	99
	List of Tables.....	100
	Acknowledgements.....	101



## Summary

Autophagy is a cellular recycling pathway that delivers material from the cytosol to the lysosomal lumen. In yeast, this process is initiated by the fusion of small vesicles to form a double-membrane sheet, the phagophore. The phagophore is continuously expanding and thereby engulfs its cytosolic cargo. Finally the membrane is sealed, giving rise to a double-membrane vesicle called autophagosome which fuses with the lysosome (or vacuole in yeast) to release its contents for degradation. Autophagy was initially discovered as response to starvation to ensure the cell's survival by degradation of bulk cytosol. However, during nutrient-rich conditions autophagy is selectively capturing cargo, such as damaged or superfluous organelles or large protein aggregates. It is thus vital for cellular homeostasis and plays a role in the protection against cancer and neurodegenerative diseases.

Autophagy is driven by a set of autophagy-related (Atg) gene products. The initiation of starvation-induced autophagy requires the transmembrane protein Atg9 and the Atg1 kinase complex. Atg9 is sorted from the Golgi to a dedicated set of small vesicles that are recruited to the site of autophagosome formation by the Atg1 kinase complex. The latter is activated in response to a starvation signal which induces the assembly of the complex. The active Atg1 kinase complex nucleates phagophore membranes by tethering Atg9 vesicles in order to prepare them for subsequent fusion. Atg17, the principle tethering subunit of the Atg1 kinase complex, is only active during starvation. How selective autophagy is initiated remains thus an open question.

Several *in vivo* studies demonstrated that another autophagy-specific factor, Atg11, interacts with Atg9 and subunits of the Atg1 kinase complex during selective autophagy. However, the molecular function of this protein remained unclear. In the present thesis this question was addressed by reconstituting autophagy initiation from purified components *in vitro*. It could be shown that Atg11 binds to Atg9 reconstituted in liposomes and is able to tether such vesicles. However, this requires dimerization of Atg11 which is inhibited by its C-terminal domain. The activation of Atg11 occurs through binding of autophagic cargo. Moreover, Atg11 and Atg17 compete for binding of Atg9 proteoliposomes, but Atg17 is inactive under physiological conditions. This allows Atg11 to initiate selective autophagy. The cargo-dependent activation of Atg11 ensures that selective autophagy only occurs if cargo is present and spatiotemporally links the nucleation of the phagophore to such cargo. Starvation induces the degradation of Atg11 and activates Atg17, which nucleates phagophores independently of cargo.



# 1 Introduction

## 1.1 Vesicular trafficking

A hallmark of eukaryotic cells is their compartmentalization with membranes generating confined spaces within the cytosol. However, it is vital for the cells that cargos can be exchanged between the different organelles which happens through small vesicles in a process called vesicular trafficking. This vesicular trafficking depends on a wide range of proteins facilitating sequestration of cargo and budding of transport vesicles (coat proteins), transport to their cellular destination (cytoskeleton and motor proteins) as well as tethering to (tethering factors) and fusion with the target membrane (SNAREs). In addition, this process needs to be tightly regulated, which is maintained via Rab GTPases and their effector molecules.

### 1.1.1 The role of Rab GTPases

Rab GTPases are a group of small GTPases switching between an active GTP-bound and an inactive GDP-bound state. They are reversibly linked to membranes via a lipid anchor and regulate trafficking processes via diverse interactions. The exchange of GDP by GTP, and thus activation, is facilitated by guanine nucleotide exchange factors (GEFs). Rab GTPases are rendered inactive by hydrolysis of GTP to GDP. The intrinsic GTPase activity is enhanced by GTPase activating proteins or GAPs (Stenmark, 2009). Sec4 was the first Rab GTPase that was shown to be required for fusion of exocytic vesicles with the plasma membrane (Salminen and Novick, 1987). Sec4-GTP interacts with a subunit of the exocyst complex that tethers these vesicles to the plasma membrane (Guo et al., 1999). Ypt7 is another example for a Rab GTPase required for a fusion step, as it was reported to play a major role in tethering preceding homotypic vacuole fusion by interaction with the tethering factor HOPS (Ungermann et al., 1998). Another Rab GTPase, Ypt1, is required for the regulation of ER-Golgi and intra-Golgi transport via its interactions with the TRAPP tethering factors (Morsomme and Riezman, 2002).

Due to their defined cellular localization and their interaction with specific downstream factors, Rab GTPases can confer membrane identity during vesicular trafficking. Another way to specify membrane identity is via the different phosphorylation states of the phospholipid phosphatidylinositol (PI). Rab GTPases coordinate the recruitment of effectors that change the phosphorylation of the inositol ring. This allows the recruitment of downstream factors with lipid binding domains (Christoforidis et al., 1999).

### 1.1.2 SNARE proteins

The fusion of membranes is an energetically highly unfavorable event and requires additional force to overcome the energy barrier. This step is catalyzed by a set of SNARE (Soluble N-ethylmaleimide-sensitive-factor attachment protein receptor) proteins. Most SNAREs are permanently anchored in membranes via a C-terminal transmembrane domain, while some are recruited for the fusion event using lipid binding motifs or lipid anchors. Their fusogenic activity derives from SNARE motifs. These are initially unfolded but form a stable four-helix bundle when they pair with three compatible partner SNARE motifs (Sutton et al., 1998). The interaction interface between the four helices is lined with unpolar amino acids. Only the center of the bundle harbors polar headgroups: one arginine (R) and three glutamine (Q) residues (Klopper et al., 2007). Based on these residues, SNAREs are classified into R-SNAREs and Q-SNAREs. Depending on additional structural similarities, Q-SNAREs are further subcategorized into Q<sub>a</sub>-, Q<sub>b</sub>-, and Q<sub>c</sub>-SNAREs. One SNARE protein of each of the four groups is necessary to form a fusogenic SNARE complex, the so-called trans-SNARE complex or SNAREpin (Südhof and Rothman, 2009). Calculations showed that the formation of three SNAREpins releases enough energy to drive membrane fusion (Li et al., 2007). After fusion, the resulting cis-SNARE complex needs to be disassembled in order to be used in another round of fusion. This requires the ATPase NSF (Mayer et al., 1996).

SNAREs localize to distinct organelles and membranes. *In vitro* studies showed that not all combinations of R-, Q<sub>a</sub>-, Q<sub>b</sub>-, and Q<sub>c</sub>-SNARE drive membrane fusion. Instead, fusion was only observed with specific sets of SNAREs that were found to act in a common pathway. Thus, cellular localization of SNAREs provides, in addition to Rab-proteins and PIPs, another layer of specificity to ensure that transport vesicles fuse with their correct target membranes (McNew et al., 2000; Parlati et al., 2000).

However, even though SNAREs alone can drive fusion *in vitro*, this requires an unphysiologically high concentration of proteins. *In vivo*, additional factors are required. The SM (Sec1/Munc18-like) protein family are key regulators of SNARE-mediated fusion. They bind to a common N-terminal H<sub>abc</sub> domain which can be found in all Q<sub>a</sub>-SNAREs. This regulatory domain adopts a three-helical structure and forms a complex with the SNARE motif. This inhibits SNAREpin formation until the H<sub>abc</sub> domain is released by the interaction with SM proteins (Demircioglu et al., 2014). Moreover, SM proteins could act as a template for SNARE complex formation as it was reported for Vps33, a subunit of the HOPS tethering complex (Baker et al., 2015).

For several SNARE proteins a role in autophagy was described. The exocytic Q<sub>a</sub>-SNARE Sso1/2 and Q<sub>bc</sub>-SNARE Sso9 are required during initial steps of autophagosome biogenesis.

While exocytic R-SNAREs are dispensable for autophagy a requirement for the ER-Golgi R-SNARE Sec22 was reported, suggesting the existence of autophagy-specific SNARE complexes (Nair et al., 2011). Furthermore, autophagy depends on the other ER-Golgi SNAREs Bet1, Bos1 and Sed5 (Tan et al., 2013). After the autophagosome is fully formed it has to fuse with the vacuolar membrane to release its content for degradation. Similar to other vacuolar fusion events this specifically requires the Q-SNAREs Vam3, Vam7 and Vti1 on the vacuolar membrane and the R-SNARE Ykt6 located on the autophagosome (Bas et al., 2018).

### **1.1.3 Tethering factors**

Tethering factors are responsible in bringing two membranes into close proximity, before SNARE mediated fusion can occur. They are Rab effectors, their specificity is thus provided by the localization and activation of Rab GTPases. Some tethers are known to regulate SNARE complex formation and hence accelerate the fusion between the tethered membranes (Yu and Hughson, 2010). Generally, tethering factors are grouped into two categories, coiled-coil tethers and multi-subunit tethering complexes. A prominent example for coiled-coil tethers are golgins. They form long, extended structures that capture vesicles and transport them to the site of fusion. Multi-subunit tethering complexes (MTCs) are composed of three to eight subunits and span a rather short distance compared to coiled-coil tethers. Through their different subunits they regulate membrane recognition and SNARE-mediated fusion (Kuhlee et al., 2015). For autophagy, two MTCs play a major role. The HOPS complex is required for fusion events with the vacuole including autophagosome-vacuole fusion. The other MTC, TRAPPIII, is an autophagy-specific variant of the TRAPPI complex and seems to direct ER-derived vesicles to the PAS (Tan et al., 2013).

#### *1.1.3.1 The HOPS complex*

The HOPS (homotypic fusion and vacuole protein sorting) complex is a well-studied example for a multi-subunit tethering complex. It is an effector of the Rab GTPase Ypt7 which is located at the vacuolar membrane. As a result it facilitates the homotypic fusion of vacuoles as well as fusion of the vacuole with late endosomes or multivesicular bodies, autophagosomes and vesicles of the AP-3 pathway (Kuhlee et al., 2015). The complex contains two Rab-binding sites, one each in the Vps39 and the Vps41 subunit. These two subunits are positioned on the opposite ends of the complex, enabling HOPS to tether two different membranes (Bröcker et al., 2012). In addition to its tethering ability, HOPS also has a regulatory role in SNARE-mediated fusion of the tethered membranes. Vacuolar fusion depends on a special set of

SNAREs: the Q-SNAREs Vam3, Vam7 and Vti1 and either of the two R-SNAREs Nyv1 and Ykt6. It is possible to fuse membranes *in vitro* only in presence of these four SNARE proteins. However, this requires an unphysiologically high SNARE concentration. At low concentrations, fusion only occurs when Ypt7-GTP and HOPS are present (Stroupe et al., 2009). This is due to the HOPS subunit Vps33 that functions as a SM protein and facilitates SNAREpin formation (Baker et al., 2015). In contrast to the other SNAREs, Vam7 is not anchored in the membrane via a transmembrane domain but by binding to PI3P via a PX domain. The HOPS subunits Vps16 and Vps18 interact with Vam7 and thus aid in its recruitment (Krämer et al., 2011).

### 1.1.3.2 The TRAPP complex

TRAPP (transport protein particle) is another example for a multisubunit tethering complex. In yeast there are three different TRAPP complexes that all act as GEFs for the Rab GTPase Ypt1. The seven-subunit complex TRAPPI is required for ER-to-Golgi transport and was shown to specifically interact with the Sec23 subunit of COPII-coated vesicles (Cai et al., 2007). TRAPPII contains additional subunits that were reported to block binding of COPII vesicles but instead allow interaction with COPI vesicles. This way, TRAPPII functions in the intra-Golgi and endosome-to-Golgi transport (Cai et al., 2005). More recently, a third TRAPP complex was described. The TRAPPIII complex shares all its subunits with TRAPPI but has one additional subunit, Trs85. This subunit has no impact on the interaction with COPII coated vesicles but is required for efficient autophagy (Lynch-Day et al., 2010). Moreover, COPII vesicles localized to the site of autophagosome biogenesis and accumulated when autophagy was blocked (Tan et al., 2013). This is in agreement with the observation that autophagosomes are formed closely to ER exit sites (ERES), where COPII vesicles pinch off the ER membrane (Graef et al., 2013). Like the other TRAPP complexes TRAPPIII is a GEF for the Rab GTPase Ypt1. Ypt1 was reported to be required for autophagy, possibly through the recruitment of the autophagy protein Atg1 (Lynch-Day et al., 2010; Wang et al., 2013a).

## 1.2 Autophagosome biogenesis

Macroautophagy, in the following called autophagy, is characterized by the de novo formation of a double-membrane vesicle. In contrast to other vesicular trafficking pathways, cargo is not transported from one organelle to another inside small vesicles. Instead, small vesicles fuse to form a double-membrane sheet, the phagophore, that encloses cytoplasmic material and

delivers it to the vacuole/lysosome. This process relies on a special set of autophagy-related (Atg) proteins and can be divided into four major events: initiation, expansion of the phagophore membrane and capturing of cargo, sealing of the membrane to form an autophagosome and fusion with the vacuole to release its contents. Cargo can be captured either non-selectively as a response to starvation or selectively through specific cargo receptors to maintain cellular homeostasis (see Figure 1).

### 1.2.1 Initiation

Autophagy captures cargo selectively during vegetative conditions or non-selectively upon starvation. In the latter case, the lack of amino acids inactivates the Target of rapamycin (TOR) complex. This in turn activates the Atg1-kinase complex, a pentameric complex and key factor in autophagy initiation, through the dephosphorylation of its subunit Atg13. The Atg1-kinase complex then recruits and tethers Atg9 vesicles, a special set of small vesicles containing the transmembrane protein Atg9.

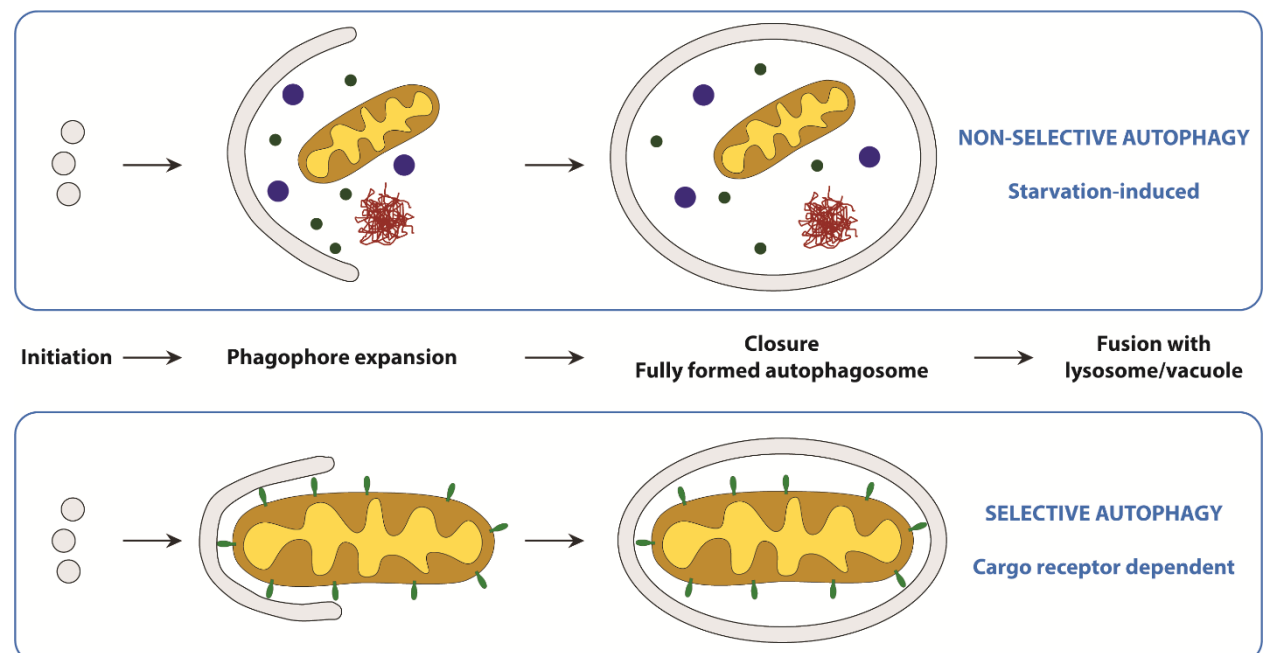


**Figure 1: Autophagosome biogenesis.** During initiation small autophagy-specific vesicles (Atg9 vesicles) fuse at the site of autophagosome biogenesis to form a phagophore. This phagophore expands, thereby capturing cargo either non-specifically as a response to starvation (upper panel) or specifically to maintain cellular homeostasis (lower panel). In the latter case, cargo-receptors ensure that no unwanted material is engulfed by the phagophore. Finally, the membrane is sealed to form a double-membrane vesicle, the autophagosome, that fuses with the lysosome or vacuole for cargo degradation.

### 1.2.1.1 *Atg1-kinase complex*

The Atg1-kinase complex consists of five different subunits: Atg1, Atg13, Atg17, Atg29, and Atg31. Atg1 is a kinase that phosphorylates several Atg proteins and itself. However, its kinase activity is not required for initiation of autophagy (Matsuura et al., 1997). Atg1 forms a constitutive complex with Atg13 independently of nutrient conditions (Kraft et al., 2012). However, Atg13 is hyperphosphorylated during nutrient-rich conditions by the TOR kinase, whereas TOR is deactivated upon starvation and Atg13 is partially dephosphorylated (Kamada et al., 2000). The other three subunits of the Atg1-kinase complex, Atg17, Atg29 and Atg31, form a stable complex in the cytosol with Atg31 linking the other two proteins. The formation of this complex is as well independent of the nutrient status of the cell (Kabeya et al., 2009). However, only upon starvation-induced dephosphorylation of Atg13 the trimeric Atg17-Atg31-Atg29 complex and Atg1-Atg13 will form the fully active Atg1 kinase complex (Kawamata et al., 2008).

Structural analysis of the Atg17-Atg31-Atg29 subcomplex revealed that Atg17 has a three-helical, crescent-shaped structure leading to the hypothesis that it could bind curved membranes. Additionally, Atg17 dimerizes via its C-terminal domain and the resulting S-shaped structure was suggested to allow vesicle tethering. Atg31 binds to Atg17 via its C-terminal helix, thereby forming a four-helix bundle. Atg29 only interacts with Atg31 but not with Atg17. Atg31-Atg29 is positioned within the Atg17 crescent which suggests a regulatory function on Atg17 membrane binding efficiency (Ragusa et al., 2012).

Previous work in the group was able to decipher the molecular function of the Atg1-kinase complex and its role in vesicle tethering (Rao et al., 2016). Atg17 specifically binds to Atg9 that was reconstituted into liposomes. Furthermore, Atg17 is sufficient to tether these proteoliposomes as shown by dynamic light scattering and cryo-EM experiments. However, Atg17 always forms a stable complex with Atg29 and Atg31 in the cytosol. Interaction with the Atg31-Atg29 subcomplex reduces the binding of Atg17 to Atg9 and inhibits its tethering function. This inhibition is released by the binding of Atg1-Atg13 to form the fully assembled Atg1 kinase complex (see Figure 2). Thus, tethering of Atg9 vesicles is prevented during nutrient-rich conditions and specifically induced upon starvation.

### 1.2.1.2 *Atg9*

Atg9 is the only autophagy-specific transmembrane protein essential for selective and non-selective autophagy (Noda et al., 2000). Atg9 consists of a highly conserved core domain

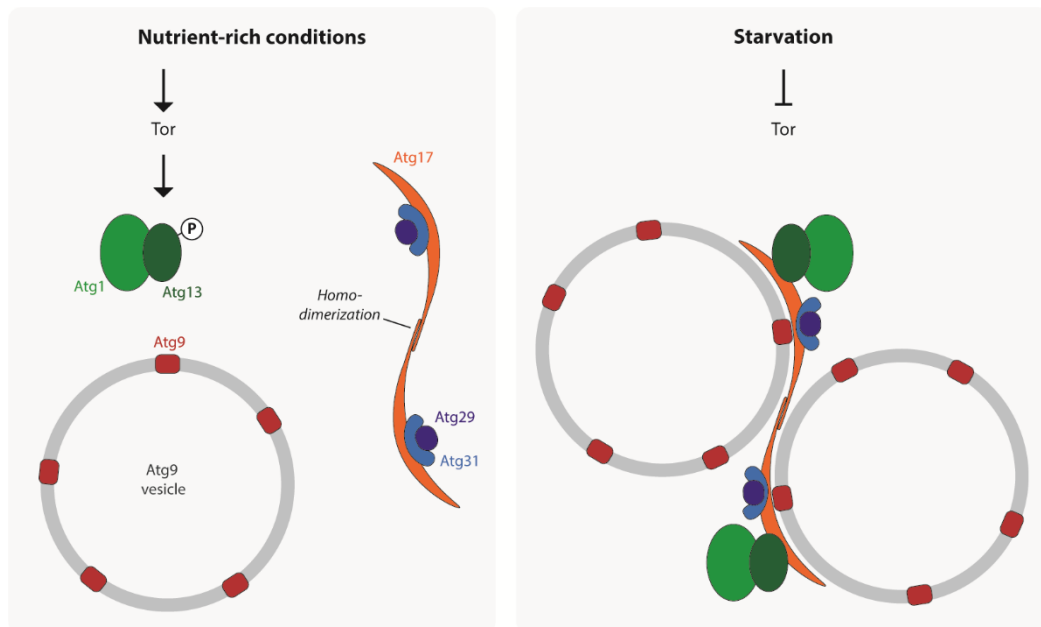


**Figure 2: Activation of the Atg1 kinase complex.** During nutrient-rich conditions (left panel) Atg13 is phosphorylated by the Tor kinase which prevents interaction with Atg17. Atg29-Atg31 binds to the crescent of Atg17 thereby inhibiting interaction with Atg9. During starvation (right panel) Atg13 is dephosphorylated and the full pentameric complex can assemble. This releases the inhibition by Atg29-Atg31 and Atg17 can bind Atg9 vesicles. Due to the homo-dimerization of Atg17 through its C-terminal domain the Atg1 kinase complex can tether two vesicles.

comprising six transmembrane helices and a cytoplasmic domain between helices two and three. Additionally, Atg9 contains largely disordered N- and C-terminal domains. These regions have been suggested to be required for trafficking of Atg9 ensuring its correct intracellular localization. However, the core domain (residues 281 to 779) is sufficient for the interaction of Atg9 with the Atg1 kinase complex *in vitro* (Rao et al., 2016). Atg9 is co-translationally inserted into the ER membrane and transported to the Golgi. Atg9 traffics from the Golgi to a specialized peripheral compartment that consists of small vesicles independently from the secretory and endocytic pathways (Mari et al., 2010). Upon starvation, the number of Atg9 vesicles increases, suggesting that starvation stimulates trafficking of Atg9 from the Golgi to its peripheral compartment (Yamamoto et al., 2012). Yamamoto et al. reported that the diameter of these Atg9 vesicles is in the range of 30 – 60 nm with 24 – 32 Atg9 molecules per vesicle. It was suggested that three Atg9 vesicles coalesce at the PAS in order to nucleate the phagophore but that no additional Atg9 vesicles are recruited during later steps of autophagosome biogenesis. Furthermore, Atg9 is primarily located at the outer membrane of autophagosomes but is not accumulating in the vacuolar membrane. Thus, a mechanism might exist that recycles Atg9 before or immediately after fusion of autophagosomes with the vacuole (Yamamoto et al., 2012).

## 1.2.2 Expansion

After initiation of autophagosome biogenesis the phagophore expands to engulf its cytoplasmic cargo. However, the membrane sources for this process are still a matter of debate. While Atg9 vesicles are suggested to be required only for initiation, an increasing number of studies report evidence for a direct role of ER-derived COPII vesicles in autophagosome biogenesis. Phagophore expansion also depends on a set of essential Atg proteins, including an autophagy-specific PI3-kinase that generates binding sites for downstream factors. Furthermore, expansion requires two ubiquitin-like systems that lead to the conjugation of the small protein Atg8 to the phagophore membrane.

### 1.2.2.1 PI3-kinase

There are two PI3-kinase complexes in yeast known so far that phosphorylate phosphatidylinositol at the D-3 position of the inositol ring. They consist of four subunits each, three of which are shared by both complexes. Vps15 is a serine/threonine kinase that is linked to the membrane via a myristoyl-anchor. It phosphorylates and thereby activates Vps34 that bears the PI3-kinase activity. The third common subunit, Vps30, is linked to Vps34 by the specific subunits Atg14 or Vps38 in complex I or II, respectively. These subunits define, whether the PI3-kinase complex functions in autophagy (complex I) or in the CPY pathway that transports carboxypeptidase Y from the Golgi to the vacuole (complex II) (Kihara et al., 2001). The interaction between Atg14 and the N-terminal domain of Atg13 results in the recruitment of the PI3-kinase I to the PAS (Jao et al., 2013). Atg14 was also implicated in the regulation of the size of autophagosomes (Obara et al., 2006).

The generation of PI3P allows the recruitment of a range of downstream factors to the phagophore membrane, most importantly Atg18 and Atg21. They both are homologous to each other, yet Atg21 but not Atg18 was reported to be dispensable for starvation-induced autophagy (Krick et al., 2006). Both proteins contain WD-40 repeats which are predicted to fold into a  $\beta$ -propeller structure. This domain facilitates the specific binding of proteins to PI3P as well as to PI(3,5)P<sub>2</sub>. Atg18 and Atg21 then further recruit downstream factors to the growing phagophore. Both proteins were reported to facilitate the recruitment of Atg16 and Atg8 to the phagophore membrane (Nair et al., 2010).

### 1.2.2.2 Ubiquitin-like conjugation systems

During phagophore expansion, two different ubiquitin-like conjugation systems create a covalent bond between Atg12 and Atg5 as well as the linkage of Atg8 to phosphatidylethanolamine (PE) on the phagophore membrane. The canonical ubiquitin system involves the processing of the ubiquitin precursor, activation by conjugation to a cysteine in the active center of an E1 enzyme, transfer to an E2 enzyme, and finally transfer to the target protein with the help of an E3 enzyme (Hershko and Ciechanover, 1998). Similarly, Atg12 is activated by a thioester linkage to Atg7 (E1-like) and is then transferred to Atg10 (E2-like). Finally, Atg12 forms a covalent bond with Atg5 without the requirement for an E3 enzyme (Mizushima et al., 1998). Atg5 binds non-covalently to the coiled-coil protein Atg16 forming a constitutive Atg12-Atg5-Atg16 complex (Mizushima et al., 1998). It was further reported that Atg16 is capable of oligomerization and drives the formation of a large complex suggested to consist of a tetramer of Atg12-Atg5-Atg16 (Kuma et al., 2002).

Another ubiquitin-like conjugation system results in the conjugation of Atg8 to phosphatidylethanolamine (PE) present in the phagophore membrane. First, Atg8 is processed by the protease Atg4 to expose a C-terminal glycine residue (Kirisako et al., 2000). Afterwards it is conjugated to the active site of Atg7 and transferred to Atg3 (E2-like). Atg12-Atg5 functions as an E3-like ligase that facilitates the transfer of Atg8 from Atg3 to PE (Hanada et al., 2007). In contrast to Atg12-Atg5 conjugation this process is reversible and Atg8 can be cleaved from the membrane by Atg4 (Kirisako et al., 2000). Another difference to Atg12-Atg5 is that the majority of Atg8 molecules is not conjugated during vegetative conditions but Atg8-PE strongly increases upon starvation (Huang et al., 2000). Interestingly, although all Atg12-Atg5 is bound to Atg16 *in vivo*, its enzymatic function is independent of Atg16 *in vitro* (Kaufmann et al., 2014).

Further investigations using purified Atg12-Atg5-Atg16 on model membranes with conjugated Atg8 revealed the formation of a meshwork-like protein coat. This scaffold formation is dependent on the oligomerization of Atg16 into tetramers with an anti-parallel arrangement of dimers. The interaction between two Atg16 dimers is also required for normal levels of autophagy *in vivo* suggesting an essential role of the Atg12-Atg5-Atg16 scaffold in autophagosome biogenesis (Kaufmann et al., 2014).

Atg8 also plays an essential role in selective autophagy. If specific cargo is destined for degradation by autophagy it is marked with a specific cargo receptor protein. These receptors harbor a conserved Atg8 interacting motif (AIM) that links the cargo to the phagophore membrane (Noda et al., 2008; Kondo-Okamoto et al., 2012).

### **1.2.3 Completion of autophagy**

After the phagophore has captured its cargo, the growing edges will seal to form the complete double-membrane autophagosome. Only then the autophagosome is able to release its contents into the vacuolar lumen by fusion of its outer membrane with the vacuole membrane. However, the mechanism behind the sealing event and the responsible factors are still unclear.

Prior to the fusion with the vacuole the PI3Ps in the outer membrane of the autophagosome are dephosphorylated by the phosphatase Ymr1 in order to release the autophagic proteins that were recruited via their lipid binding domains (Gebollero, 2012). A recent study also reported a decrease in autophagic flux when the cleavage of Atg8 from the autophagosomal membrane was blocked, indicating a possible requirement for Atg8 deconjugation for autophagosome-vacuole fusion (Nair et al., 2012).

The fusion of the autophagosome with the vacuole depends on factors involved in other vacuolar fusion events. One of those is the Rab GTPase Ypt7. It is activated by the Mon1-Ccz1 complex which is specifically recruited to autophagosomes via its Atg8 interacting motif (Gao et al., 2018). Active Ypt7 recruits the HOPS complex that tethers autophagosomes to the vacuolar membrane and facilitates SNARE-mediated fusion. Two vacuolar SNAREs, Vam7 and Ykt6, contain lipid anchors instead of transmembrane domains and thus cycle between a cytosolic and membrane-bound state. Recently, it was reported that both SNAREs are specifically recruited to autophagosomes (Bas et al., 2018; Liu et al., 2016).

In contrast to other autophagy proteins on the autophagosome membrane, Atg9 cannot be simply released from the autophagosome. Atg9 is not degraded in the vacuole, indicating that it is preferentially located in the outer membrane of completed autophagosomes. However, the absence of accumulated Atg9 in the vacuolar membrane suggests that Atg9 is recycled (Yamamoto et al., 2012). Still, it remains unclear when Atg9 is retrieved from the membrane and the molecular mechanism of this process.

### **1.3 Selective autophagy**

During nutrient-rich conditions cargo is selectively degraded by autophagy. This process is essential for cellular homeostasis as it removes damaged organelles and protein aggregates. In yeast, selective autophagy has also a biosynthetic function: The cytoplasm-to-vacuole targeting (Cvt) pathway delivers precursors of vacuolar proteases to the vacuolar lumen. In contrast to starvation-induced autophagy Atg17 is dispensable for selective autophagy.

Instead, another protein, Atg11, is essential for the initiation of selective autophagy. However, its exact molecular function was unclear. The different cargoes that are targeted by selective autophagy are recognized via specific cargo receptors through their interactions with Atg11 and Atg8.

### **1.3.1 The Cvt pathway**

The Cvt pathway is the best-characterized selective autophagy pathway in yeast. It delivers precursors of vacuolar proteases, mainly aminopeptidase1 (Ape1), to the vacuole where they are activated. The premature form of Ape1, prApe1, interacts with other prApe1 molecules to form a homo-dodecamer (Su et al., 2015). The propeptide can form a trimeric coiled-coil with two other propeptides which allows the interaction of different dodecamers and thus the formation of a large aggregate, called the Ape1 complex (Yamasaki et al., 2016). The Ape1 complex is then targeted by the Cvt pathway and delivered to the vacuole. The Ape1 complex is specifically recognized by the cargo receptor Atg19. Atg19 binding was also reported to limit the size of the Ape1 complex for efficient clearance by the Cvt pathway (Yamasaki et al., 2016). There are also other cargo molecules targeted by the Cvt pathway, for example Ams1 and Ty1. However, these proteins are incapable of forming large aggregates. Instead, they bind to the Ape1 complex and thus depend on Ape1 for their transport to the vacuole (Yamasaki and Noda, 2017). At its C-terminus, Atg19 contains an AIM for interaction with Atg8. The specific binding to Atg8 is essential for the Cvt pathway, but not for clearance by starvation-induced autophagy, as it might favor the expansion of the phagophore membrane around the Ape1 complex while excluding other cytosolic material (Noda et al., 2008b). Atg19 contains also a C-terminal Atg11 binding site. However, binding of Atg11 to Atg19 depends on the phosphorylation of several serine residues in the Atg11 binding region of Atg19 by the Hrr25 kinase (Pfaffenwimmer et al., 2014).

### **1.3.2 Mitophagy**

Being the energy-producing organelles of the cell, mitochondria can accumulate reactive oxygen species (ROS). An excess of ROS can lead to DNA damages and ageing and leakage of proteins from damaged mitochondria induce cell death (Yen and Klionsky, 2008). To prevent adverse effects on the cell, these organelles are removed by selective autophagy, termed mitophagy. Mitochondria are specifically targeted via the autophagy receptor Atg32 that is anchored in the outer mitochondrial membrane via a transmembrane domain. The importance of Atg32 for mitophagy is further demonstrated by the observation that Atg32

levels increase under mitophagy-inducing conditions, for example increased oxidative stress (Okamoto et al., 2009).

Little is known about the intra-mitochondrial C-terminal domain, although it reportedly plays a role in the regulation of Atg32 (Wang et al., 2013b). However, the cytosolic N-terminal domain plays a major role in autophagy as it contains binding sites for Atg8 and Atg11. Thus, Atg32 provides a link between mitochondria and the autophagic machinery. Upon induction of mitophagy, residues Ser-114 and Ser-119 are phosphorylated and recruit Atg11 to the mitochondrial membrane. However, interaction with Atg8 is independent of the phosphorylation state (Aoki et al., 2011).

### **1.3.3 Pexophagy**

Superfluous peroxisomes are quickly degraded by autophagy, termed pexophagy. This is initiated by the binding of Atg36 to the peroxisomal membrane protein Pex3. Like the cargo receptors discussed above, Atg36 is interacting with Atg8 and Atg11 (Motley et al., 2012). Similar to Atg19 in the Cvt pathway, phosphorylation of Atg36 by the Hrr25 kinase is necessary for pexophagy (Tanaka et al., 2014).

### **1.3.4 Aggrephagy**

Aggrephagy is the specific degradation of aggregates of misfolded proteins. In humans, autophagy plays a major protective role in neurodegenerative diseases, e.g. Alzheimer's, Parkinson's and Huntington's disease. The misfolded proteins are ubiquitinated but cannot be cleared by the proteasomal pathway due to their aggregated state. These aggregates are then captured by autophagosomes for lysosomal degradation (Hyttinen et al., 2014). In humans, the poly-ubiquitin binding protein p62 was shown to enable autophagic degradation of ubiquitinated protein aggregates (Pankiv et al., 2007). However, the existence of a similar pathway in yeast was unknown. Only recently a study identified CUET proteins, a new class of ubiquitin receptors conserved from yeast to human. Cue5 and its human homologue Tollip facilitate the autophagy-dependent degradation of polyQ protein aggregates, which are linked to Huntington's disease in humans (Lu et al., 2014).

### **1.3.5 Atg11**

Atg11 is a large protein of 1178 amino acid residues and a molecular weight of 135 kDa. Until now its structure has not been solved but the presence of four coiled-coil domains was

predicted (Yorimitsu and Klionsky, 2005). Several interaction partners are identified and their binding regions were mapped to the different coiled-coil domains (CCs, see Figure 3). The C-terminal domain containing CC4 is indispensable for interaction with the Cvt pathway cargo receptor Atg19 (Yorimitsu and Klionsky, 2005). Likewise, this domain is also required for interaction with the mitophagy-specific cargo receptor Atg32 (Aoki et al., 2011). The C-terminal region is thus the key player in linking specific cargo to the autophagic pathway. Coiled-coil domains CC2 and CC3 were reported to have several interaction partners, including core components of the autophagic machinery like Atg17 and Atg20 (binding region mapped to CC2) as well as Atg1 which required both, CC2 and CC3 (Yorimitsu and Klionsky, 2005). Furthermore, Atg11 self-interaction was reported via CC2 and CC3. Another study found that Atg11 is interacting with Atg9 via CC1 and CC2 (Chang et al., 2006). More recently, interaction between Atg11 and Atg29 was reported, which requires the starvation-induced phosphorylation of Atg29. Binding between Atg11 and phosphorylated Atg29 or Atg1 was crucial for efficient autophagy. Thus, Atg11 might aid in non-selective autophagy as well by recruiting the active Atg1 kinase complex to the PAS (Mao et al., 2013). These data suggest a fundamental role of Atg11 in autophagy initiation and in linking selective cargoes to the autophagic machinery. However, the molecular function of this protein remained poorly understood.

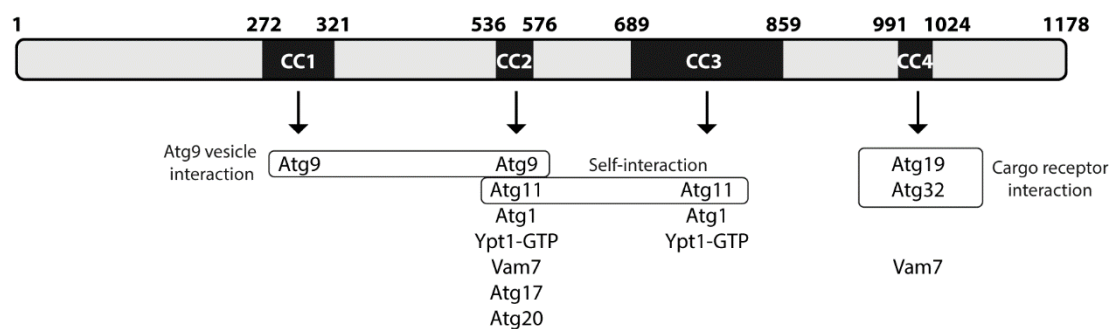


**Figure 3: Interactions with Atg11.** Atg11 has four predicted coiled-coil domains (CC1 to CC4). Several interaction partners had been discovered by yeast two-hybrid and immunoprecipitation assays and binding regions were mapped to the different coiled-coil domains. Atg11 shows self-interaction via CC2 and CC3 and interacts with Atg9 via CC1 and CC2 and cargo receptors via CC4.

## 1.4 Human homologues of the yeast system

Many insights that were obtained from studying yeast could contribute to the understanding of autophagy in human cells. Autophagy is a highly conserved pathway and many proteins of the core machinery in yeast have known human homologues (see Table 1). Initiation in human cells requires the Ulk1/2 complex as compared to the Atg1-kinase complex in yeast. Ulk1/2 and Atg13 are homologous to yeast Atg1 and Atg13, respectively, and FIP200 is considered to be a potential homologue of Atg17 (Noda and Fujioka, 2015). Because of its large size compared to Atg17, FIP200 might comprise additional functions. Thus, it might combine the function of Atg17 and Atg31-Atg29, as for the latter no homologous proteins are known so far. However, the exact role of FIP200 remains unclear. Also, it is still uncertain whether there is a human homologue of Atg11. However, it was suggested recently that Huntingtin is a scaffolding protein comprising a similar function as Atg11. While aggregates of mutant Huntingtin cause Huntington's Disease, its normal function was reported to be required for selective autophagy. Moreover, its C-terminal domain shares structural similarities with Atg11 and interacts with the Ulk1/2 complex, cargo receptors and Atg8 family proteins (Ochaba et al., 2014).

**Table 1: Human orthologues of yeast ATGs.** The following table lists several autophagy-related proteins in *S. cerevisiae* and their known or proposed orthologues in humans.

	Yeast	Human
Autophagy initiation	Atg1	Ulk1, Ulk2
	Atg13	Atg13
	Atg17	FIP200?
	Atg29/31	Part of FIP200?
	Atg11	Huntingtin?
	Atg9	Atg9A
PI3-kinase	Atg14	Atg14/Bakor
PI3P interactors	Atg18	WIPI2
	Atg4	Atg4A, -B, -C, -D
	Atg7	Atg7
Conjugation machinery	Atg10	Atg10
	Atg12	Atg12
	Atg5	Atg5
	Atg16	Atg16-L1
	Atg8	LC3A, LC3B, LC3C, GABARAP, GABARAPL1, GATE-16

Human homologues have also been identified for the transmembrane protein Atg9, for the PI3-kinase subunit Atg14 and the PI3P-binding protein Atg18 (Imai et al., 2016; Itakura et al., 2008; Wilson et al., 2014). Furthermore, the proteins of the ubiquitin-like conjugation machinery are highly conserved as well (Wilson et al., 2014). However, while most of them have only one orthologue, several homologues have been identified for yeast Atg8. They can be divided into two subgroups, the LC3 subfamily (LC3A, LC3B and LC3C) and the GABARAP/GATE-16 subfamily (GABARAP, GABARAPL1 and GATE-16) which are both required for autophagy but may act at different steps of autophagosome biogenesis (Weidberg et al., 2010).

## **1.5 Aim of the thesis**

The selective removal of cytoplasmic cargo by autophagy is a crucial process to maintain cellular homeostasis and plays an important role in the protection against cancer, neurodegenerative diseases and ageing. In contrast to non-selective autophagy, which leads to the degradation of bulk cytoplasm, selective autophagy exclusively degrades distinct cargo. Consequently, differences in the morphology of autophagosomes and the composition of the protein-machinery exist between both pathways. It is therefore of high interest to decipher how the cell switches between these two pathways and how this process is regulated.

One key player in selective autophagy is Atg11. Several interaction partners had been identified *in vivo* including cargo receptors, the transmembrane protein Atg9 and subunits of the Atg1 kinase complex. However, it is not essential for starvation-induced autophagy. In contrast, Atg17 is required for non-selective but not for selective autophagy. It functions as a tether for Atg9 vesicles during autophagy initiation upon starvation but tethering is impaired during nutrient-rich conditions. The structure of Atg11 is unknown but its N-terminal domain shares some sequence homology with Atg17. This gave rise to the hypothesis that Atg11 might tether Atg9 vesicles during selective conditions when Atg17 is inactive.

The aim of this thesis was to decipher the molecular function of Atg11 and its regulation. This required the reconstitution of autophagy initiation *in vitro* utilizing purified proteins and artificial Atg9 vesicles as it was previously developed to investigate the function of Atg17. One goal was to examine physical protein-protein interactions in the defined *in vitro* system. Furthermore, it was aimed to identify a possible tethering function of Atg11 its regulation, especially in respect to the mitochondrial cargo receptor Atg32. Moreover, it was investigated whether Atg11 and Atg17 facilitate the recruitment of each other or whether their binding to

Atg9 vesicles is competitive. Additionally, *in vivo* experiments should support the *in vitro* observations. The findings acquired for this thesis could finally contribute to a new model of autophagy initiation during selective conditions.

## 2 Materials and methods

### 2.1 Materials

If not mentioned otherwise, chemicals were purchased from Fisher Scientific, Roth, Sigma-Aldrich, or Thermo Scientific. Enzymes for cloning were purchased from New England Biolabs, lipids from Avanti Polar lipids. Enzymes used for protein purification (Sm DNase, PreScission, TEV protease) were produced in-house by the MPIB core facility. DNA primer synthesis and sequencing were carried out by Eurofins Genomics. More details on *E. coli* and *S. cerevisiae* strains, plasmids and antibodies are summarized in Table 2 to Table 5.

#### 2.1.1 Bacterial strains

Table 2 lists the *E. coli* strains that were used for cloning (XL-1 Blue and Omnimax) and protein expression (BL21 and Rosetta) and their respective phenotypes.

**Table 2:** List of *E. coli* strains.

Strain	Genotype
XL-1 Blue	<i>recA1 endA1 gyrA96 thi-1 hsdR17 supE44 relA1 lac [F' proAB lacIqZΔM15 Tn10 (Tetr)]</i>
Omnimax	<i>F' {proAB+ lacIq lacZ ΔM15 Tn10(TetR) Δ(ccdAB)} mcrA Δ(mrr-hsdRMS-mcrBC) φ80(lacZ)ΔM15 Δ(lacZYA-argF) U169 endA1 recA1 supE44 thi-1 gyrA96 relA1 tonA pand</i>
BL21 (DE3)	<i>E. coli B F- dcm ompT hsdS(rB- mB-) gal λ(DE3)</i>
Rosetta (DE3)	<i>F- ompT hsdSB(rB- mB-) gal dcm (DE3) pRARE (CamR)</i>
DH10Bac	<i>F-mcrA Δ(mrr-hsdRMS-mcrBC) Φ80lacZΔM15 ΔlacX74 recA1 endA1 araD139 Δ(ara, leu)7697 galU galK λ-rpsL nupG/pMON14272/pMON7124</i>
XL10 Gold	<i>Tet<sup>r</sup>Δ (mcrA)183 Δ(mcrCB-hsdSMR-mrr)173 endA1 supE44 thi-1 recA1 gyrA96 relA1 lac Hte [F' proAB lacI<sup>q</sup>ZΔM15 Tn10(Tetr) Amy Cam<sup>r</sup>]</i>

#### 2.1.2 Plasmids

Table 3 lists the plasmids that were used either for heterologous expression of proteins in bacteria for subsequent purification or expression in or modification of yeast for *in vivo* studies.

**Table 3:** List of plasmids for bacterial and yeast expression.

Plasmid	Details	Source
pCoofy1	pBR322-His <sub>6</sub> -PreScission-ccdB ccdB substituted by gene of interest	MPIB core facility
pCoofy37	pBR322-MBP-PreScission-ccdB-His <sub>6</sub> ccdB substituted by gene of interest	MPIB core facility
pCoofy37-Atg11	Expression of MBP-PreScission-Atg11-His <sub>6</sub>	Nena Matscheko
pCoofy37-Atg11-linker	Expression of MBP-PreScission-Atg11-TEV-His <sub>6</sub> -linker-His <sub>6</sub>	This study
pCoofy37-Atg11 <sup>ΔC</sup>	Expression of MBP-PreScission-Atg11 <sup>1-677</sup> -His <sub>6</sub>	Nena Matscheko
pCoofy37-Atg11 <sup>Δdim</sup>	Expression of MBP-PreScission-Atg11 <sup>1-456</sup> -His <sub>6</sub>	This study
pCoofy1-Atg32	Expression of His <sub>6</sub> -PreScission-Atg32 <sup>1-376</sup>	Nena Matscheko
pCoofy1-Atg32 <sup>SE</sup>	Expression of His <sub>6</sub> -PreScission-Atg32 <sup>1-376, S114E</sup>	Nena Matscheko
pST39-Atg17 <sup>TC</sup>	Polycistronic expression of His <sub>6</sub> -PreScission-Atg17-myc, Atg29 and Atg31	Yijian Rao
pST39-Atg17	Expression of His <sub>6</sub> -PreScission-Atg17-myc	Yijian Rao
pST39-Atg29-Atg31	Polycistronic expression of His <sub>6</sub> -PreScission-Atg29 and Atg31	Yijian Rao
pST39-Atg29 <sup>SD</sup> -Atg31	Polycistronic expression of His <sub>6</sub> -PreScission-Atg29 <sup>S197D, S199D, S201D</sup> and Atg31	Yijian Rao
pST39-Atg17 <sup>TC,SD</sup>	Polycistronic expression of His <sub>6</sub> -PreScission-Atg17-myc, Atg29 <sup>S197D, S199D, S201D</sup> and Atg31	This study
pET28a(+)-Atg9 <sup>core</sup>	Expression of Atg9 <sup>281-779, I327V, L328F, M439L</sup> -PreScission-StrepTag-His <sub>6</sub>	Yijian Rao
pCoofy37-Atg13-TEV	Expression of MBP-PreScission-Atg13-TEV-His <sub>6</sub>	Marco Perna
pCoofy29-Atg1	Vector for translocation of MBP-PreScission-Atg1-TEV-His <sub>6</sub> into bacmid DNA for insect cell expression	Marco Perna
pTL58(pAtg11)-Atg11-3HA	CEN plasmid, expression of HA-tagged Atg11 in yeast under endogenous promoter	Nena Matscheko
pG-KJE8	Expression of chaperones dnaK, dnaJ, grpE, groES, groEL	Takara Bio Inc.

### 2.1.3 Yeast strains

Table 4 lists the yeast strains used for this study. Proteins were tagged or deleted using PCR amplified cassettes as described in paragraph 2.2.3. The respective selection markers are indicated.

**Table 4:** List of yeast strains.

Strain	Details	Source
BY4741	S288C MATa <i>his3Δ1 leu2Δ0 met15Δ0 ura3Δ0</i>	Euroscarf
BY4741 Atg11-9myc	BY4741 Atg11-9x myc tag (natNT2)	Nena Matscheko
BY4741 Atg11-9myc <i>pdr5Δ</i>	BY4741 Atg11-9x myc tag (natNT2) <i>pdr5::hphNT1</i>	Nena Matscheko
BY4741 <i>pdr5Δ</i>	BY4741 <i>pdr5::hphNT1</i>	This study
BY4741 <i>atg7Δ</i>	BY4741 <i>atg7::kanMX6</i>	Viola Beier
BY4741 Atg17-9myc	BY4741 Atg17-9x myc tag (natNT2)	Viola Beier
BY4741 <i>pep4Δ</i>	BY4741 <i>pep4::kanMX6</i>	Viola Beier

### 2.1.4 Antibodies

Table 5 lists the antibodies that were used in experiments, either for Western blots (the used dilution is given in brackets) or bound to Protein A coupled magnetic beads for immunoprecipitation.

**Table 5:** List of antibodies.

Target	Host organism	Manufacturer	Application
c-myc	Rabbit	Santa Cruz	Western blot, primary antibody (1:1,000)
c-myc	Mouse	(in house)	Immunoprecipitation
HA	Mouse	Santa Cruz	Western blot, primary antibody (1:200)
Ubiquitin	Mouse	Enzo	Western blot, primary antibody (1:500), Immunoprecipitation
Pgk1	Mouse	Invitrogen	Western blot, primary antibody (1:1,000)
GFP	Mouse	Roche	Western blot, primary antibody (1:1,000)
Mouse IgG (HRP-conjugated)	Goat	Thermo	Western blot, secondary antibody (1:10,000)
Rabbit IgG (HRP-conjugated)	Goat	Rockland	Western blot, secondary antibody (1:5,000)

### 2.1.5 Insect cell lines

Insect cells were used as an additional expression system for protein purification by baculovirus infection of Sf9 (derived from *Spodoptera frugiperda* pupal ovarian tissue) or High Five cells (BTI-TN-5B1-4, derived from a *Trichoplusia ni* cell line). Sf9 cells were used

for transfection, virus production and expression whereas High Five cells were only used for expression.

## **2.2 Molecular biology methods**

### **2.2.1 Competent bacteria**

Chemocompetent bacteria for plasmid transformation were prepared as described (Inoue et al., 1990). Bacteria were grown in 100 ml of LB medium to an OD<sub>600</sub> of 0.6 at 18°C. The cells were collected and resuspended in 30 ml TB buffer (10 mM HEPES, 15 mM CaCl<sub>2</sub>, 250 mM KCl, and 55 mM MnCl<sub>2</sub>). After 10 min incubation on ice, cells were pelleted and resuspended in 8 ml TB buffer supplemented with DMSO to 7% final concentration. The cells were incubated for another 10 min. Aliquots of competent cells were flash-frozen in liquid nitrogen and stored at -80°C.

### **2.2.2 Cloning and plasmid preparation**

For DNA amplification Phusion polymerase was used. PCRs were carried out as described in the manual. For DNA insertions into plasmids the Sequence and Ligation Independent (SLIC) method was used as described (Scholz et al., 2013). Briefly, inserts were amplified by PCR using primers that contained 25 bp overhangs homologous to the 5' and 3' flanking regions of the target plasmid. The plasmid was linearized by PCR using the reverse complements of the overhangs as primers. For the recombination reaction 100 ng of linearized plasmid were mixed with the insert PCR product (molar ratio of plasmid:insert = 1:3) in RecA buffer (NEB). 1 µl RecA (2 µg/ml) was added, the sample was incubated at 37°C for 30 min and transformed into chemocompetent *E. coli* Omnimax cells. For this, the sample was mixed with 50 µl of cells on ice and incubated for 30 min, followed by a heat-shock at 42°C for 45 s. After cooling down on ice, the sample was supplemented with 1 ml of LB medium and incubated at 37°C for 1 h. The bacteria were then spread on LB agar plates containing the appropriate antibiotics and incubated at 37°C. Plasmids were prepared from 5 ml cultures in LB medium after overnight incubation using the NucleoSpin Plasmid miniprep kit (Macherey-Nagel).

For small inserts the RecA reaction was rather inefficient. In this case, the insert was introduced via primers for plasmid linearization followed by re-ligation. The reverse and forward primers were homologous to the 5' and 3' flanking regions of the insertion site, respectively, and contained the sequence of either half of the insert in their overhangs. The PCR product was then treated with DpnI to remove template DNA and purified via an agarose

gel. The DNA was incubated with T4 polynucleotide kinase at 37°C for 30 min to phosphorylate the ends of the PCR products. Afterwards, T4 DNA ligase was added and the sample was incubated at 16°C overnight. This method, however, required to screen a larger set of colonies. First, colony-PCR was performed with one primer binding to the insert, the other one to the backbone. Positive colonies then were checked by sequencing as base pair deletions happened frequently at the ligation site.

### 2.2.3 Genomic manipulation of yeast

Deletions and genomic addition of tags in yeast were carried out using homologous recombination of transformed DNA cassettes. The cassettes were amplified from a set of cassette plasmids and primers were designed accordingly (Janke et al., 2004). The PCR was carried out as described above.

The strain to be manipulated was grown at 30°C until an  $OD_{600}$  of 0.3. 10 ml of culture per reaction were centrifuged at 1,000 g for 10 min. The pellet was resuspended in 1 ml of sterile water and transferred to an Eppendorf tube. After centrifugation at 1,000 g for 5 min the pellet was washed with 1 ml LiAc Buffer (100 mM lithium acetate, 10 mM Tris pH 8.0, 1 mM EDTA). Afterwards, the pellet was resuspended in 50  $\mu$ l LiAc Buffer per reaction and incubated at 30°C for 15 min. 50  $\mu$ l of this suspension were mixed with 5  $\mu$ l of ssDNA (salmon sperm DNA heated to 95°C for 5 min and cooled on ice), 10  $\mu$ l PCR product and 300  $\mu$ l PEG Buffer (40% PEG 3350, 100 mM lithium acetate, 10 mM Tris pH 8.0, 1 mM EDTA). Samples were incubated at 30°C for 1 h at moderate shaking. Then, 35  $\mu$ l DMSO were added, carefully mixed and the samples were heat-shocked at 42°C for 30 min. The cells were pelleted at 500 g for 5 min and the pellet was resuspended in 2 ml YPD and incubated by shaking at 30°C for 5 h. The culture was pelleted at 1,000 g for 5 min, resuspended in 100  $\mu$ l YPD and plated on a YPD-agar plate containing the appropriate antibiotics. If the cassette contained an autotrophic marker, cells were washed once with PBS after the heat-shock and directly plated on SD-agar plates lacking the appropriate amino acid.

The plates were incubated for at least two days at 30°C. Colonies were picked and streaked out on fresh plates to ensure there was no contamination with background colonies. The correct insertion of the cassette was verified by PCR. Colonies were picked and resuspended in 100  $\mu$ l Extraction Buffer (200 mM lithium acetate, 1% SDS) and incubated for 15 min at 70°C. The samples were mixed with 300  $\mu$ l pure ethanol and centrifuged at 17,000 g for 3 min. The pellet was washed with 500  $\mu$ l of 70% ethanol and then dissolved in 20  $\mu$ l of water. Cell debris was pellet by centrifugation at 17,000 g for 20 s and 1  $\mu$ l of DNA solution was used in the PCR reaction.

#### **2.2.4 Plasmid transformation into yeast cells**

CEN plasmids were expressed in yeast cells without integration into the genome. For the transformation of these plasmids a modified protocol was used. 1 µg of plasmid was mixed with 85 µl One Step Buffer (47% PEG 3550, 0.24 M lithium acetate), 10 µl of 1 M DTT and 5 µl ssDNA (salmon sperm DNA heated to 95°C for 5 min and cooled down on ice). A small amount of the yeast strain to be transformed was picked from an agar plate and resuspended in the transformation mix. The samples were incubated for 30 min at 45°C, pelleted by centrifugation at 500 g for 5 min, washed once in PBS and plated on SD-agar plates lacking the corresponding amino acid.

### **2.3 Biochemical methods**

#### **2.3.1 SDS-PAGE and Western blotting**

For most applications SDS-acrylamide gels were prepared as follows: The mix for the separation gel contained 10 to 15% acrylamide (Rotiphorese Gel 30 acrylamide/bis-acrylamide solution, Roth), 375 mM Tris pH 8.8, 0.1% SDS, 0.1% ammonium persulfate, and 0.1% TEMED (N,N,N',N'-tetramethylethane-1,2-diamine). The separation gel was topped with a stacking gel containing 4% acrylamide, 125 mM Tris pH 6.8 and 0.1% each of SDS, ammonium persulfate and TEMED. The gel was run in a Mini-Protean chamber (BioRad) filled with SDS Running Buffer (25 mM Tris, 192 mM glycine, 0.1% SDS) with 80 V for the stacking and 160 V for the separation gel. The samples were loaded together with the BenchMark Protein Ladder (Invitrogen) or the Novex Sharp Pre-stained Protein Standard (Invitrogen) as marker for Coomassie stained gels or Western blots, respectively. For direct staining of the protein bands the gel was incubated in Coomassie Staining solution (0.2% Coomassie Brilliant Blue R250, 30% ethanol, 10% acetic acid) for 1 h, followed by incubation in Destaining solution (40% ethanol, 10% acetic acid) until the background was fully destained. For antibody detection of proteins Western blots were performed. The gel was incubated in Blotting buffer (50 mM Tris base, 39 mM glycine, 20% methanol, 0.037% SDS) for 10 min. A PVDF membrane corresponding to the size of the gel (BioRad) was first incubated in 100% methanol for 1 min and then 10 min in Blotting buffer. The gel and the membrane were sandwiched between two pieces of Extra thick filter paper (BioRad) soaked in Blotting buffer. Blotting was performed in a Transblot SD semidry blotting chamber (BioRad) at 15 V for 30 min to 1 h depending on the size of the protein. Afterwards, the membrane was blocked in TBS-T (25 mM Tris pH 7.4, 150 mM NaCl, 0.05% Tween-20) containing 5% milk powder for

1 h at room temperature. The membrane was washed with TBS-T and incubated with the primary antibody diluted in TBS-T containing 2% BSA and 0.02% sodium azide. After incubation for 2 h at room temperature or at 4°C over night, the membrane was washed three times in TBS-T for 5 min and incubated for 1 h at room temperature with the secondary antibody (HRP-conjugated) diluted in TBS-T with 5% milk powder. The membrane was washed again three times. It was incubated with SuperSignal West Pico Plus chemiluminescence substrate (Thermo) and subsequently imaged in a G:Box chamber (Syngene). To stain different proteins in the same sample, the membrane was incubated in Stripping buffer (100 mM NaOH, 2% SDS, 0.5% DTT) for 30 min at room temperature, washed five times with TBS-T and incubated with 5% milk powder in TBS-T for 1 h. Staining with a different antibody was then performed as described before. Band intensities were quantified using ImageJ and its built-in band-quantification tool.

### 2.3.2 Crosslinking

As crosslinkers react with primary amines such as Tris-HCl, size exclusion chromatography during Atg11 purification was performed using Atg11 HEPES buffer (25 mM HEPES pH 7.2, 275 mM KCl, 5% glycerol). Other proteins that contained Tris-HCl were re-buffered into Atg11 HEPES buffer using Zeba Desalting spin columns (Thermo). For glutaraldehyde crosslinking, proteins were diluted with Atg11 HEPES buffer to a final concentration of 5  $\mu$ M, supplemented with up to 5 mM glutaraldehyde and incubated at room temperature for up to 5 min. The reactions were stopped by addition of Tris pH 8.0 to a final concentration of 100 mM. To overcome the problems of aggregation with glutaraldehyde crosslinking, the photocrosslinker Sulfo-LC-SDA (Thermo) was used. Either Atg11 or Atg32<sup>SE</sup> were mixed with the crosslinker (molar ratio protein:crosslinker between 1:10 and 1:50). The reaction was carried out for 30 min at room temperature and quenched with Tris pH 8.0 at 100 mM final concentration. To remove residual crosslinker the sample was applied to a Zeba Desalting spin column equilibrated in Atg11 HEPES buffer. Labeled Atg11 was mixed with unlabeled Atg32<sup>SE</sup> (molar ratio = 1:3) or vice versa and exposed to UV light for 30 s to 30 min.

## 2.4 Protein purification

### 2.4.1 Purification of Atg11

To improve the expression of full-length Atg11 the pCoofy37-Atg11-linker plasmid was co-transformed with the pG-KJE8 plasmid (Takara) into *E. coli* BL21 (DE3). The bacteria were

grown at 37°C in 3 l of TB (Terrific broth) medium (2.4% yeast extract, 1.2% tryptone, 0.5% glycerol, 0.017 mM KH<sub>2</sub>PO<sub>4</sub>, 0.072 mM K<sub>2</sub>HPO<sub>4</sub>) supplemented with 35 µg/ml kanamycin and 24 µg/ml chloramphenicol. After 1 h, expression of chaperones was induced by adding arabinose to 0.2% and tetracycline to 5 ng/ml final concentration. Cells were grown to an OD<sub>600</sub> of 0.6 and shifted to 18°C. Expression of Atg11 was induced with 0.3 mM IPTG at an OD<sub>600</sub> of 1.6 and carried out at 18°C for 20 h. The cells were harvested by centrifugation (15 min at 4,500 g and 4°C) and resuspended in Atg11 Lysis Buffer (100 mM Tris pH 8.0, 300 mM KCl, 10% glycerol, 20 mM imidazole, 0.2% Tween-20, 5 mM β-mercaptoethanol, 1 mM PMSF) to a final volume of 150 ml and supplemented with 500 µl Protease Inhibitor cocktail (Sigma-Aldrich) and 20 µl Sm DNase. The sample was sonicated four times for 1 min with 80% amplitude and 2s/5s on/off pulse (Ultrasonic 500 W, Fisher Scientific). The lysate was cleared by centrifugation for 1 h at 50,000 g and 4°C. The supernatant was loaded on a HisTrap 5 ml column with an Äkta Prime system, the flow through was collected and loaded two more times resulting in a total incubation time of 3 h. The column was washed with 200 ml of Atg11 Wash Buffer (50 mM Tris pH 8.0, 500 mM KCl, 10% glycerol, 80 mM imidazole) and eluted with 20 ml of Atg11 Elution Buffer (25 mM Tris pH 7.2, 500 mM KCl, 10% glycerol, 250 mM imidazole). 2 ml fractions were collected and the peak fractions of the elution were pooled (8-10 ml total volume) and concentrated to 400 µl using an Amicon Ultra-20 centrifugal filter with 50 kDa MWCO (Merck Millipore). The sample was supplemented with DTT and EDTA to 1 mM final concentration each and mixed with 5 µl His-PreScission and 5 µl His-TEV. The sample was incubated at 4°C over night and centrifuged for 20 min at 17,000 g to remove larger aggregates. The supernatant was loaded on a Superose 6 Increase 10/300 (GE) size exclusion column equilibrated in Atg11 Buffer (25 mM Tris pH 7.2, 275 mM KCl, 5% glycerol). Peak fractions were pooled and concentrated using an Amicon Ultra-4 centrifugal filter with 50 kDa MWCO (Merck Millipore). Due to the low stability of Atg11, the concentrated sample was kept at 4°C and used within the following two days. To remove possible aggregates that formed after size exclusion, the sample was ultracentrifuged at 160,000 g for 20 min prior to use.

#### **2.4.2 Purification of Atg11 variants**

Atg11<sup>ΔC</sup> and Atg11<sup>Δdim</sup> were expressed from the pCoofy37 plasmid in *E. coli* BL21. Cells were grown at 37°C in 3 l LB medium supplemented with 50 µg/ml kanamycin. The expression was induced with 0.3 mM IPTG at an OD<sub>600</sub> of 0.8 and carried out at 18°C for 20 h. Cells were harvested by centrifugation for 15 min at 4,500 g and 4°C. The pellet was resuspended in Atg11 Lysis Buffer (100 mM Tris pH 8.0, 300 mM KCl, 10% glycerol, 20 mM imidazole, 0.2%

Tween-20, 5 mM  $\beta$ -mercaptoethanol, 1 mM PMSF, 0.25% PI, 10  $\mu$ l Sm DNase) to a final volume of 100 ml. The cells were lysed by sonicating four times for 30 s at 80% amplitude and 2s/5s on/off pulse (Ultrasonic 500 W, Fisher Scientific). The lysate was cleared by centrifugation for 1 h at 50,000 g and 4°C. The supernatant was mixed with 2 ml of washed Ni-NTA agarose beads and incubated at 4°C for 2 h. The beads were washed 6 times with 25 ml KCl Wash Buffer (25 mM Tris pH 8.0, 300 mM KCl, 10% glycerol, 20 mM imidazole) in a glass column with fritted disc and the protein was eluted with 5 ml KCl Elution Buffer (25 mM Tris pH 7.4, 300 mM NaCl, 500 mM imidazole, 10% glycerol). The MBP-tag was cleaved off by addition of 10  $\mu$ l His-PreScission and incubation at room temperature for 1 h. Then the sample was loaded on a Superdex 200 16/60 size exclusion column equilibrated in Atg11 Buffer (25 mM Tris pH 7.2, 275 mM KCl, 5% glycerol). Peak fractions were pooled and concentrated using a Spin-X UF concentrator with 30 kDa MWCO (Corning). Concentrated samples were flash-frozen in liquid nitrogen and stored at -80°C until further use.

### 2.4.3 Purification of other Atg proteins

#### 2.4.3.1 *Atg17, Atg29, Atg31*

*Atg17*, *Atg29* and *Atg31* were co-expressed from the pST39 plasmid for polycistronic expression. Different constructs were used to co-express all three proteins, to co-express *Atg29* (wild type and phosphomimetic mutant) with *Atg31*, and to express *Atg17* alone. All constructs were transformed into the *E. coli* BL21 Rosetta strain for improved codon usage and grown in 3 l LB medium supplemented with 100  $\mu$ g/ml ampicillin and 24  $\mu$ g/ml chloramphenicol. The expression was induced with 0.3 mM IPTG at an OD<sub>600</sub> of 0.8 and carried out at 18°C for 20 h. Cells were harvested by centrifugation for 15 min at 4,500 g and 4°C. The pellet was resuspended in Lysis Buffer 8.0 (100 mM Tris pH 8.0, 300 mM NaCl, 10 mM imidazole, 10% glycerol, 5 mM  $\beta$ -mercaptoethanol, 1 mM PMSF, 0.25% Protease Inhibitor, 10  $\mu$ l Sm DNase) to a final volume of 100 ml. The cells were lysed by sonicating four times for 30 s at 80% amplitude and 2s/5s on/off pulse (Ultrasonic 500 W, Fisher Scientific). The lysate was cleared by centrifugation for 1 h at 50,000 g and 4°C. The supernatant was mixed with 2 ml of washed Ni-NTA agarose beads and incubated at 4°C for 2 h. Then, the suspension was moved to a glass column with fritted disc. The beads were washed 6 times with 25 ml Wash Buffer 7.4 (25 mM Tris pH 7.4, 300 mM NaCl, 20 mM imidazole, 10% glycerol) and the protein was eluted with 5 ml Elution Buffer 7.4 (25 mM Tris pH 7.4, 300 mM NaCl, 500 mM imidazole, 10% glycerol). Finally, the eluate was applied to a Superdex 200 16/60 size exclusion column and peak fractions were pooled and concentrated using a Spin-X UF concentrator with 30 kDa

MWCO (Corning). Concentrated samples were flash-frozen in liquid nitrogen and stored at -80°C until further use.

#### 2.4.3.2 *Atg13*

The pCoofy37-Atg13-TEV-His plasmid was transformed into the *E. coli* BL21 Rosetta strain. Bacteria were grown in 6 l of LB medium and induced with 0.3 mM IPTG at an OD<sub>600</sub> of 0.5. Proteins were expressed for 4 h at 27°C. Cells were harvested and the cell pellet was resuspended in Lysis Buffer 8.0 (100 mM Tris pH 8.0, 300 mM NaCl, 10 mM imidazole, 10% glycerol, 0.2% Tween-20, 5 mM β-mercaptoethanol, 1 mM PMSF, 0.25% Protease Inhibitor, 10 μl Sm DNase) to a final volume of 100 ml. The cell suspension was passed three times through an Emulsiflex C3 (Avestin) applying 1.5 kbar pressure. The lysate was cleared by centrifugation for 1 h at 50,000 g and 4°C. The supernatant was loaded on a HisTrap FF 5 ml (GE) and the flowthrough was loaded again. The column was washed with 30 ml of Wash Buffer 7.4 (25 mM Tris pH 7.4, 300 mM NaCl, 20 mM imidazole, 10% glycerol) supplemented with 0.05% Tween-20 and 5 mM β-mercaptoethanol and eluted with a gradient of 0-20% Elution Buffer 7.4 (25 mM Tris pH 7.4, 300 mM NaCl, 500 mM imidazole, 10% glycerol) supplemented with 5 mM β-mercaptoethanol. Atg13 containing fractions were pooled and mixed with 30 μl each of His-PreScission and His-TEV to cleave N- and C-terminal tags, respectively. After incubation at 4°C over night, the sample was diluted with Atg13 Dilution Buffer (25 mM Tris pH 7.4, 5% glycerol, 2 mM DTT) to a final concentration of 135 mM NaCl. The sample was loaded on a HiTrap Q 1 ml (GE) anion exchange column. The column was washed with 5 ml of Atg13 HiTrap Buffer (25 mM Tris pH 7.4, 125 mM NaCl, 5% glycerol, 2 mM DTT) and Atg13 was eluted with a linear gradient from 125 mM to 250 mM NaCl in Atg13 HiTrap Buffer over 50 ml. To concentrate, the Atg13 peak fractions were pooled and diluted with Atg13 Dilution Buffer to 135 mM NaCl. The sample was loaded again on the cleaned and equilibrated HiTrap Q 1 ml column, followed by an elution step with Atg13 HiTrap Buffer containing 300 mM NaCl. Peak fractions were pooled, flash-frozen in liquid nitrogen and stored at -80°C until further use.

#### 2.4.3.3 *Atg9*

The pET28a-Atg9<sup>core</sup> plasmid, containing the core domain of Atg9 (residues 281-779) with three mutations (I327V, L328F, M439L), was transformed into the *E. coli* BL21 Rosetta strain. The bacteria were grown in 3 l TB medium and induced at an OD<sub>600</sub> of 1.0 with 0.3 mM IPTG. Protein expression was carried out for 20 h at 18°C. Cells were harvested and resuspended in

Atg9 Lysis Buffer (100 mM Tris pH 8.0, 500 mM KCl, 10% glycerol) supplemented with 1 mM PMSF, 0.15% protease inhibitor and 20  $\mu$ l Sm DNase to final volume of 200 ml. Cells were lysed by passing the suspension three times through an Emulsiflex C3 (Avestin) applying 1.5 kbar pressure. The lysate was centrifuged 10 min at 24,000 g. The supernatant was collected and centrifuged for another 10 min. Finally, the supernatant was transferred to an ultracentrifuge and membranes were collected for 1 h at 150,000 g. The membrane pellet was resuspended in 100 ml Atg9 Lysis Buffer supplemented with 0.1% protease inhibitor and centrifuged again for 1 h at 150,000 g. The pellet was resuspended with 80 ml of Atg9 Lysis Buffer per g of pellet, supplemented with 0.1% of protease inhibitor, 20 mM imidazole and 0.5% (w/v) LDAO. The membranes were solubilized for 1 h at 4°C and remaining particles were removed by ultracentrifugation at 150,000 g for 30 min. The supernatant was passed two times over a HisTrap FF 5 ml column. The column was washed with 100 ml of Atg9 Wash Buffer (25 mM Tris pH 8.0, 500 mM KCl, 40 mM imidazole, 10% glycerol, 0.1% LDAO) and Atg9 was eluted with Atg9 Elution Buffer (25 mM Tris pH 8.0, 200 mM KCl, 500 mM imidazole, 10% glycerol, 0.1% LDAO). Peak fractions were pooled and concentrated to 4 ml. The sample was loaded on a Superdex 200 16/60 size exclusion column equilibrated with Atg9 SEC Buffer (25 mM Tris pH 8.0, 150 mM NaCl, 0.05% LDAO). Fractions of monomeric Atg9 (elution volume of 73 ml) were pooled and concentrated to 4 mg/ml using an Amicon Ultra-20 centrifugal filter with 30 kDa MWCO (Merck Millipore). The sample was flash-frozen in liquid nitrogen and stored at -80°C.

#### 2.4.3.4 *Atg1*

Atg1 was expressed in baculovirus-infected insect cells based on a protocol developed for multi-gene expression (Fitzgerald et al., 2006). The pCoofy29-Atg1 plasmid was transformed into chemocompetent DH10Bac cells according to the standard protocol with some changes. After the heat-shock, cells were incubated for 4 h and plated on LB agar plates containing 50  $\mu$ g/ml kanamycin, 7  $\mu$ g/ml gentamicin, 10  $\mu$ g/ml tetracyclin, 40  $\mu$ g/ml IPTG, and 100  $\mu$ g/ml Bluo-gal. The plates were incubated for 2 days at 37°C allowing the negative clones to show a strong blue color. Colonies with successful transfer of the Atg1 gene to the bacmid DNA lacked the blue color and were streaked on fresh plates to confirm the phenotype.

Bacmid DNA was prepared from a 2 ml overnight culture in LB medium containing kanamycin and gentamicin. The cell pellet was lysed by alkaline lysis using Resuspension (A1), Lysis (A2) and Neutralization Buffer (N3) from the Qiagen Miniprep Kit. The lysate was centrifuged at 17,000 g for 5 min and the supernatant was transferred to a new tube and centrifuged for another 15 min to completely remove the particles. Isopropanol was added to the

supernatant to 40% concentration and DNA was pelleted by centrifugation for 10 min at 17,000 g and 4°C. The pellet was washed twice with 500 µl 70% ethanol and was dried under a sterile hood. The pellet was resuspended in 50 µl sterile water.

Sf9 cells were diluted to  $0.4 \times 10^6$  cells/ml and seeded into a 6-well plate (2 ml culture per well). Cellfectin II was mixed with 1 µg bacmid DNA in 200 µl medium and incubated for 45 min at room temperature. The transfection mix was added to the cells followed by an incubation for 3-5 h at 27°C. Afterwards, the medium was substituted with 3 ml of fresh medium. After 65 h, the medium was collected and centrifuged for 5 min at 200 g to remove cells and debris. The cleared supernatant (Virus stock V0) was added to 25 ml of Sf9 cell culture at a density of  $0.8 \times 10^6$  cells/ml. The cells were counted every 24 h and if required, medium was added to keep the cell number below  $1.0 \times 10^6$ . After proliferation arrest, the culture was incubated for another 48 h. The cells were removed by centrifugation for 5 min at 150 g and the supernatant was transferred to a fresh tube (Virus stock V1).

Atg1 expression was performed in High Five cells. The cells were diluted into 3 l of ExCell 420 insect cell medium (Sigma-Aldrich) to reach a final density of  $0.8 \times 10^6$  cells/ml and infected with Virus stock V1 at a volume ratio of 200:1 followed by incubation at 27°C. Cells were counted every 24 h and medium was added to keep cell number below  $1.0 \times 10^6$  cells/ml if needed. After proliferation arrest, the culture was incubated for 48 h. Cells were harvested by centrifugation (2,000 g, 20 min) and the pellet was resuspended in 100 ml Atg1 Lysis Buffer (100 mM Tris pH 7.4, 300 mM NaCl, 20 mM imidazole, 5% glycerol, 1% Triton-X100, 5 mM β-mercaptoethanol, 1 mM PMSF, 0.5% protease inhibitor, 10 µl Sm DNase). Cells were lysed using a douncer and the lysate was cleared by centrifugation for 1 h at 50,000 g and 4°C. The supernatant was loaded on a HisTrap FF 5 ml column using a 150 ml superloop. The column was washed with 50 ml Atg1 Wash Buffer (25 mM Tris pH 7.4, 300 mM NaCl, 20 mM imidazole, 5% glycerol, 0.1% Triton X-100). Protein was eluted with Atg1 Elution Buffer (25 mM Tris pH 7.4, 300 mM NaCl, 500 mM imidazole, 5% glycerol) and peak fractions were concentrated to 4 ml using an Amicon Ultra-20 centrifugal filter with 50 kDa MWCO. The sample was loaded on a Superdex 200 16/60 size exclusion column equilibrated with Atg1 Buffer (25 mM Tris pH 7.4, 300 mM NaCl, 5% glycerol). Atg1 fractions (peak elution volume of 65 ml) were pooled and concentrated to a concentration of about 2 mg/ml using an Amicon Ultra-4 centrifugal filter with 50 kDa MWCO.

## 2.5 Biophysical methods

### 2.5.1 Preparation of small unilamellar vesicles (SUVs)

Synthetic lipids were mixed in chloroform to give 1 mg of total lipid consisting of 20 mol% cholesterol, 60% 1-palmitoyl-2-oleoyl-sn-glycero-3-phosphocholine (POPC), 10% 1-palmitoyl-2-oleoyl-sn-glycero-3-phospho-L-serine (POPS), 10% 1-palmitoyl-2-oleoyl-sn-glycero-3-phosphoethanolamine (POPE) and 0.1% 1,2-dioleoyl-sn-glycero-3-phosphoethanolamine-N-(lissamine rhodamine B sulfonyl) (rhodamine-PE). Lipids were dried under a nitrogen stream and traces of chloroform were removed by applying vacuum for 1 h. The lipid film was resuspended in 1 ml of Liposome Buffer (20 mM HEPES pH 7.0, 100 mM NaCl) by vortexing for 1 min giving rise to a suspension of multilamellar vesicles (MLVs). To be used as control samples, the suspension was sonicated under the same conditions as for Atg9 proteoliposomes to obtain SUVs.

### 2.5.2 Reconstitution of Atg9 into proteoliposomes

A suspension of MLVs was prepared as described above except that the lipid film was resuspended in 1 ml of detergent-free Atg9 Buffer (25 mM Tris pH 8.0, 150 mM NaCl). Then, LDAO was added to 0.15% (6.5 mM) final concentration to solubilize the lipids. Purified Atg9<sup>core</sup> was centrifuged for 20 min at 17,000 g to remove larger aggregates and was added to the lipids in a molar protein:lipid ratio of 1:200 (460 µg Atg9<sup>core</sup> per mg of lipids). After 20 min incubation at room temperature, the sample was mixed with 30 ml of detergent-free Atg9 Buffer to quickly dilute to well below the critical micellar concentration (1.7 mM). Then, the solution was ultracentrifuged for 30 min at 150,000 g to collect the liposomes. The supernatant was completely removed and the pellet was resuspended in 1 ml of Liposome Buffer (20 mM HEPES pH 7.0, 100 mM NaCl).

### 2.5.3 Flootation assays

Atg9 liposomes or protein-free MLVs were sonicated 10 times for 30 s with 20 s break in-between to break down the liposome aggregates and generate LUVs. 100 µl of liposomes were immediately mixed with the proteins of interest and buffer to a total sample volume of 280 µl. For the competition assay, Atg9 proteoliposomes were incubated with Atg11 for 10 min on ice before Atg17 was added. After 30 min incubation on ice, 250 µl of the liposome mix was mixed with a 80% Histodenz solution to reach a final concentration of 40% Histodenz, transferred to an ultracentrifuge tube and overlaid with 300 µl of 30% Histodenz in Liposome

Buffer, followed by 200  $\mu$ l Liposome Buffer. The samples were ultracentrifuged at 165,000 g for 1 h at 4°C and liposomes that floated at the Histodenz/buffer interface were collected in a final volume of 80  $\mu$ l, mixed with 20  $\mu$ l 5x SDS sample buffer and incubated overnight at room temperature.

#### **2.5.4 Cryo-electron microscopy**

500  $\mu$ l of Atg9 proteoliposomes were sonicated for 10 s to break down large aggregates and mixed with 160  $\mu$ g Atg11. The sample was co-sonicated for 20 min with 0.2 s on / 1.8 s off time with the lowest power setting (21%) on a Sonics Vibra-Cell VC750 sonicator. The sample was divided into two halves and mixed with either Atg32<sup>SE</sup> (1:3 molar ratio of Atg11 to Atg32<sup>SE</sup>) or an equal amount of buffer. Cryo-electron microscopy was performed with Gérard Pehau-Arnaudet at the UTechS Biomagery Ultrastructurale, Institut Pasteur. Samples were loaded on a glow discharged Lacey carbon grid and mounted on a Leica EM GP system, blotted for 1 sec and plunge-frozen in liquid ethane. The samples were visualized on a Tecnai F20 cryo-electron microscope and images were recorded in low-dose mode on a Falcon II direct electron detector.

## **2.6 *In vivo* methods**

### **2.6.1 Growth of yeast cultures**

Genomically modified yeast strains were stored at -80°C in medium containing 20% glycerol and were streaked out on agar plates prior to use. For expression from CEN plasmids, yeast cells were freshly transformed as described before. Pre-cultures were inoculated with colonies from the plate in either YPD medium (1% yeast extract, 2% peptone, 2% glucose, supplemented with antibiotics depending on the selection marker) or SD medium (0.67% yeast nitrogen base, 2% glucose, 0.2% amino acid mix lacking the appropriate amino acid depending on the selection marker) and grown overnight at 30°C. Large cultures were inoculated from the pre-cultures and grown to an OD<sub>600</sub> of 0.8 to 1.0. For starvation experiments, cells were pelleted at 1,000 g for 5 min, washed twice in SD-N starvation medium (0.17% yeast nitrogen base, 2% glucose) and resuspended in the initial culture volume with SD-N. Culturing of the cells was continued for up to 6 h.

### **2.6.2 Preparation of whole cell lysates**

To compare protein levels in different samples by Western blot, whole cell extracts were prepared basically as described (Zhang et al., 2011). 1 OD of yeast cells was taken for each sample. The cells were pelleted and resuspended in 100  $\mu$ l of 2 M lithium acetate. After 5 min incubation on ice, cells were pelleted and resuspended in 100  $\mu$ l of 0.4 M NaOH. After another 5 min incubation on ice, cells were pelleted, the NaOH was completely removed and the pellet was resuspended in 50  $\mu$ l 1x SDS sample buffer. The samples were incubated at 95°C for 5 min and debris was removed by centrifugation.

### **2.6.3 Immunoprecipitation experiments**

Yeast cells corresponding to 50 OD of yeast culture were harvested by centrifugation. For the anti-ubiquitin IP the amount was increased to 500 OD. The pellet was resuspended in 0.5 to 2.0 ml of IP Buffer (25 mM Tris pH 7.2, 150 mM NaCl, 200 mM sorbitol, 1 mM MgCl<sub>2</sub>, 0.1% Tween-20) supplemented with 3 mM PMSF and 3-5% protease inhibitor mix. Acid-washed glass beads (425-600  $\mu$ m) were added to the suspension to 50% of the total volume. The samples were vortexed six times for 1 min with 1 min of cooling time in-between. The lysate was transferred to a fresh tube and larger components were removed by centrifugation for 1 min at 5000 g. The supernatant was supplemented with Tween-20 to 1% final concentration and was incubated for 10 min on ice. The sample was centrifuged for 15 min at 17,000 g and the supernatant was mixed with 10  $\mu$ g of antibody (20  $\mu$ g for anti-ubiquitin antibody). After incubation for 2 h at 4°C the sample was mixed with 20  $\mu$ l (40  $\mu$ l for anti-ubiquitin antibody) of Protein A coupled magnetic beads (Thermo Scientific). The suspension was incubated for 30 min at 4°C, the lysate was removed and the beads were washed four times with IP buffer containing 0.5% Tween-20. Finally, the beads were resuspended in 50  $\mu$ l SDS-PAGE loading buffer and incubated for 5 min at 95°C.

### **2.6.4 Proteasomal block assay**

The function of the proteasome was specifically inhibited by the chemical MG132. The strains used for the proteasomal block assays contained an additional deletion of the drug efflux pump Pdr5 to increase the intracellular concentration of the inhibitor. Cells were grown in SD medium and split into two at an OD<sub>600</sub> of 0.7. Either a 5 mM MG132 solution in DMSO was added to a final concentration of 50  $\mu$ M, or the same volume of DMSO as a control. After incubation at 30°C for 1 h cells were harvested and resuspended in SD-N starvation medium.

MG132 was added to a final concentration of 75  $\mu$ M, or the same volume of DMSO as a control, and cultures were incubated at 30°C for 4 h. 1 OD of cells was taken at various time points and whole cell lysates were prepared as described above.

## **2.7 Mass spectrometry**

For the cross-linking experiment samples were run on a NuPage 4-12% Bis-Tris polyacrylamide gel (Thermo Fisher) and stained with Bio-Safe Coomassie Solution (Bio-Rad). Bands were cut out, digested with trypsin and analyzed by nanoLC-MS/MS in the Mass Spectrometry for Biology Utechs (MSBio) platform at Institut Pasteur. Measurements were performed by Christian Malosse and the data was analyzed by Christian Malosse and Julia Chamot-Rooke.

### 3 Results

#### 3.1 Protein purifications

##### 3.1.1 Purification of Atg11

Atg11 is a large protein of about 135 kDa rendering expression in *E. coli* inefficient. The gene encoding Atg11 was cloned into the pCoofy37 plasmid by Dr. Nena Matscheko. This plasmid contains an N-terminal MBP-tag for increased solubility followed by a PreScission protease cleavage site, as well as a C-terminal His<sub>6</sub>-tag. The His<sub>6</sub>-tag served to remove C-terminally degraded fragments of Atg11. Although the protein was expressed with a MBP-tag, the solubility was very low. To increase folding of Atg11 in *E. coli*, the Atg11 fusion protein was co-expressed with chaperones from the Takara pG-KJE8 plasmid. Figure 4 shows an anti-His<sub>6</sub> Western blot of cell lysates from different expression conditions. This test revealed that the yield of full-length Atg11 is strongly enhanced when expressed in the presence of chaperones at a temperature of 18°C for 16 h. The yield was further increased when cells were grown in

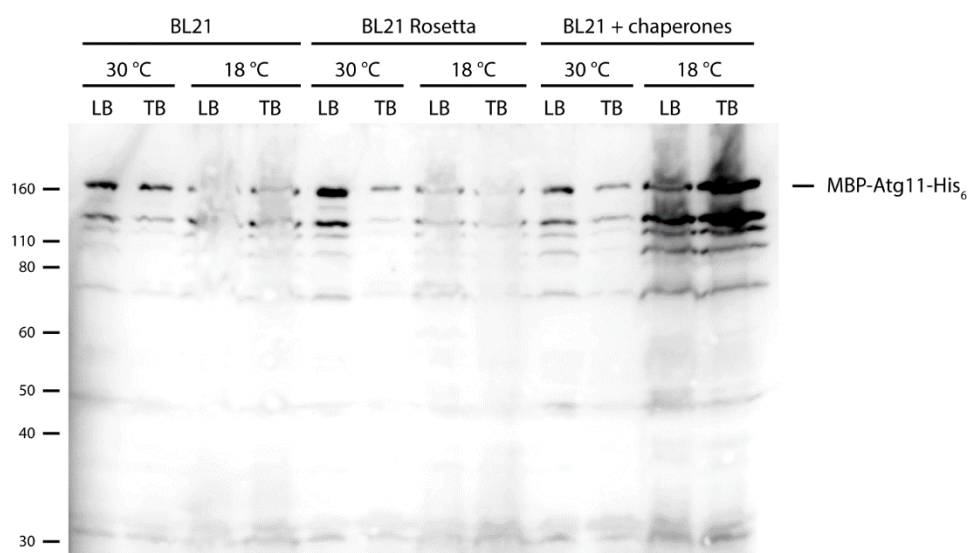


**Figure 4: Expression test for the Atg11 fusion protein.** Western blot of samples prepared from whole cell pellets and stained using anti-His antibody. Tested conditions included the medium (LB or TB), the temperature after IPTG induction (3 h expression at 30°C or 16 h at 18°C), and the bacterial strain (BL21, BL21 Rosetta for improved codon usage or BL21 co-transformed with pG-KJE8 for chaperone expression).

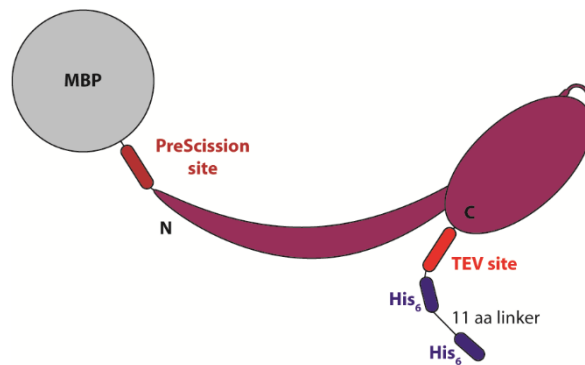


**Figure 5: Schematic of the Atg11 fusion protein for improved binding to the HisTrap.** The drawing illustrates the self-inhibition of Atg11 by its C-terminal domain, which might render a C-terminal tag less accessible. A double His<sub>6</sub>-tag was designed to improve binding to the resin (the tags are not drawn to scale).

Terrific Broth (TB) medium compared to LB medium (last two lanes in Figure 4). Even though the C-terminal His<sub>6</sub>-tag helped to remove N-terminal Atg11 fragments, the binding efficiency of the full-length fusion protein to the HisTrap resin was very low. To overcome this problem a longer C-terminal tag was designed by introducing a TEV recognition site for a later cleavage of the tag, followed by a His<sub>6</sub>-tag, a 11 amino acid spacer and a second His<sub>6</sub>-tag (Figure 5). With this change the yield of Atg11 could be strongly increased.

The large scale purification of Atg11 using a HisTrap column is depicted in Figure 6. Major contaminations could be washed from the column at low imidazole concentrations (lane "1"). A slight increase in imidazole concentration and continuous washing over several column volumes could strongly enhance the purity of the protein preparation, even though some Atg11 was lost at this step (lane "2"). The eluate was concentrated and both N- and C-terminal tags were cleaved prior to size exclusion chromatography (last two lanes of the SDS-PAGE in Figure 6). Gel filtration was performed on a Superose 6 Increase column and the chromatogram is depicted in Figure 7. Atg11 was primarily detected in the elution volume range of 9 ml to 15 ml (grey box 1). This can be explained by the aggregation-prone nature of Atg11. Monomeric Atg11 eluted at 13.1 ml (marked by an asterisk) and was detected as a strong band in SDS-PAGE. This elution volume corresponds roughly to that of thyroglobulin with a molecular weight of 669 kDa (product information by GE Life Sciences) indicating an elongated shape of Atg11. The Superose 6 Increase column was chosen because of its resolution capacity in the high molecular weight range, which allowed the separation of monomeric Atg11 from Atg11 aggregates.

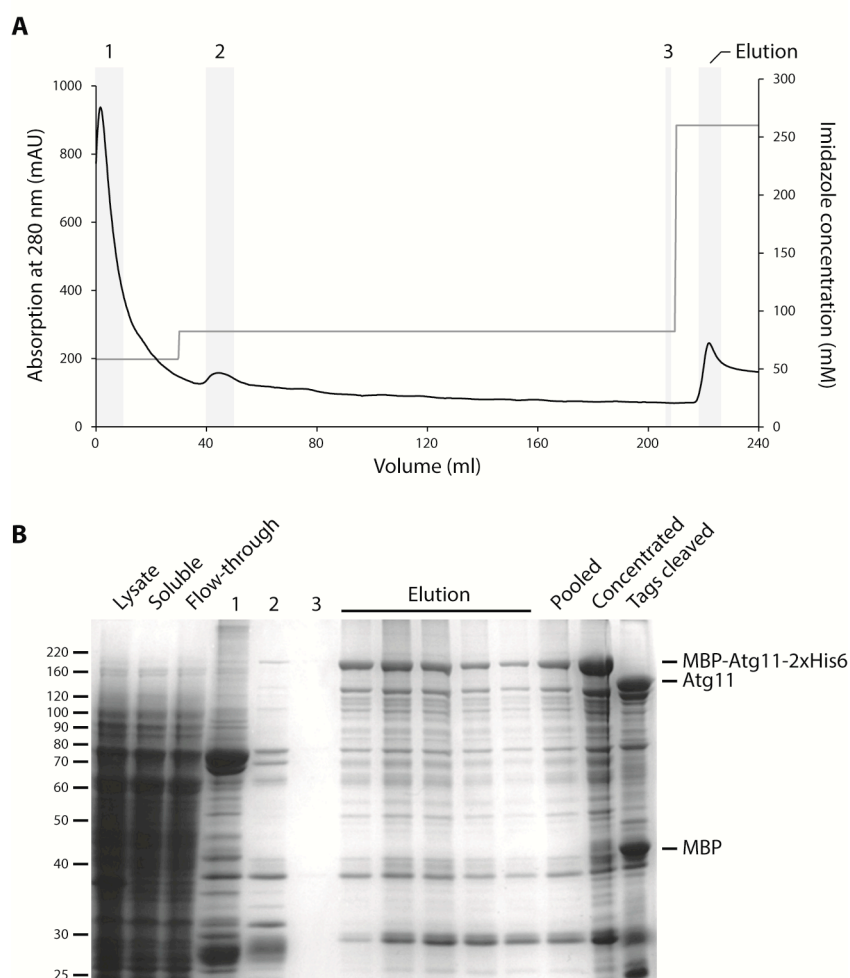


**Figure 6: HisTrap purification of Atg11.** (A) Chromatogram of the washing and elution step. Absorption at 280 nm is drawn in black, imidazole concentrations in grey. (B) Samples of different purification steps were analyzed by SDS-PAGE and Coomassie staining.

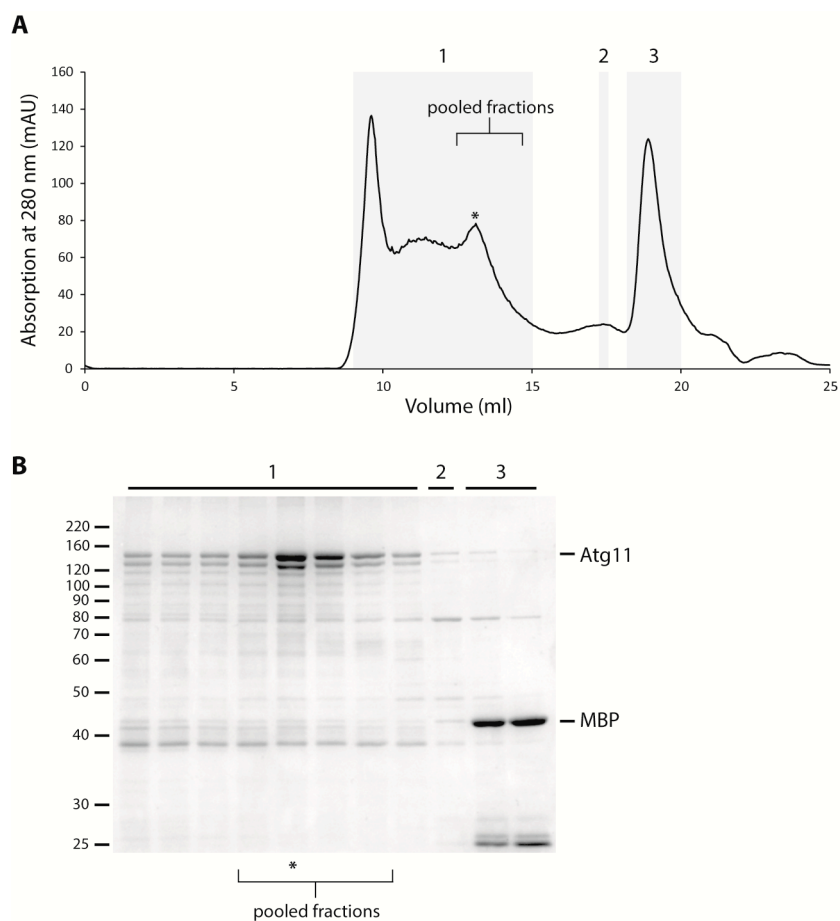


**Figure 7: Size exclusion chromatography of Atg11.** (A) Chromatogram of the gelfiltration on a Superose 6 Increase column showing the absorption at 280 nm. (B) Samples of elution fractions were analyzed by SDS-PAGE.

### 3.1.2 Purification of other Atg proteins

#### 3.1.2.1 *Atg11* variants

Atg11<sup>ΔC</sup> (residues 1-667) lacks the C-terminal domain comprising coiled-coil domains CC3 and CC4. It was expressed in *E. coli* BL21 from the pCoofy37 plasmid with a cleavable N-terminal MBP-tag and a C-terminal His<sub>6</sub>-tag. The fusion protein was bound to a Ni-NTA resin and the MBP-tag was cleaved off after imidazole elution (Figure 8A, SDS-PAGE, first lane). The sample was further purified on a Superdex 200 16/60 size exclusion column to remove aggregates and smaller impurities including the MBP tag. Atg11<sup>ΔC</sup> eluted at 62 ml (grey area 2). Another impurity of about 65 kDa could not be separated from the Atg11<sup>ΔC</sup> construct, which is most likely a N-terminally truncated degradation product as already observed for full-length Atg11. By comparison with the elution volumes of different globular proteins (aldolase has a molecular weight of 158 kDa and elutes at a volume of 65 ml; product

information by GE Life Sciences) the molecular weight of Atg11<sup>ΔC</sup> is estimated to be about 200 kDa. This suggests that Atg11<sup>ΔC</sup> has an elongated shape as expected for full-length Atg11 and/or that this variant is forming dimers. The possible dimerization is consistent with analytical ultracentrifugation experiments conducted by Dr. Nena Matscheko. These showed an increase of the sedimentation coefficient at higher protein concentration in the sample, indicating the formation of oligomers.

Atg11<sup>Δdim</sup> (residues 1-456) is a N-terminal fragment of Atg11 that only contains coiled-coil domain CC1. Thus, it lacks the coiled-coil domains reported to be required for Atg11 self-interaction (Yorimitsu and Klionsky, 2005). Atg11<sup>Δdim</sup> was expressed and purified as

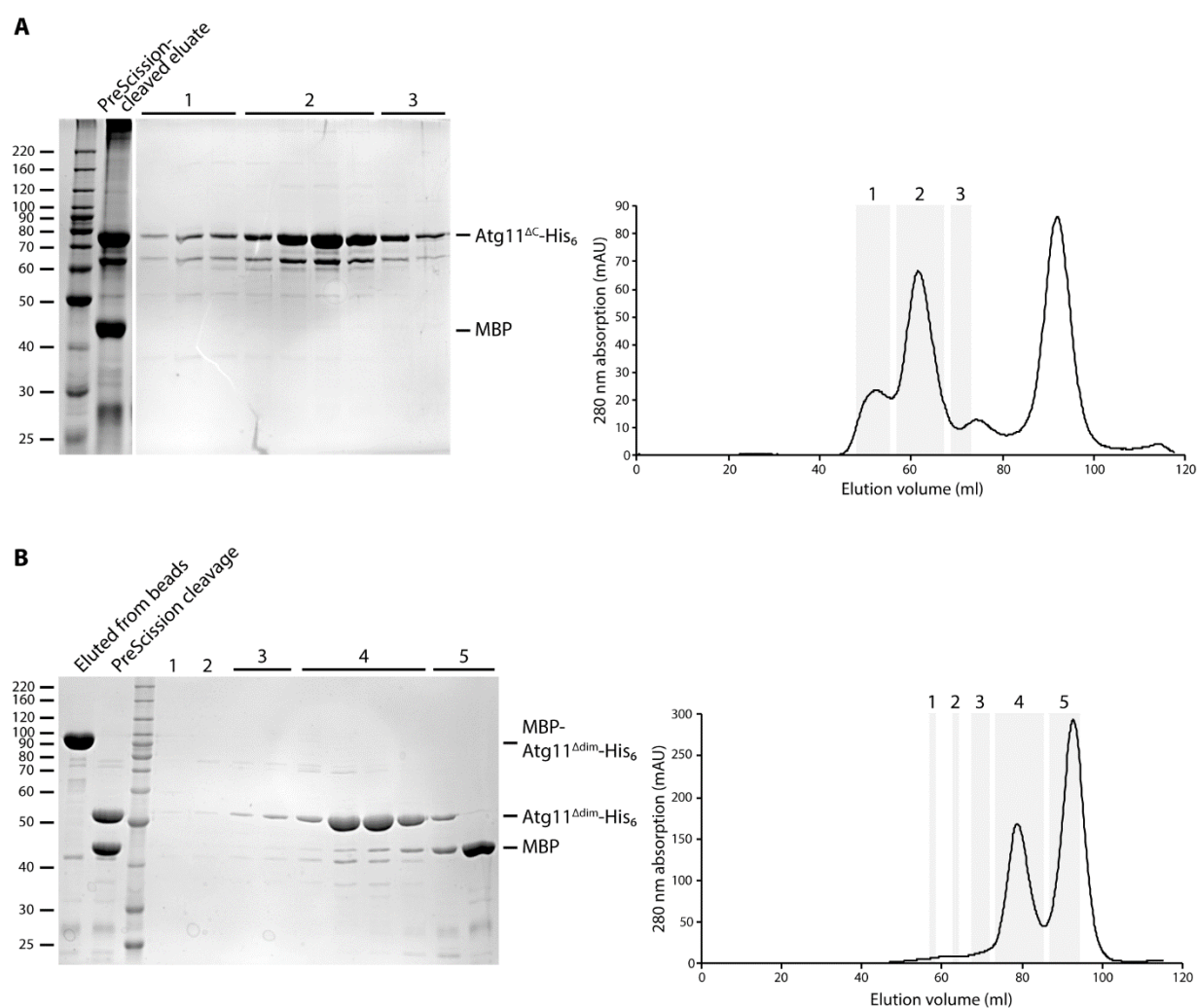


**Figure 8: Purification of Atg11 variants.** MBP-Atg11<sup>ΔC</sup>-His<sub>6</sub> (A) and MBP-Atg11<sup>Δdim</sup>-His<sub>6</sub> (B) were bound to Ni-NTA resin, the MBP-tag was cleaved after elution and the sample was applied to a Superdex 200 size exclusion column. Gelfiltration profiles (280 nm absorption) are shown on the right, Coomassie-stained acrylamide gels of gelfiltration samples are shown on the left.

described for Atg11<sup>ΔC</sup>. Purification using Ni-NTA resin already achieved a high purity (Figure 8B, SDS-PAGE lane 1). The MBP-tag was cleaved using PreScission protease and removed via size exclusion chromatography on a Superdex 200 16/60 column alongside other impurities. Atg11<sup>Δdim</sup> eluted at 78 ml (grey box 4). This elution volume corresponds to a globular protein of about 60 kDa, which is close to the molecular weight of Atg11<sup>Δdim</sup> of 53 kDa. This strongly indicates that Atg11<sup>Δdim</sup> is a monomer in solution. As for full-length Atg11 and Atg11<sup>ΔC</sup>, but only to a small percentage, a N-terminally truncated contamination of 10 kDa difference co-eluted with Atg11<sup>Δdim</sup> from the column.

### 3.1.2.2 *Components of the trimeric complex*

Atg17, Atg31-Atg29 and the Atg17-Atg31-Atg29 trimeric complex were expressed from a pST39a polycistronic vector and purified according to an established protocol (Rao et al., 2016). Atg17 was purified via a His-Trap column. The N-terminal His<sub>6</sub>-tag was cleaved off by PreScission protease treatment and Atg17 was separated from remaining impurities on a Superdex 200 size exclusion column with a peak elution volume of 64 ml (Figure 9A). The Atg31-Atg29 subcomplex was bound to Ni-NTA resin via an N-terminal His<sub>6</sub>-tag on Atg29. The tag was cleaved off by PreScission protease treatment and the sample was separated on a Superdex 200 16/60 size exclusion column (Figure 9B). The complex eluted at 72 ml but was partly overlapping with the elution volume of a larger contamination of about 70 kDa and a contamination of about 35 kDa that could be a truncated version of Atg31. Therefore, only fractions from 66 ml to 73 ml elution volume were collected.

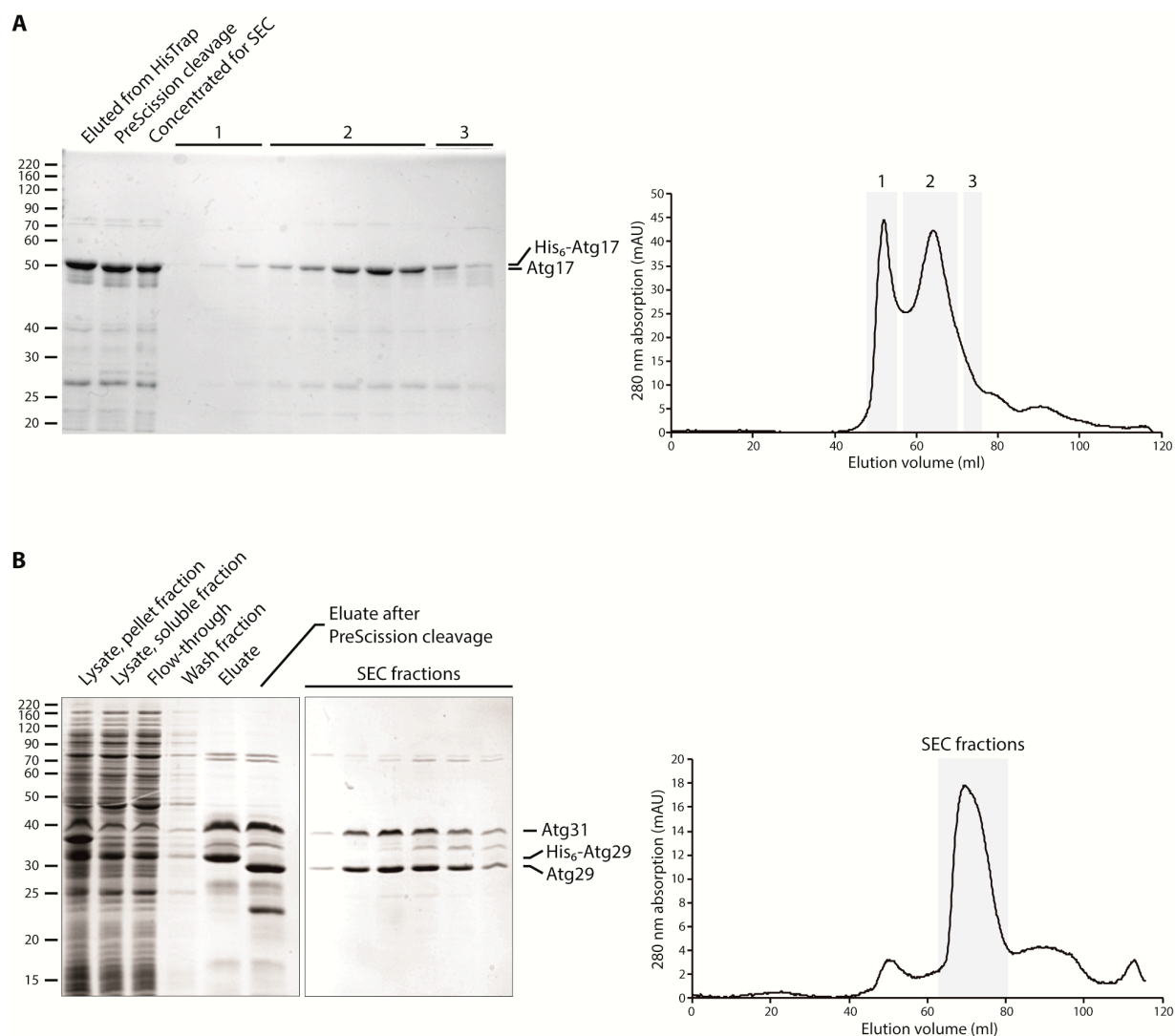


**Figure 9: Purification of trimeric complex subunits.** His<sub>6</sub>-Atg17 (A) and His<sub>6</sub>-Atg29-Atg31 (B) were bound to a HisTrap column or Ni-NTA beads, respectively. The His-tag was cleaved after elution by PreScission protease and the sample was applied to a Superdex 200 size exclusion column. Gelfiltration profiles (280 nm absorption) are shown on the right, Coomassie-stained acrylamide gels of gelfiltration samples are shown on the left.

### 3.1.2.3 *Atg32<sup>SE</sup>*

Atg32 was purified as a C-terminally truncated protein (Atg32<sup>1-376</sup>) lacking the transmembrane and intramitochondrial domain. Additionally, serine 114 was mutated to a glutamate (Atg32<sup>SE</sup>) to obtain a phosphomimetic variant resembling active Atg32 (Aoki et al., 2011). Atg32<sup>SE</sup> was expressed in *E. coli* from a pCoofy1 plasmid with a N-terminal His<sub>6</sub>-tag cleavable via a PreScission site. The protein was purified by affinity chromatography using a

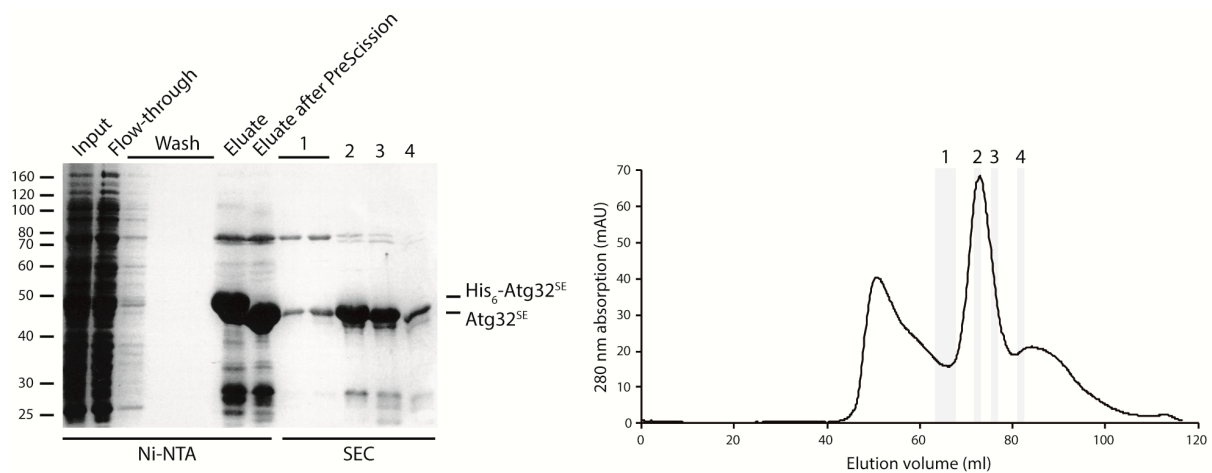


**Figure 10: Purification of Atg32<sup>SE</sup>.** His<sub>6</sub>-Atg32<sup>SE</sup> was bound to Ni-NTA beads, eluted with high imidazole concentration and separated on a Superdex 200 size exclusion column. Gelfiltration profiles (280 nm absorption) are shown on the right, Coomassie-stained acrylamide gels of protein samples are shown on the left.

Ni-NTA resin. After cleaving the tag the sample was further purified by size exclusion chromatography. Atg32<sup>SE</sup> eluted at a volume of 75 ml from a Superdex 200 16/60 gelfiltration column Figure 10.

#### 3.1.2.4 Atg9

For in vitro experiments a truncated version of Atg9 was used, termed Atg9<sup>core</sup> (Rao et al., 2016). The Atg9<sup>core</sup> was expressed in *E. coli* and purified from the membrane fraction via a C-terminal His<sub>6</sub>-tag (Figure 11). The supernatant after low-speed centrifugation of the cell lysate (S24) was applied to ultracentrifugation to collect the membrane fraction (P140). The membrane pellet was solubilized in presence of detergent and Atg9<sup>core</sup> was purified by affinity chromatography using a HisTrap column. The protein was then further purified by size exclusion chromatography. Even though there is no Atg9 band visible in the elution fraction on the acrylamide gel, UV absorption indicated a high protein concentration of the sample. Generally, it could be observed that Atg9 bands were hardly visible in samples from HisTrap elution fractions. This was probably due to the KCl and imidazole in the buffer, as strong bands were seen in samples of gelfiltration samples where KCl was replaced by NaCl (lanes 1-5). Monomeric Atg9 eluted at 72 ml from a Superdex 200 16/60 gelfiltration column. However, as seen in the SDS-PAGE image the majority of Atg9 was in an oligomeric or aggregated state and eluted close to the void volume.

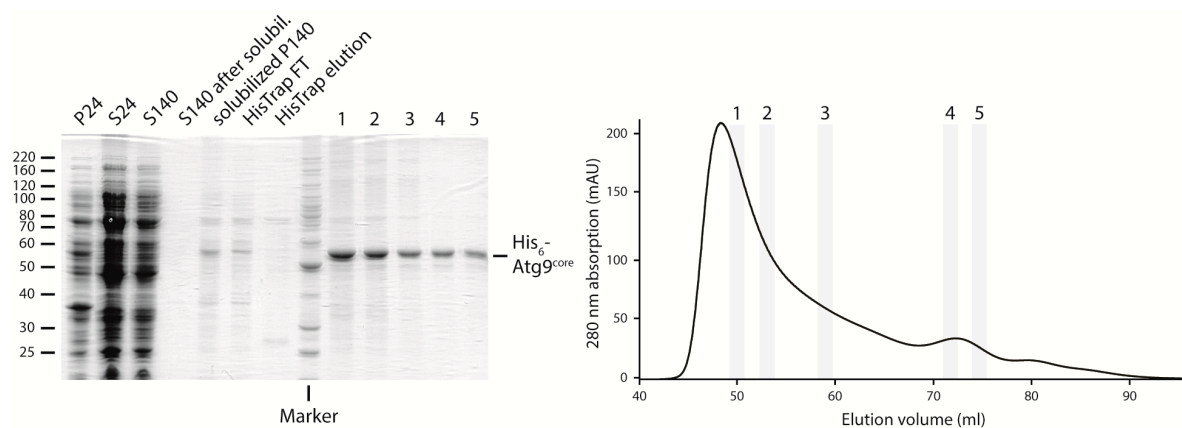


**Figure 11: Purification of Atg9<sup>core</sup>.** His<sub>6</sub>-Atg9<sup>core</sup> was purified from the solubilized membrane fraction (P140). In a first step the protein was purified by affinity chromatography using a HisTrap column followed by size exclusion chromatography on a Superdex 200 column. Gelfiltration profiles (280 nm absorption) are shown on the right, Coomassie-stained acrylamide gels of protein samples are shown on the left.

### 3.1.2.5 *Atg13*

Atg13 was expressed with a N-terminal MBP-tag for better solubility and a C-terminal His<sub>6</sub>-tag, both of them cleavable. Purification was performed basically as described (Rao et al., 2016). The fusion protein was bound to a HisTrap, eluted with high imidazole and the tags were cleaved off. Due to poor separation from contaminations on a size exclusion column, the sample was bound to a HiTrap anion exchange column. Atg13 was eluted in a 125 mM to 260 mM NaCl gradient over 50 ml (Figure 12). Peak fractions were pooled and concentrated by binding to a HiTrap anion exchange column followed by a step elution with 300 mM NaCl.

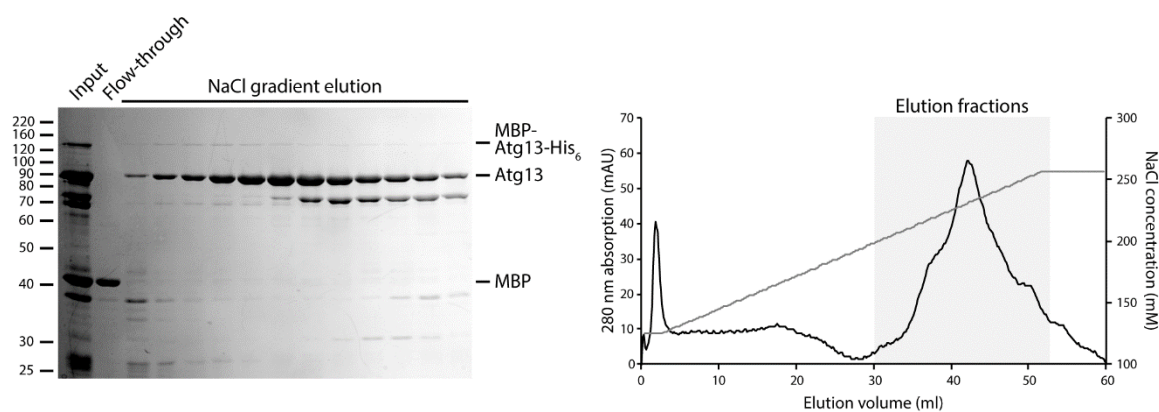


**Figure 12: Purification of Atg13.** Anion exchange chromatography of Atg13 was performed as a second purification step after HisTrap purification. A NaCl gradient from 125 mM to 260 mM was applied to elute Atg13. The anion exchange and profile (280 nm absorption) is shown on the right, the Coomassie-stained acrylamide gel of protein samples is shown on the left.

### 3.1.2.6 *Atg1*

*Atg1* was expressed using baculovirus infection of insect cells (HighFive) due to the improved expression and protein folding. *Atg1* was purified basically as described, with a N-terminal MBP-tag and a C-terminal His<sub>6</sub>-tag (Rao et al., 2016). The initial method of choice was to induce expression by adding a frozen stock of baculovirus infected insect cells (BIICs) to the cell culture (Wasilko et al., 2009). However, this was not suitable for *Atg1* as the prolonged storage of BIICs resulted in a strong decrease of *Atg1* expression. In order to maintain a high yield the virus had to be used for *Atg1* expression immediately after virus production. As the virus degraded quickly after harvesting, the time required to perform a virus titer determination would have been enough to decrease the expression of *Atg1*. Therefore, a protocol was used that does not rely on measuring the virus titer and that allowed to directly add the freshly produced virus stock to the expression culture (Fitzgerald et al., 2006). This way, high yield (around 1 mg protein / liter) and purity were achieved. *Atg1* was purified by affinity chromatography using a HisTrap column. Both N- and C-terminal tags were cleaved off. The sample was then further separated by gelfiltration and it eluted at a volume of 64 ml from a Superdex 200 16/60 size exclusion column (Figure 13).

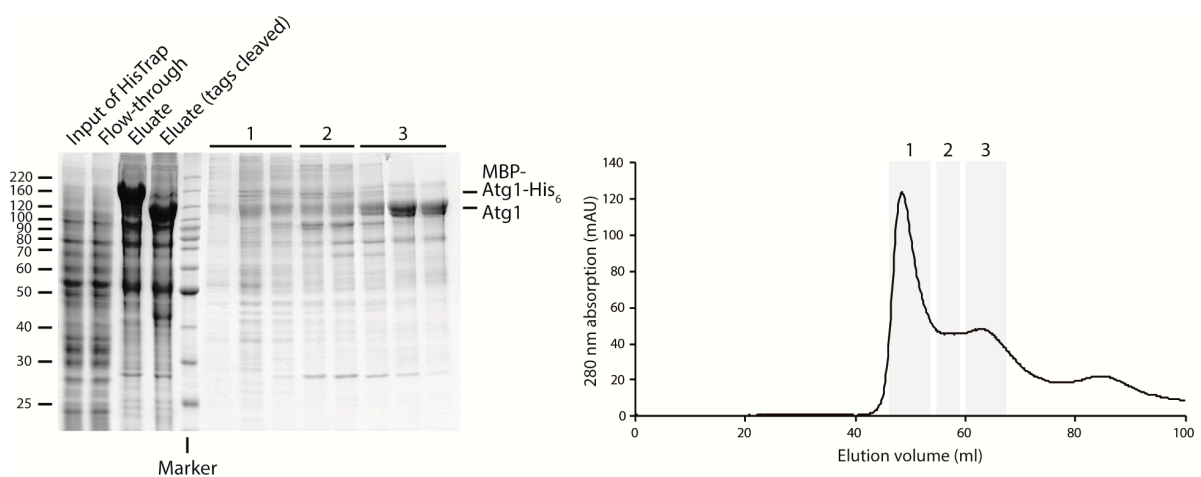


**Figure 13: Purification of *Atg1*.** *Atg1* was purified on a HisTrap followed by cleavage of the tags and separation on a Superdex 200 16/60 size exclusion column. The gelfiltration profile (280 nm absorption) is shown on the right, the Coomassie-stained acrylamide gel of protein samples is shown on the left.

### 3.2 In vitro analysis of Atg11-Atg32 interaction

Atg32 is the mitochondrial cargo receptor that is integrated into the outer mitochondrial membrane. In vivo studies, based on co-immunoprecipitation and yeast two-hybrid assays, suggested that Atg11 directly interacts with Atg32 when the latter is phosphorylated on serine 114 (Aoki et al., 2011). To confirm that both proteins indeed physically interact, the binding of purified recombinant proteins was investigated.

#### 3.2.1 Requirement of Atg9 for interaction of Atg11 with Atg32

It was not possible to identify the formation of an Atg11-Atg32 complex in solution by size exclusion chromatography. To test, whether the recruitment of the proteins to a membrane facilitates their interaction, floatation assays with Atg9 proteoliposomes were performed. For this, the Atg9<sup>core</sup> was reconstituted into synthetic liposomes to obtain Atg9 proteoliposomes. During ultracentrifugation in a Histodenz gradient these liposomes move to an area of lower density together with bound proteins while unbound proteins stay at the bottom of the tube (the experimental setup is illustrated in Figure 14).

Figure 15 shows a floatation assay performed to evaluate the binding of full-length Atg11, Atg11<sup>ΔC</sup> and Atg11<sup>Δdim</sup> to Atg9 proteoliposomes in presence and absence of Atg32<sup>SE</sup>. All three Atg11 variants were co-floating with Atg9 proteoliposomes which confirms direct interaction with Atg9 independently of Atg32. Although Atg11 coiled-coil domains CC1 and CC2 were reported to be required for interaction with Atg9 (Chang et al., 2006), Atg11<sup>Δdim</sup>, which lacks CC2, was sufficient to bind Atg9 in vitro. For Atg32 some binding to Atg9 proteoliposomes was observed even in absence of other factors. A similar amount of Atg32 was co-floating in

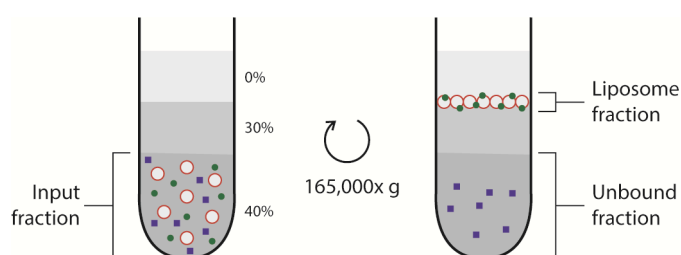


**Figure 14: Illustration of a floatation assay.** Left: Liposomes (red-white circles) are mixed with proteins (green and blue) as well as Histodenz to 40% final concentration at the bottom of a tube (input fraction). A layer each of 30% Histodenz and buffer is put on top. Right: After ultracentrifugation, liposomes float at the 30%/0% interface together with the bound proteins while unbound proteins remain in the bottom fraction.

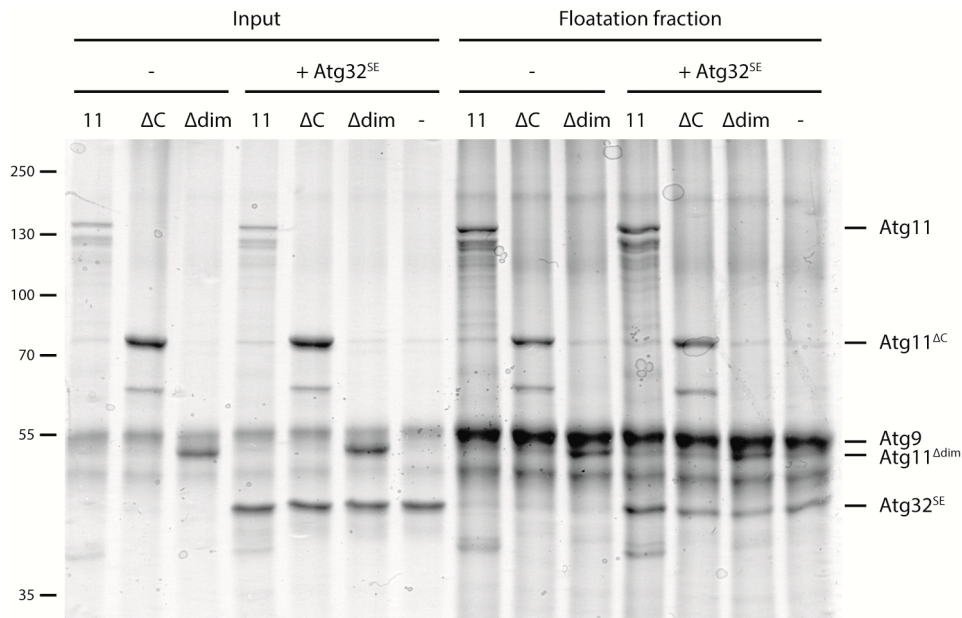


**Figure 15: Interaction of Atg11 variants and Atg32 with Atg9 proteoliposomes.** Binding was assessed by floatation and subsequent SDS-PAGE of liposome fractions. All Atg11 variants interact with Atg9 proteoliposomes independently of Atg32. Atg32 itself shows some binding to Atg9 proteoliposomes (last lane) but the amount of bound protein was increased in presence of full-length Atg11.

presence of both truncated Atg11 variants. However, in presence of full-length Atg11 a stronger binding of Atg32 was observed, consistent with previous studies that claim a direct interaction of Atg32 with the C-terminal domain of Atg11 (Aoki et al., 2011).

Interestingly, an *in vivo* co-immunoprecipitation experiment conducted by Dr. Nena Matscheko showed decreased levels of Atg9 co-precipitating with Atg11<sup>ΔC</sup> and Atg11<sup>Δdim</sup> compared to full-length Atg11 (data not shown). While all variants were co-floating with Atg9 proteoliposomes *in vitro*, the interaction with Atg32 might be required *in vivo* for efficient recruitment of Atg11 to the autophagic cargo.

### 3.2.2 Atg32-dependent dimerization of Atg11

Atg11 was reported to self-interact via its coiled-coil domains CC2 and CC3 (Yorimitsu and Klionsky, 2005). When recombinant Atg11 was analyzed by analytical ultracentrifugation by Dr. Nena Matscheko and Stefan Uebel (MPIB core facility), its sedimentation coefficient was independent of protein concentration. This suggested that Atg11 is present as a monomer in solution. In contrast, Atg11<sup>ΔC</sup> showed a concentration-dependent sedimentation coefficient, which is typical for an oligomer. As Atg32 interacts with the C-terminal domain of Atg11, it was reasoned that the cargo receptor might induce dimerization or oligomerization of Atg11.

To test this hypothesis crosslinking was used, in order to identify specific complexes by SDS-PAGE.

As Atg11<sup>ΔC</sup> was observed to oligomerize in solution it was used to establish crosslinking conditions. As shown on the SDS-PAGE depicted in Figure 16, a distinct band of 150 kDa appeared under all tested conditions. This corresponds to double the molecular weight of Atg11<sup>ΔC</sup> (77 kDa) indicating the specific formation of an Atg11<sup>ΔC</sup> dimer. In addition, larger structures could be observed in the acrylamide gel that correspond to oligomers and aggregates. However, these might be artifacts due to excessive crosslinking by glutaraldehyde. Considering the elution volume of Atg11<sup>ΔC</sup> from the size exclusion column (see paragraph 3.1.2.1), these results suggest that Atg11<sup>ΔC</sup> forms dimers in solution.

Next, crosslinking was performed with full-length Atg11 in presence and absence of Atg32<sup>SE</sup>. Furthermore, a mix of Atg11, Atg32<sup>SE</sup> and Atg9 proteoliposomes was treated with glutaraldehyde due to the Atg11-Atg32 interaction observed by floatation. However, incubation with glutaraldehyde either had no effect at lower concentrations or led to the extensive formation of aggregates, but not a distinct complex, at higher concentrations (Figure 17).

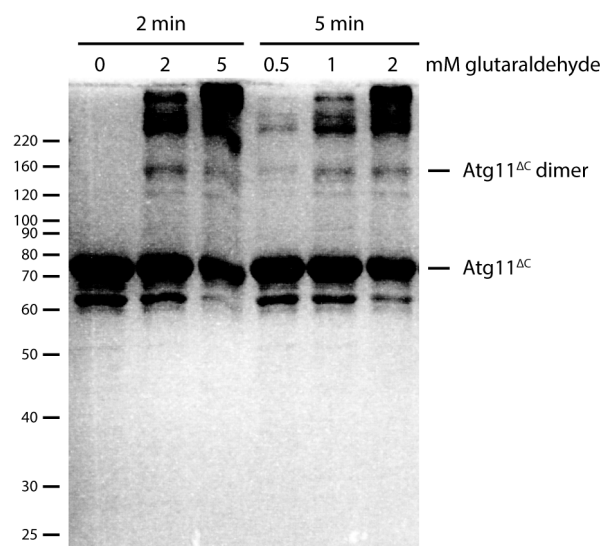


**Figure 16: Crosslinking of Atg11<sup>ΔC</sup>.** Purified Atg11<sup>ΔC</sup> (molecular weight of 77 kDa) was mixed with glutaraldehyde in different concentrations for two different incubation times and analyzed by SDS-PAGE and Coomassie staining. Besides larger crosslinked complexes at the top of the gel there was a distinct band of about 150 kDa corresponding to an Atg11<sup>ΔC</sup> dimer. Thus, truncation of Atg11 results in dimerization without the requirement for additional factors.

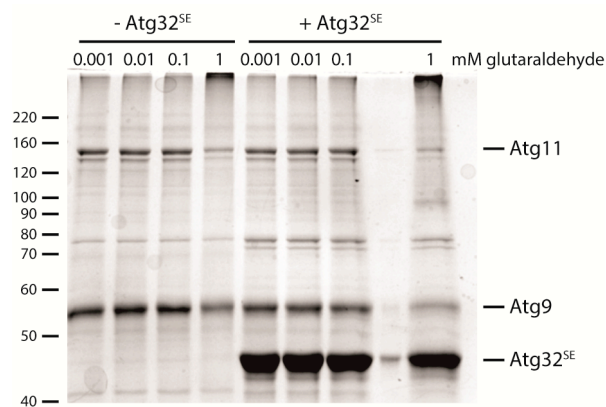


**Figure 17: Glutaraldehyde crosslinking of full-length Atg11.** Atg11 was incubated with Atg9 proteoliposomes and mixed with different concentrations of glutaraldehyde in presence or absence of Atg32<sup>SE</sup>. Samples were analyzed by SDS-PAGE and Coomassie staining.

Therefore, another crosslinker, Sulfo-LC-SDA, was used. This compound is a heterobifunctional crosslinker. The N-hydroxysuccinimide (NHS) ester group reacts with primary amines while the diazirine group, upon induction by UV light, reacts with any amino acid side chain or the peptide backbone. Upon incubation with one specific protein, unreacted crosslinker was removed before addition of other proteins, followed by exposure to UV light. Thus, this system allows a better control as crosslinking events are restricted to the vicinity of a specific protein. First, the initial crosslinking step was carried out with Atg11 before Atg32<sup>SE</sup> was added. However, only the formation of aggregates but no distinct complex was observed. This was likely due to the tendency of Atg11 to form aggregates in solution. To overcome this problem, the crosslinker was first added to Atg32<sup>SE</sup> and crosslinking was induced in presence of unlabeled Atg11. Indeed, a distinct band could be observed upon UV exposure of the mixture but not for Atg11 or Atg32<sup>SE</sup> alone, indicating specific complex formation between Atg32 and Atg11 (Figure 18A). The samples of the cross-linked complex were re-applied to a 7% acrylamide gel for better resolution in the high molecular weight region (Figure 18B). Besides confirming the presence of a prominent complex band upon UV light exposure, a weaker band of lower molecular weight was detectable as well. This might correspond to a complex with a different subunit combination. To estimate the possible complex compositions, the approximate size of the complex was calculated from the running distance in the acrylamide gel. The running distance of the marker bands was used to fit a logarithmic trendline (Figure 19). This gave a calculated mass of 340 kDa for the stronger band and 294 kDa for the weaker band (compare Table 6). Table 6 further lists the theoretical masses of possible Atg11-Atg32 complexes. The estimated size of the larger complex roughly corresponds to two Atg11 and two Atg32<sup>SE</sup> molecules. This suggests that Atg32<sup>SE</sup> indeed induces the dimerization of Atg11.

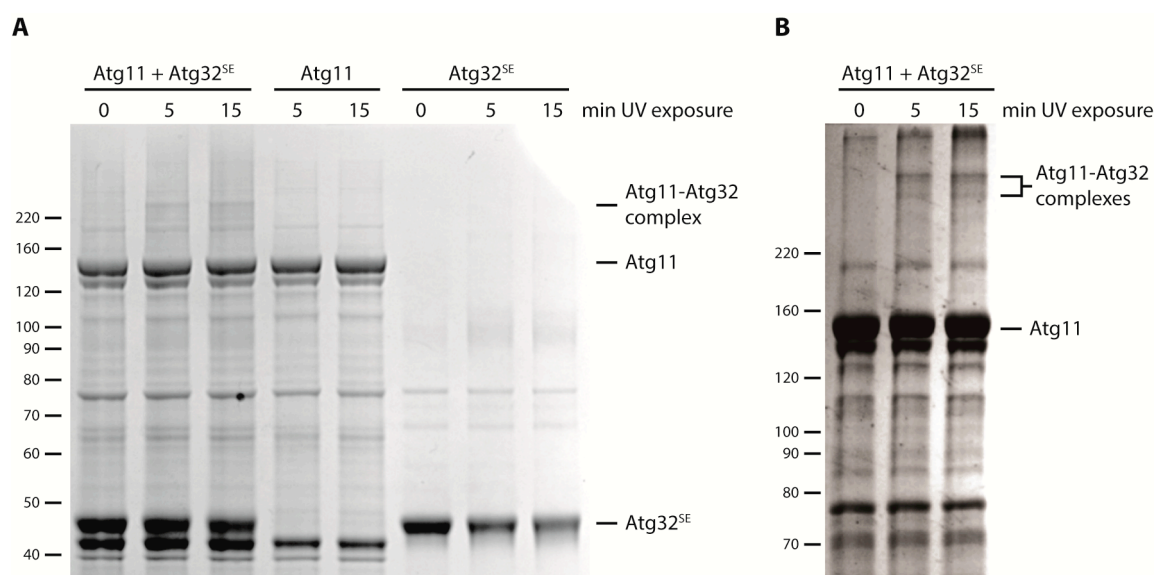


**Figure 18: Crosslinking of Atg11 and Atg32.** (A) Atg32<sup>SE</sup> was labelled with LC-SDA before incubation with Atg11. Samples were exposed to UV light for up to 15 min. Specific bands emerged after UV exposure of a mix of both protein. Crosslinked and control samples were run on a pre-cast 4-12% Bis-Tris gradient gel. (B) Crosslinked samples from Fig. B were run on a 7% acrylamide gel for better separation in the high molecular weight region, revealing a second, weaker complex band. The gel was used for the size estimation of the cross-linked complexes (Figure 19 and Table 6).

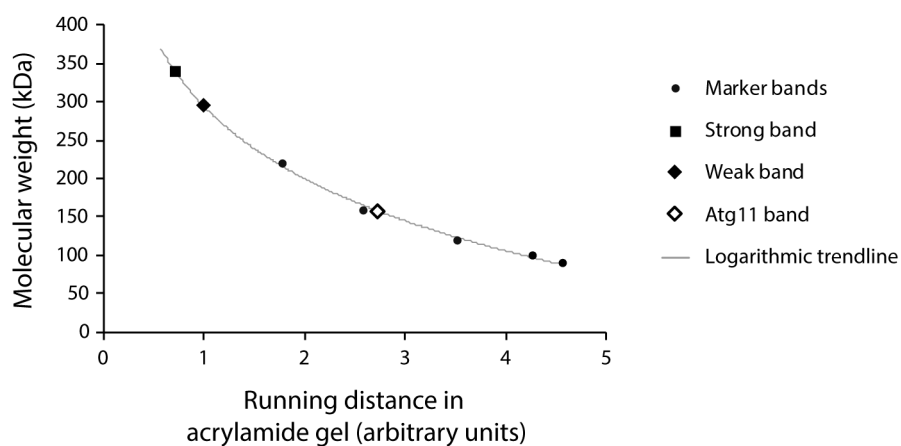


**Figure 19: Size estimation of crosslinked complexes.** A logarithmic trendline was fitted to the running distance of the marker bands (circles). This was used to calculate the molecular weight of the crosslinked complexes visible as a strong and a weak band (square and diamond, respectively) in Figure 18B. Values are given in Table 6.

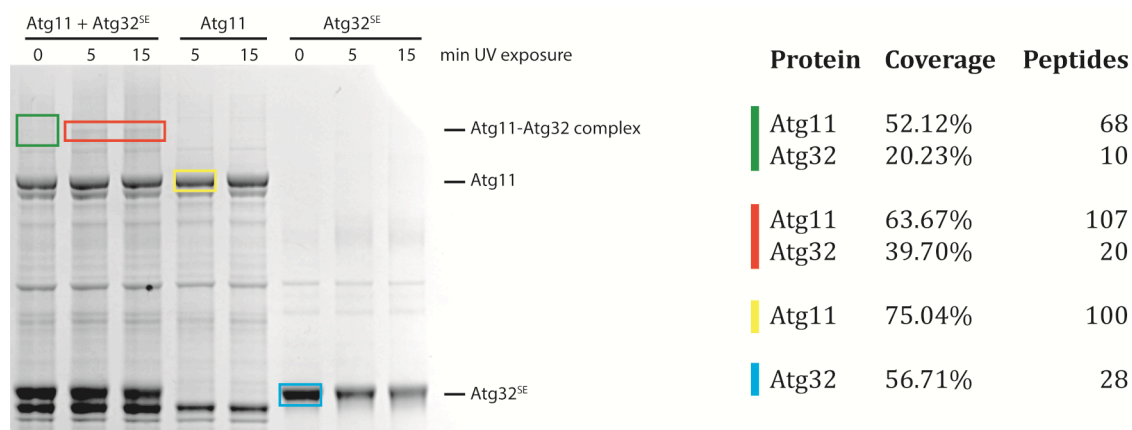
**Table 6: Size estimation of crosslinked complexes.** The molecular weight of the crosslinked complexes was calculated from the running distance as shown in Figure 19. The complex most likely contains an Atg11 dimer with either one or two Atg32 molecules.

<b>Sample</b>	<b>Calculated mass</b>
Strong band	340 kDa
Weak band	294 kDa
Atg11 band	152 kDa

<b>Complex combinations</b>	<b>Theoretical mass</b>
Atg11	135 kDa
Atg32	42 kDa
Atg11 + Atg32	177 kDa
Atg11 + 2x Atg32	219 kDa
2x Atg11 + Atg32	312 kDa
2x Atg11 + 2x Atg32	354 kDa

To further verify that the crosslinked complex contained both, Atg11 and Atg32<sup>SE</sup>, mass spectrometry was performed. Bands were cut out from the acrylamide gel as indicated by colored boxes in Figure 20. Proteins were digested, extracted from the gel and analyzed by mass spectrometry. The measurement and the data analysis were carried out by Christian Malosse and Julia Chamot-Rooke at the UTechS MSBio core facility at Institut Pasteur. The number of peptides corresponding to Atg11 and Atg32 as well as the sequence coverage are indicated in Figure 20. As expected, only Atg11 (yellow) or Atg32 (blue) were identified in the single protein controls. In the sample of the protein band emerging after crosslinking (red) both proteins were detectable, indicating that they indeed are forming a complex. The sample taken prior to UV light exposure served a negative control (green box) but Atg11 and Atg32 were detectable as well. This might be due to contaminations or crosslinking events that happened without additional activation by UV light. However, the number of peptides of Atg11 and Atg32 was significantly higher after UV exposure, confirming they both participate in complex formation.



**Figure 20: Results of mass spectrometry analysis of crosslinking experiment.** Proteins were extracted from gel slices. Bands from the gel already shown in Figure 18A were cut out (as indicated by colored boxes) and analyzed by mass spectrometry. The number of peptides for both, Atg11 and Atg32, was increased upon UV exposure (red box) as compared to the unexposed sample (green box). This confirms that the cross-linked species contains Atg11 and Atg32.

### 3.2.3 Atg11 dimerization leads to tethering of Atg9 proteoliposomes

Atg11 is a monomer in solution but dimerizes upon interaction with Atg32<sup>SE</sup>. Furthermore, Atg11 strongly binds to Atg9 proteoliposomes. This raised the question whether Atg11 can tether Atg9 proteoliposomes upon dimer formation, as observed for Atg17 homodimers. To test the effects of Atg11 on Atg9 proteoliposomes their hydrodynamic radius was measured by dynamic light scattering (DLS). This method had been used previously to investigate liposome tethering by Atg17 (Rao et al., 2016). Figure 21 shows the hydrodynamic radii of Atg9 proteoliposomes and protein-free SUVs in presence of the indicated proteins (measurements were conducted by Dr. Yijian Rao). SUVs had a hydrodynamic radius of approximately 50 to 60 nm, independently of the added proteins (black columns). In absence of any additional protein, Atg9 proteoliposomes tend to cluster. Due to this polydisperse solution it was not possible to measure the hydrodynamic radius (Figure 21A). The addition of the tether Atg17 resulted in a monodisperse signal with a hydrodynamic radius of about 130 nm. Thus, the tethering function of Atg17 leads to an approximately two-fold increase in the size of the liposomes. A similar result was obtained for Atg11<sup>ΔC</sup>, while in presence of full-length Atg11 the size of the Atg9 proteoliposomes was comparable to SUVs. As Atg11<sup>ΔC</sup> is, like Atg17, a constitutive dimer but full-length Atg11 is a monomer in solution, dimerization of Atg11 might be required for the increase in the hydrodynamic radius.

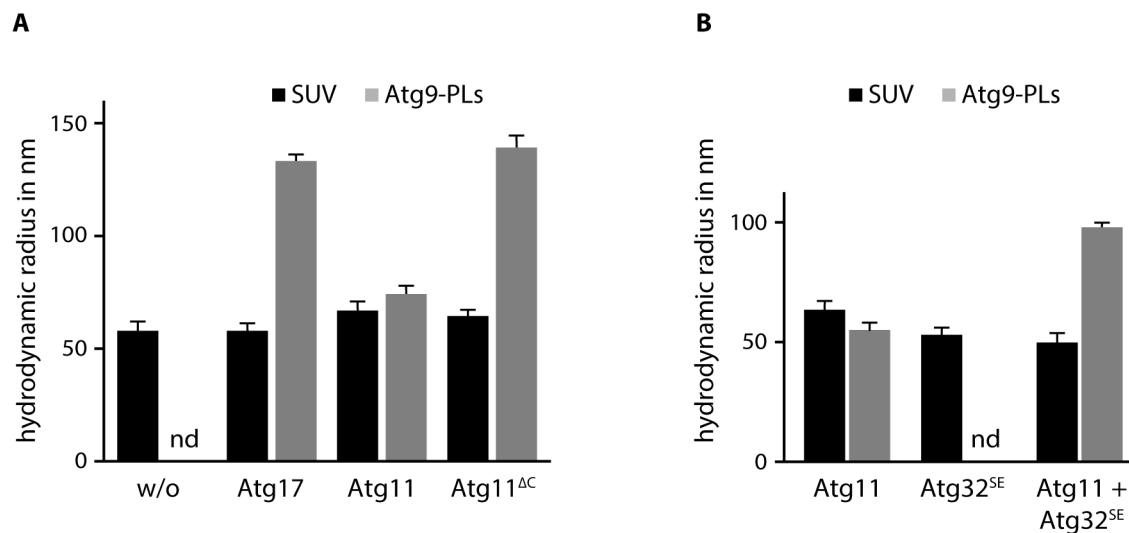


**Figure 21: Dynamic light scattering to determine tethering.** Atg9 proteoliposomes or protein-free liposomes were co-sonicated with the indicated proteins and their hydrodynamic radius was measured by DLS. (A) Full length Atg11 does not tether Atg9 proteoliposomes. However, the Atg11<sup>ΔC</sup> variant tethers vesicles in a similar fashion as Atg17. (B) Atg11 is able to tether Atg9 proteoliposomes when the cargo receptor Atg32 is present.

nd: In absence of a tethering factor Atg9 proteoliposome tend to cluster and no monodisperse signal is detectable. DLS measurements were conducted by Dr. Yijian Rao.

To test whether a similar effect can be achieved with an Atg11-Atg32 complex, Atg32<sup>SE</sup> was added to the sample (Figure 21B). Indeed, presence of Atg32<sup>SE</sup> significantly increased the hydrodynamic radius of Atg9 proteoliposomes as compared to Atg11 alone. This is in agreement with the observed induction of Atg11 dimerization by Atg32<sup>SE</sup>.

Even though the changes in radii resembled the observations made previously for Atg17-dependent tethering, other possible effects could not be ruled out. The increase in size could also be explained by fusion of the liposomes or the assembly of elongated Atg11 dimers on the liposomes. In order to identify the function of Atg11 dimers cryo-electron microscopy was performed. Figure 22 shows cryo-EM images of Atg9 proteoliposomes that were either incubated with Atg11 or with both, Atg11 and Atg32<sup>SE</sup>. When Atg32<sup>SE</sup> was present in the sample (right panel) tethering events could be observed that resulted in membrane deformation (indicated by white arrow heads). Membranes of adjacent liposomes were flattened and forming tight contacts of about 25 nm on average in size. This is remarkable, as such membrane deformations are energetically unfavorable and cannot be explained by unspecific effects. Furthermore, cryo-EM revealed that in each case the lipid bilayers were still separated and no fusion of the liposomes was induced. When only Atg11 was present in the sample, Atg9 proteoliposomes were mostly dispersed (left panel). While some of the liposomes came into close proximity to each other, no tight tethering could be observed.

Therefore, these results support the model that Atg11 specifically and tightly tethers Atg9 proteoliposomes upon its dimerization when activated by interaction with Atg32.

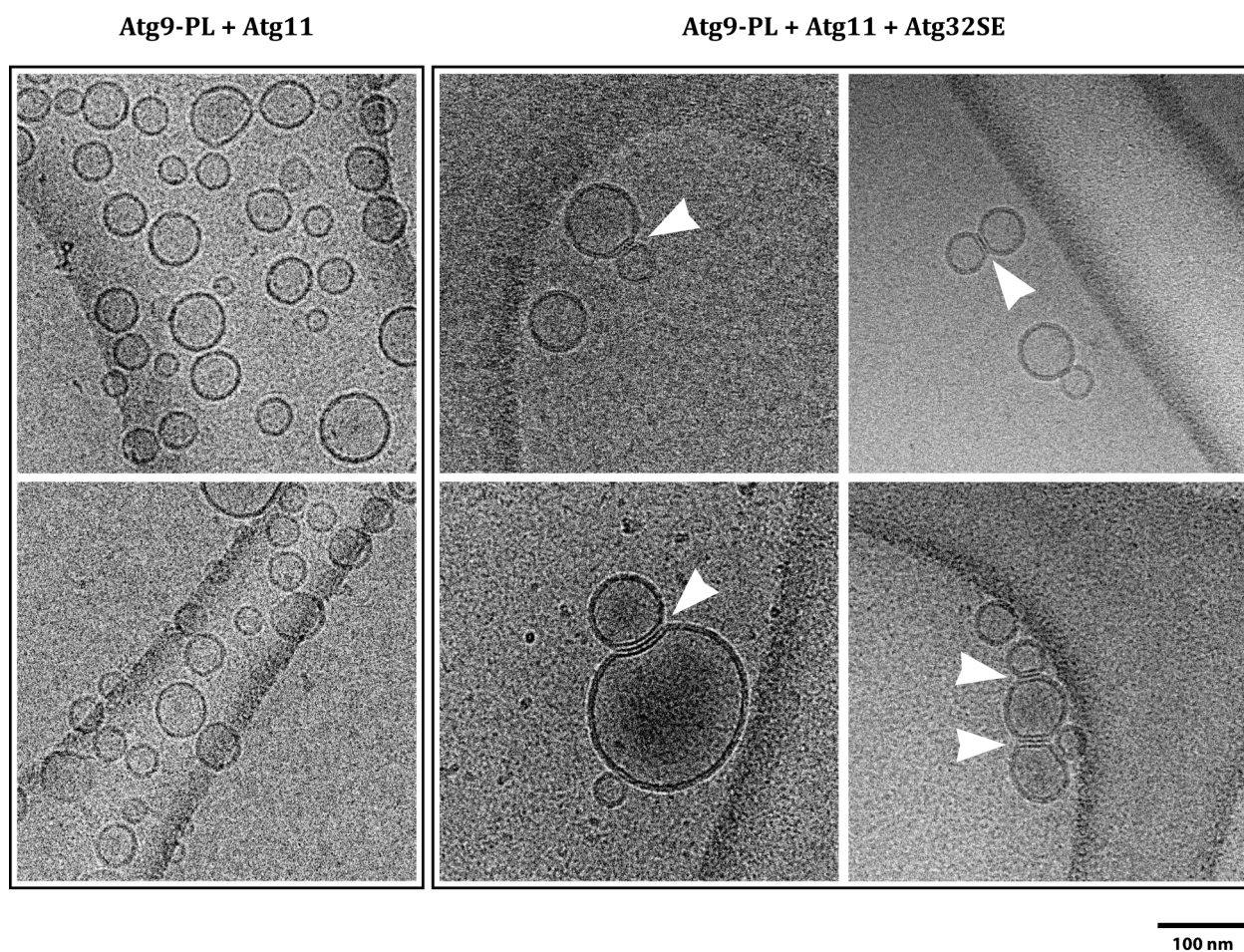


**Figure 22: Cryo-electron microscopy imaging of Atg9 proteoliposome tethering.** Atg9 proteoliposomes were co-sonicated with Atg11, frozen in liquid ethane and imaged by cryo-EM. Images show single liposomes without specific tethering events (left panel). However, in presence of Atg32<sup>SE</sup>, tethering of liposomes was observed (right panel). The resulting tethering was very tight leading to membrane deformation and the formation of large contact areas (marked with white arrow heads).

### 3.3 Atg11 and Atg17 compete for liposome binding

In vitro experiments confirmed that Atg11 as well as Atg17 bind to Atg9 proteoliposomes. Furthermore, both proteins share a similar mode of action by tethering these liposomes through dimer formation. However, it was unclear how their binding to Atg9 vesicles is influenced by each other. To address this question a floatation-based competition assay was established. Atg9 proteoliposomes were incubated with Atg11 followed by the addition of increasing amounts of Atg17 (from equimolar amounts to a 50-times excess). Protein binding was then assessed by a floatation assay and subsequent SDS-PAGE (see Figure 23A). For statistical analysis, the amount of protein co-floating with Atg9 proteoliposomes was determined from the measured band intensities and the known protein amounts in the “1:1” input sample (9 pmol Atg11, 14 pmol Atg9 and 9 pmol Atg17). To correct for different liposome concentrations in the floatation fractions, Atg11 and Atg17 amounts were corrected by the amount of Atg9 in each sample relative to the Atg9 amount in the “1:0” floatation fraction. The quantification result is presented in Figure 23B. When the same molar amount of both proteins was present in the input, the floatation fraction contained 16 pmol of Atg11 but only 3 pmol of Atg17 (sample “1:1”). This indicates a strong binding of Atg11 to Atg9 compared to Atg17. Atg17 amounts in the floatation fractions increased with the amount of Atg17 in the input (10 pmol co-floating Atg17 at a 50-times stoichiometric excess in the input). In contrast, Atg11 amounts declined to 7 pmol in the 1:50 sample. Still, a 25-fold excess of Atg17 was required to achieve binding of similar amounts of Atg11 and Atg17. Interestingly, the sum of the molar amounts of both proteins remained almost constant over all ratios tested, with an estimated Atg9 saturation of 65% (Figure 23C). This takes into account that only half of the Atg9 molecules are inserted correctly with the cytoplasmic side exposed to the buffer, while the others are inverted with the cytoplasmic side facing to the liposome lumen. The constant saturation suggests that Atg11 and Atg17 both compete for the same or at least overlapping Atg9 binding sites. The results further confirm the high affinity of Atg11 to Atg9 and the requirement for a high stoichiometric excess of Atg17 to replace Atg11. However, similar expression levels were reported for Atg11 and Atg17 in vivo (Kulak et al., 2014). Thus, under physiological conditions most Atg9 vesicles might be sequestered by Atg11. Upon starvation additional regulatory mechanisms would then be required to facilitate the replacement of Atg11 by Atg17.

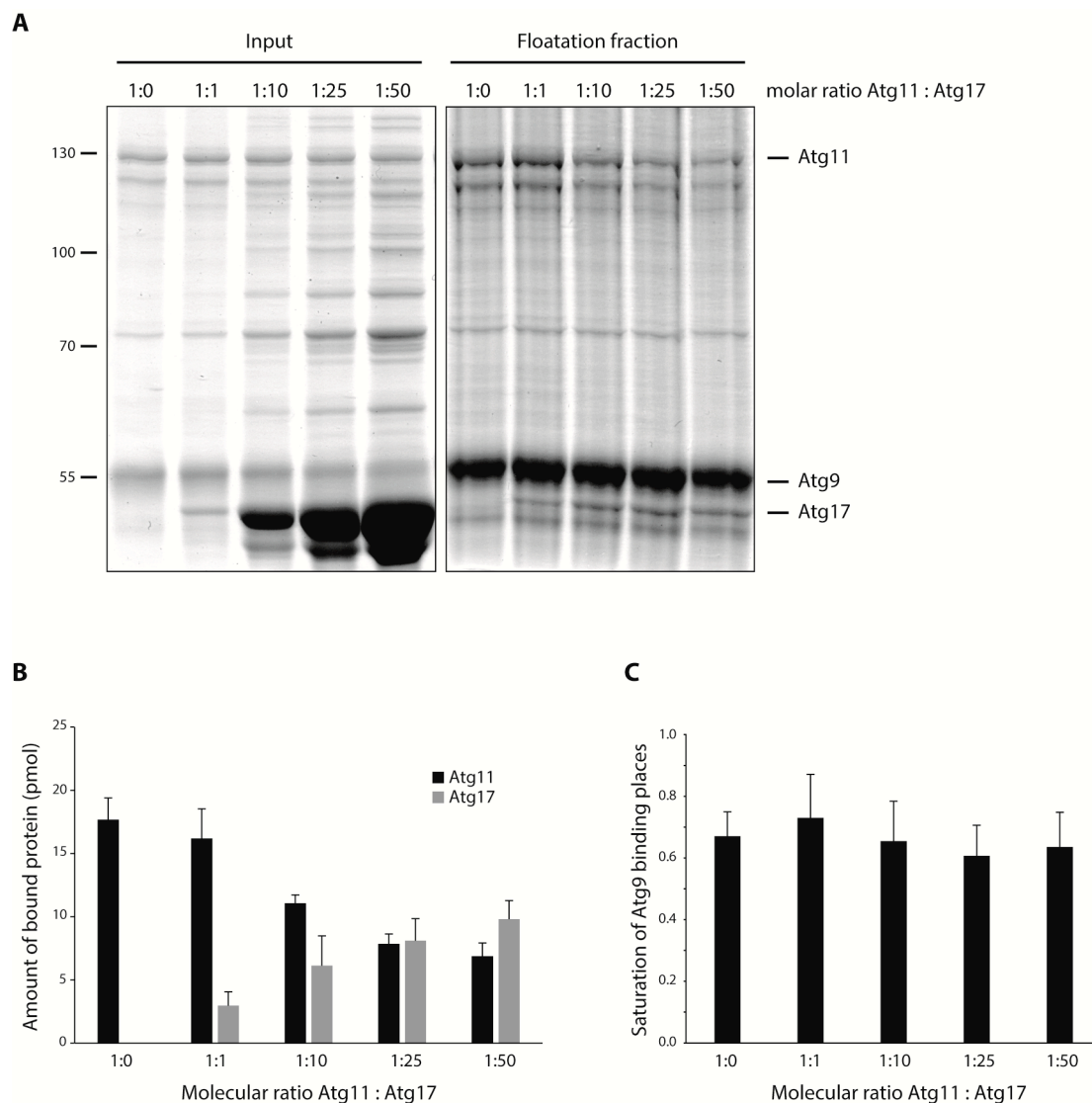


**Figure 23: Competition for Atg9 proteoliposome binding.** Atg11 bound to Atg9 proteoliposomes can be replaced by Atg17. (A) Coomassie-stained polyacrylamide gel showing the result of a floatation assay. Atg17 was added to Atg11-bound Atg9 proteoliposomes in up to 50-times molar excess. The liposome fractions after floatation showed increased binding of Atg17 with increased amounts in the input, while the amount of bound Atg11 was decreasing. (B) Molar amount of bound Atg11 (black) and Atg17 (grey) calculated from quantified band intensities. (C) The total amount of bound protein is independent of the amount of added Atg17. On average, Atg9 was saturated to 65% without significant changes between the different ratios.

### 3.4 The role of Atg29 phosphorylation in autophagy initiation

Atg29 was reported to be phosphorylated upon starvation by a yet uncharacterized kinase. Furthermore, Atg11 was demonstrated to co-immunoprecipitate with Atg29 from lysates of starved cells but not with an Atg29 mutant where all phosphorylation sites were changed to alanine (23STA). Atg29<sup>23STA</sup> also exhibited a significant decrease in autophagic flux, suggesting the requirement of interaction between Atg29 and Atg11 to initiate non-selective autophagy. The mutation of only three residues close to the C-terminus, serines 197, 199 and 201 (Atg29<sup>3SA</sup>), resulted in a higher autophagic activity yet less than a mutation of the 20 other residues (Atg29<sup>20STA</sup>). This indicated the importance of the C-terminal serines in autophagy (Mao et al., 2013). In order to avoid excessive modification of Atg29, only mutations of serines 197, 199 and 201 were considered in this thesis. These three residues were mutated to aspartate to generate a phosphomimetic mutant (Atg29<sup>SD</sup>). Under nutrient-rich conditions the co-localization of fluorescent labelled Atg17 and Atg9 in living yeast cells was significantly increased in presence of Atg29<sup>SD</sup> compared to wild-type Atg29 (experiment conducted by Dr. Nena Matscheko; data not shown). This indicated that phosphorylation of Atg29 might drive the recruitment of Atg17 to Atg9 vesicles. To further investigate the interactions between Atg9, Atg11 and subunits of the Atg1 kinase complex, these components were reconstituted *in vitro*.

#### 3.4.1 Differences in the stability of the Atg17<sup>TC</sup> and Atg17<sup>TC,SD</sup> complex

In order to purify the wild-type (Atg17-Atg31-Atg29 or Atg17<sup>TC</sup>) and mutant (Atg17-Atg31-Atg29<sup>SD</sup> or Atg17<sup>TC,SD</sup>) trimeric complexes for subsequent *in vitro* experiments, His-tagged Atg17 was co-expressed with Atg31 and wild-type or mutant Atg29. After affinity chromatography, Atg17<sup>TC</sup> eluted as a single peak from the size exclusion column, indicating the formation of a stable complex. However, for the mutant only Atg17 was recovered from the Ni-NTA resin while Atg31 and Atg29<sup>SD</sup> remained in the flow-through and the wash fractions. This indicates that the phosphorylation of Atg29 might have a direct effect on the stability of the trimeric complex. However, it does not influence the interaction with Atg31 as both, the wild-type and mutant Atg31-Atg29 complex, could be purified without any difference.

To further characterize the trimeric complex formation, Atg17 and Atg31-Atg29 or Atg31-Atg29<sup>SD</sup> were purified separately, reconstituted and purified by size exclusion chromatography on a Superdex 200 10/300 column. Under these conditions both, wild-type and mutant trimeric complex, formed and eluted at a volume of 14.7 ml (Figure 24A).

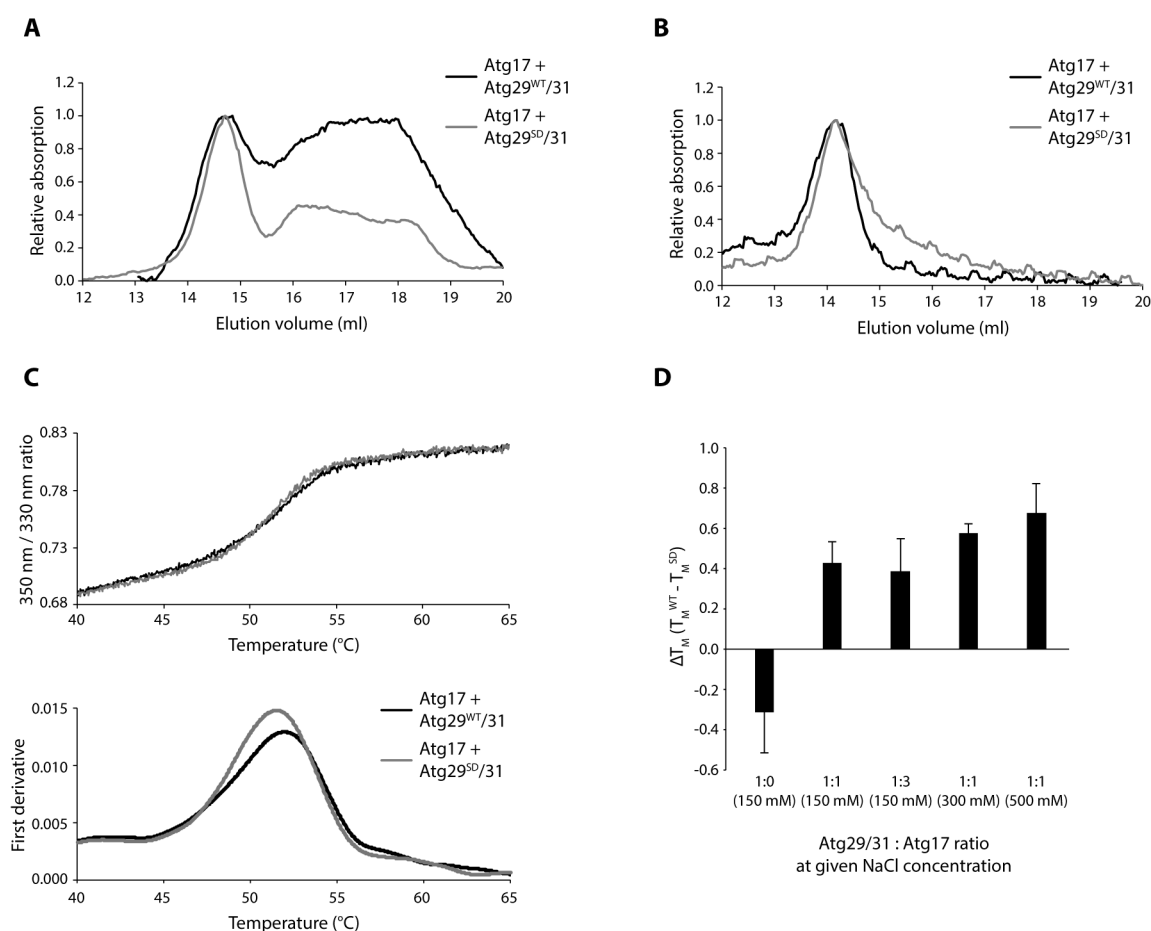


**Figure 24: Stability of the trimeric complex in respect to Atg29 phosphorylation.** (A) Size exclusion chromatography reveals that incubation of Atg17 with both, Atg31-Atg29 (black) and Atg31-Atg29<sup>SD</sup> (grey) results in incomplete complex formation. (B) The isolated complexes showed comparable stability when re-applied to SEC, independent of wild-type or mutant Atg29. (C) DSF measurement to determine the melting temperature. Atg17 was incubated with Atg31-Atg29 or Atg31-Atg29<sup>SD</sup> in a 1:1 molar ratio. Top: Intrinsic fluorescence given as 350 nm to 330 nm ratio. Bottom: First derivative of the fluorescence curve with the maximum giving the melting temperature. (D) The graph displays the difference in melting temperatures between wild-type and mutant ( $T_M^{WT} - T_M^{SD}$ ). The  $T_M$  of the wild-type trimeric complex was significantly higher for all protein ratios and salt concentrations tested compared to the mutant (second to fifth column). In contrast, without Atg17 the  $T_M$  of wild-type Atg31-Atg29 was lower than the mutant complex indicating a specific effect of the mutation on trimeric complex formation.

Moreover, complex formation was incomplete independently of the Atg29 variant as additionally elution of the subunits was observed. When the fractions containing the trimeric complex were re-applied to size exclusion chromatography no dissociation could be observed (Figure 24B). Thus, even though the conditions during co-expression or affinity chromatography disassembled Atg17<sup>TC,SD</sup>, Atg29<sup>SD</sup> is still able to form a trimeric complex. To test whether Atg29<sup>SD</sup> indeed destabilizes the trimeric complex the stability of Atg17<sup>TC</sup> and Atg17<sup>TC,SD</sup> were analyzed by differential scanning fluorimetry (DSF). This method uses the intrinsic tryptophan fluorescence of proteins that changes depending on the environment of

the amino acid. Thus, protein unfolding can be recorded as an increase in the ratio of 350 nm to 330 nm fluorescence. Figure 24C shows the fluorescence ratio for an equimolar mix of Atg17 with Atg31-Atg29 (black) or Atg31-Atg29<sup>SD</sup> (grey) at increasing temperatures (upper graph). The inflection point, determined from the maximum of the first derivative as shown in the lower graph, corresponds to the melting temperature and can be used as a measurement for complex stability. Indeed, the melting temperature was significantly lower in the presence of Atg29<sup>SD</sup>. This shift was observed at different salt concentrations and different ratios between Atg17 and Atg31-Atg29. As shown in Figure 24D, the melting temperature of the wild-type complex was between 0.4 and 0.7°C higher than the mutant complex. To exclude that this temperature difference was caused by a change in Atg29 stability due to the mutation, Atg31-Atg29 and Atg31-Atg29<sup>SD</sup> were tested in absence of Atg17. In contrast to the trimeric complex the melting temperature of Atg31-Atg29 was slightly decreased compared to Atg31-Atg29<sup>SD</sup> (Figure 24D). This suggests that the phosphomimetic mutation of Atg29 specifically influences the interaction of Atg17 with the Atg31-Atg29 subcomplex.

### 3.4.2 Atg29 phosphorylation has no effect on interaction with Atg9 or Atg11

In order to test the direct interactions of Atg29 and its phosphomimetic variant with Atg9 and Atg11 floatation assays were performed. Atg29 and Atg29<sup>SD</sup> were purified as subcomplexes with Atg31 to ensure their stability and solubility. SDS-PAGE of the floatation fractions showed binding of both subcomplexes to Atg9 proteoliposomes (Figure 25). This interaction was specific to Atg9 as no protein was co-floating with protein-free SUVs. Furthermore, the band intensities of Atg29 and Atg31 were comparable in both, the wild-type and mutant sample, indicating that interaction with Atg9 is independent of the phosphorylation state of Atg29. Next, Atg9 proteoliposomes were pre-incubated with Atg11 to test interaction of the subcomplexes with Atg11. However, while large amounts of Atg11 were recovered in the floatation fraction, there was no significant increase in Atg31-Atg29 and Atg31-Atg29<sup>SD</sup> compared to the Atg11-free samples. This suggests that there is no direct interaction of wild-type or mutant Atg29 with Atg11, at least when bound to Atg9 proteoliposomes. Interestingly, Atg11 in solution in absence of Atg9 proteoliposomes and Atg31 could be co-precipitated with GST-tagged Atg29 and Atg29<sup>SD</sup> (assay conducted by Dr. Yijian Rao; data not shown). However, even though interaction was observed in this experimental setup it was not influenced by the Atg29 mutation as well. Thus, the Atg29<sup>SD</sup> mutant is not sufficient to induce or increase interaction with Atg11.

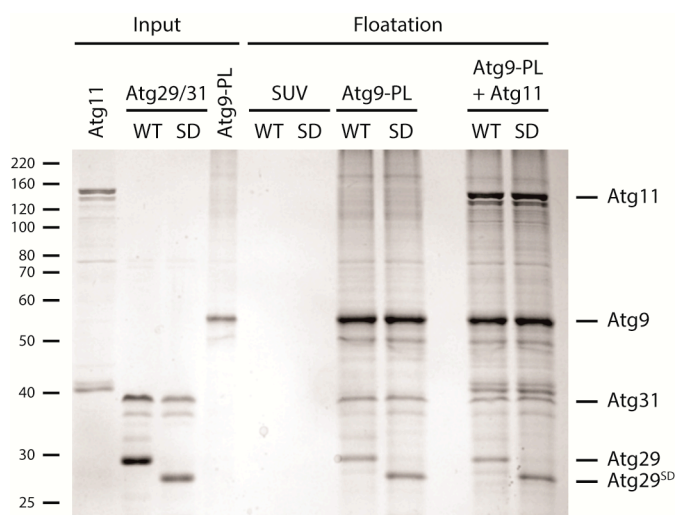


**Figure 25: Effects of Atg29 phosphorylation on protein-protein interactions.** Binding of Atg31-Atg29 was assessed by floatation assays followed by SDS-PAGE and Coomassie staining. Atg31-Atg29 as well as the phosphomimetic mutant (Atg31-Atg29<sup>SD</sup>) were incubated with protein-free SUVs or Atg9 proteoliposomes (Atg9-PL). There is specific binding to Atg9-PLs but not to SUVs; however, without significant difference between wildtype and mutant. While Atg11 bound strongly to Atg9-PLs (last two lanes) it did not increase recruitment of Atg31-Atg29.

### 3.4.3 Atg29 phosphorylation does not alter Atg17 binding to Atg9 proteoliposomes

The phosphomimetic mutation of Atg29 did not change the recruitment of the Atg31-Atg29 subcomplex to Atg9 proteoliposomes. However, Atg31-Atg29 forms a constitutive complex with Atg17 in vivo and the mutation decreased the stability of this complex in solution. Thus, floatation assays were used to investigate the binding of Atg17<sup>TC</sup> and Atg17<sup>TC,SD</sup> to Atg9 proteoliposomes and Atg11. The trimeric complexes were purified by incubation of Atg17 with Atg31-Atg29 or Atg31-Atg29<sup>SD</sup> followed by size exclusion chromatography. As shown in Figure 26 the amount of Atg17 recovered in the floatation fraction of the wild-type sample was significantly lower than that of Atg11. This is in agreement with the competition assay between Atg11 and Atg17 that confirmed a higher efficiency of Atg11 binding. However, the amount of co-floating Atg11 and Atg17 in presence of the Atg29<sup>SD</sup> mutant remained unchanged compared to the wild-type sample. This suggests that the phosphorylation of Atg29 does not directly influence the competition of Atg11 and Atg17 for Atg9 binding sites.

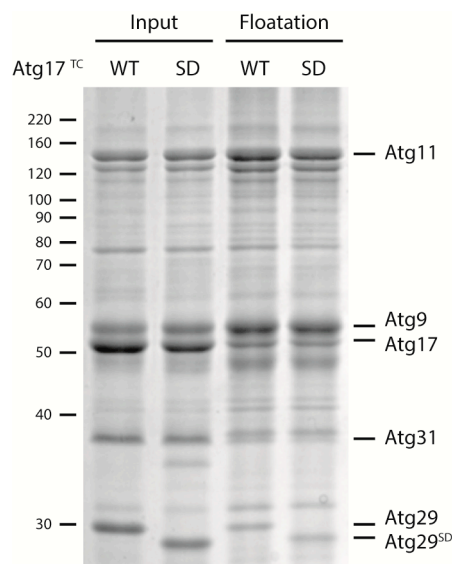


**Figure 26: Recruitment of the Atg17 trimeric complex to Atg9 proteoliposomes.** Coomassie-stained acrylamide gel of samples from floatation assay (input and liposome fraction after floatation). Atg11 binds strongly to Atg9 proteoliposomes compared to the Atg17 trimeric complex. Also, the phosphomimetic Atg29<sup>SD</sup> mutant did not influence the binding of the trimeric complex to Atg9 proteoliposomes.

### 3.4.4 Atg11 might increase recruitment of the Atg1 kinase complex in vitro

The constitutive Atg17 trimeric complex interacts with Atg1 and Atg13 upon starvation to form the fully active Atg1 kinase complex. Therefore, it was tested whether the starvation-induced phosphorylation of Atg29 impacts the recruitment of the Atg1 kinase complex to Atg9 proteoliposomes. Atg31-Atg29 or Atg31-Atg29<sup>SD</sup> were incubated with Atg17, Atg13 and Atg1 and the pentameric Atg1 kinase complexes (Atg1<sup>PC,WT</sup> or Atg1<sup>PC,SD</sup>) were purified by size exclusion chromatography. The complexes were incubated with Atg9 proteoliposomes in presence or absence of Atg11 and protein binding was assessed by floatation assays (Figure 27A). As observed previously for Atg17<sup>TC</sup> and the Atg31-Atg29 subcomplex, no improved binding of Atg1<sup>PC,SD</sup> was observed compared to wild-type Atg1<sup>PC</sup>. To better compare the effect of Atg11 on the recruitment of Atg1<sup>PC</sup> to Atg9 proteoliposomes the samples of the floatation fractions shown in Figure 27A were analyzed again by SDS-PAGE in a changed order (Figure 27B). While the Atg17 band could not be clearly separated from the Atg9 band, the band intensities of all other subunits of Atg1<sup>PC</sup> were slightly increased in presence of Atg11. This

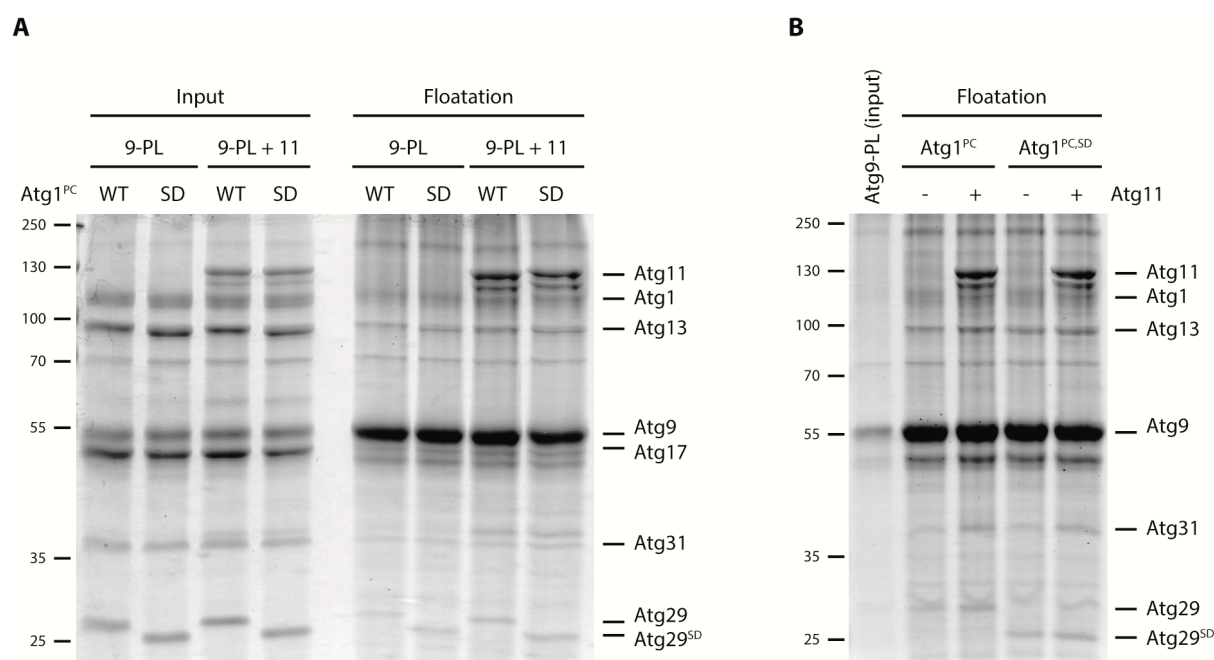


**Figure 27: Floatation assay to determine binding of the Atg1 kinase complex (Atg1<sup>PC</sup>) to Atg9 proteoliposomes.** (A) and (B) Coomassie-stained acrylamide gel of samples from input and liposome fractions after floatation. The pentameric complex containing either wild-type Atg29 (Atg1<sup>PC</sup>) or Atg29<sup>SD</sup> (Atg1<sup>PC,SD</sup>) was mixed with Atg9 proteoliposomes with or without Atg11. (B) Floatation samples from (A) were applied again to SDS-PAGE for better comparison between samples with and without Atg11. Atg11 might slightly increase the amount of bound protein while Atg29<sup>SD</sup> did not influence the recruitment of the complex.

effect has not been observed for Atg17<sup>TC</sup>, indicating that Atg1 or Atg13 might increase the recruitment of the Atg1 kinase complex in an Atg11-dependent manner. This is in agreement with a previous study suggesting a direct interaction of Atg1 with Atg11 (Mao et al., 2013). However, the observed effect was very small. Furthermore, under all tested conditions Atg11 bound more efficiently to Atg9 proteoliposomes than Atg17. Therefore, another mechanism has to exist that facilitates the binding of Atg17 and the replacement of Atg11 as a membrane tether.

### **3.4.5 Atg13 phosphorylation influences protein-protein interactions**

The TOR kinase phosphorylates Atg13 during nutrient-rich conditions but is deactivated upon starvation. The resulting dephosphorylation of Atg13 is required to induce the assembly of the Atg1 kinase complex and thus the activation of Atg17-dependent tethering of Atg9 vesicles (Rao et al., 2016). However, during nutrient-rich conditions Atg13 was reported to interact with Atg11 (Kamber et al., 2015). To test the recruitment of Atg13 by Atg11, floatation assays were performed. When incubated with Atg9 proteoliposomes in absence of other factors, very weak binding of unphosphorylated Atg13 was observed (Figure 28A). This binding was strongly enhanced in presence of Atg17<sup>TC</sup> and Atg11. This was expected and is consistent with previous studies that showed direct interaction of Atg13 with Atg17<sup>TC</sup> (Rao et al., 2016). However, Atg11 alone is not sufficient to increase the binding of Atg13 (Figure 28B). To test the possible recruitment of Atg13 by Atg11 during nutrient-rich conditions, Atg13 was phosphorylated *in vitro* by catalytic amounts of Atg1. As shown in Figure 28A, phosphorylated Atg13 migrated slower on an SDS-PAGE gel than unmodified Atg13. However, no phosphorylated Atg13 was recovered in the floatation fractions independently of other factors. As expected, Atg17<sup>TC</sup> is not sufficient to recruit Atg13 as complex formation requires Atg13 dephosphorylation. However, the absence of phosphorylated Atg13 in the floatation fraction even in presence of Atg11 indicates that there is likely no direct interaction between Atg11 and Atg13 during vegetative conditions.

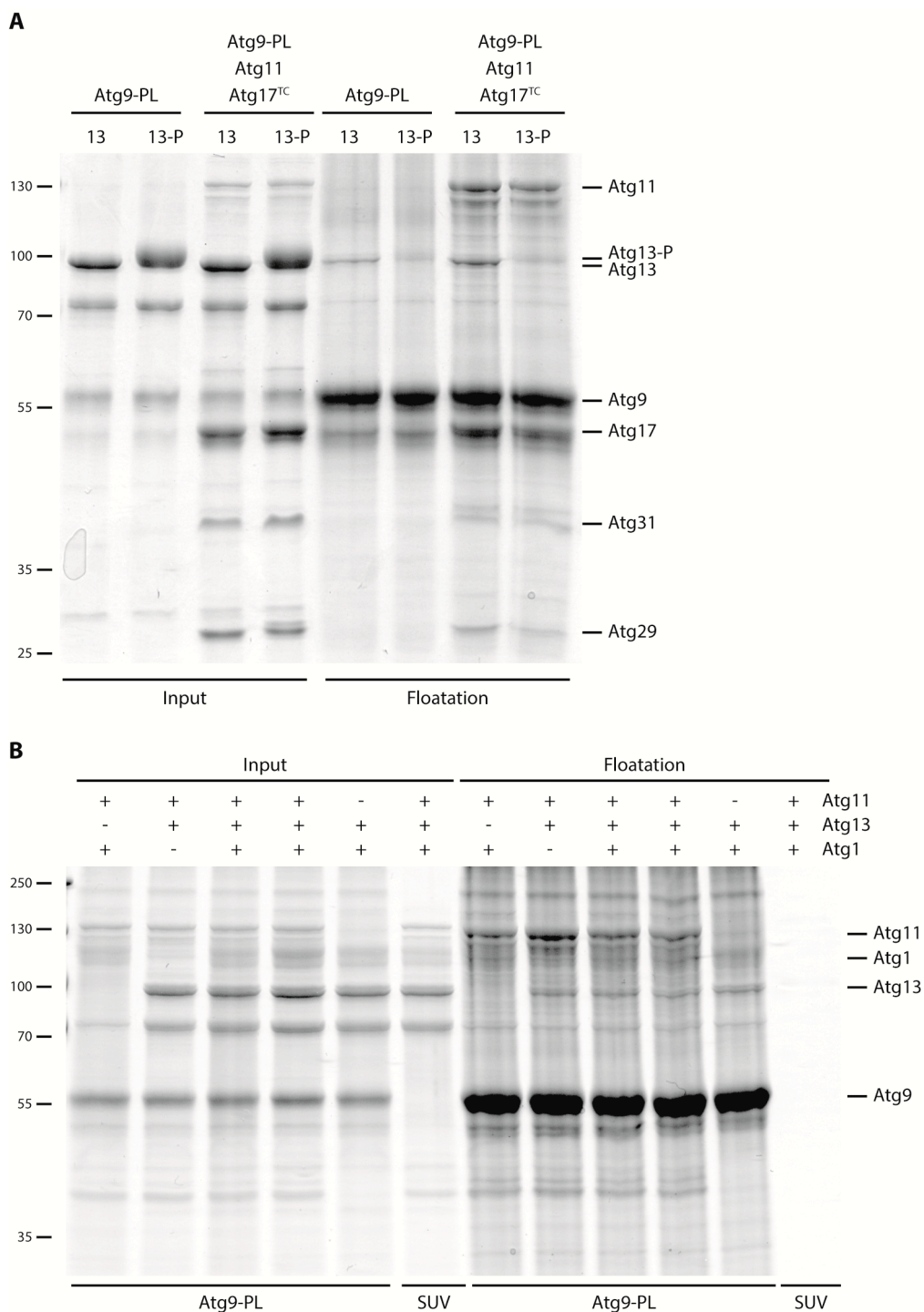


**Figure 28: Interaction of Atg13 with Atg9 proteoliposomes.** The binding of unphosphorylated and phosphorylated Atg13 to Atg9 proteoliposomes was assessed by floatation assays followed by SDS-PAGE and Coomassie staining. (A) Recruitment of unphosphorylated Atg13 to Atg9 proteoliposomes is increased in presence of Atg11 and Atg17<sup>TC</sup>. However, after phosphorylation of Atg13 (13-P), no recruitment was observed. (B) Control experiment that showed weak binding of Atg13 to Atg9 proteoliposomes but not to protein-free liposomes. Atg13 recruitment was not increased in presence of Atg11 or Atg1 and thus requires Atg17 for efficient binding.

### 3.5 Competition between Atg11 and Atg17 in vivo

Atg11 binds more efficiently to Atg9 proteoliposomes than Atg17 in vitro. This required a high stoichiometric excess of Atg17 to replace Atg11. However, similar levels of both proteins are present in the cell (Kulak et al., 2014). Interestingly, a consistent decrease of Atg11 levels had been observed in lysates of starved cells, suggesting its specific degradation upon induction of non-selective autophagy.

#### 3.5.1 Atg11 is degraded upon starvation

As non-selective autophagy degrades bulk cytoplasm, the observed decline in Atg11 levels could be caused by autophagy-dependent degradation. To test this possibility, HA-tagged Atg11 was expressed in wild-type and *atg7Δ* cells. Atg7 allows the initiation of autophagy but

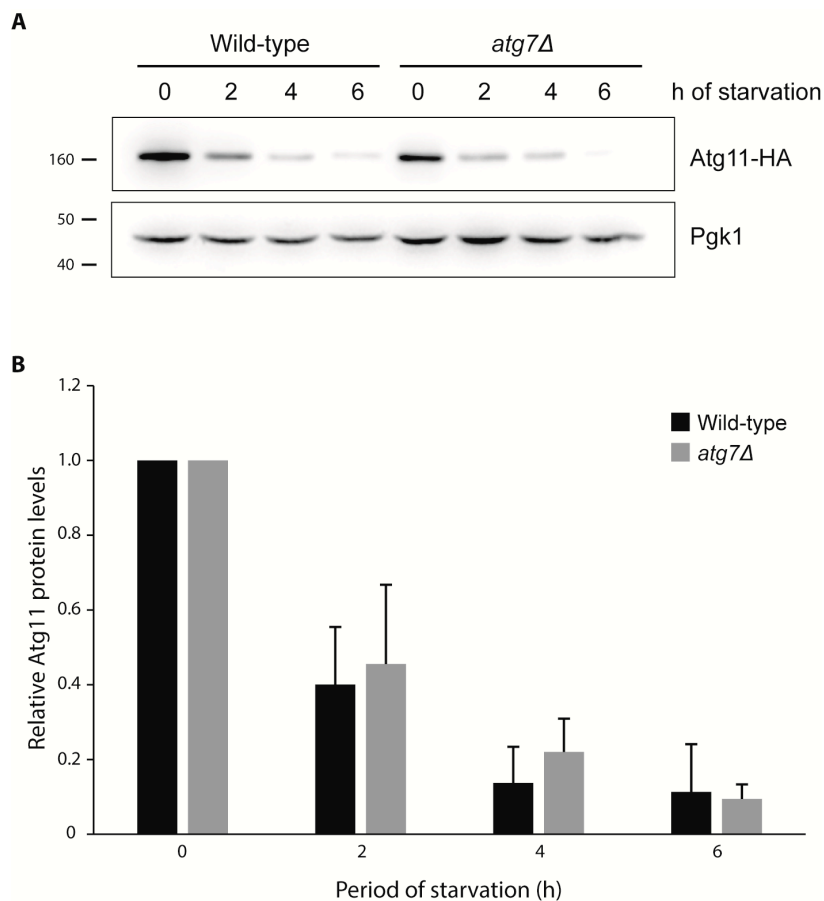


**Figure 29: Atg11 degradation upon starvation in vivo.** (A) Western blot of cell lysates of wild-type and *atg7Δ* cells expressing HA-tagged Atg11. Staining against the HA-tag showed a decrease of Atg11 protein levels in both cases. As an internal loading control, the blot was stained against Pgk1. (B) Band intensities from anti-HA blots of four independent experiments were quantified and normalized against Pgk1. The graph displays Atg11 levels relative to non-starved cells. There is no significant difference between wild-type and mutant background.

blocks the expansion of the phagophore. Atg11 levels were determined by Western blotting of lysates of starved and non-starved cells. As shown in Figure 29A, there was a strong decrease in band intensity in both, wild-type and *atg7Δ* cells. The band intensities from four independent experiments were quantified and normalized against the Pgc1 levels. Figure 29B shows the Atg11 levels relative to non-starved wild-type or mutant cells. In both cases, approximately 90% of Atg11 was degraded after 6 h of starvation and no significant difference between wild-type and *atg7Δ* cells could be observed. Thus, Atg11 is degraded upon starvation in an autophagy-independent manner. To further confirm that Atg11 is not transported to the vacuole for degradation, Atg11 levels in the *pep4Δ* strain were determined.

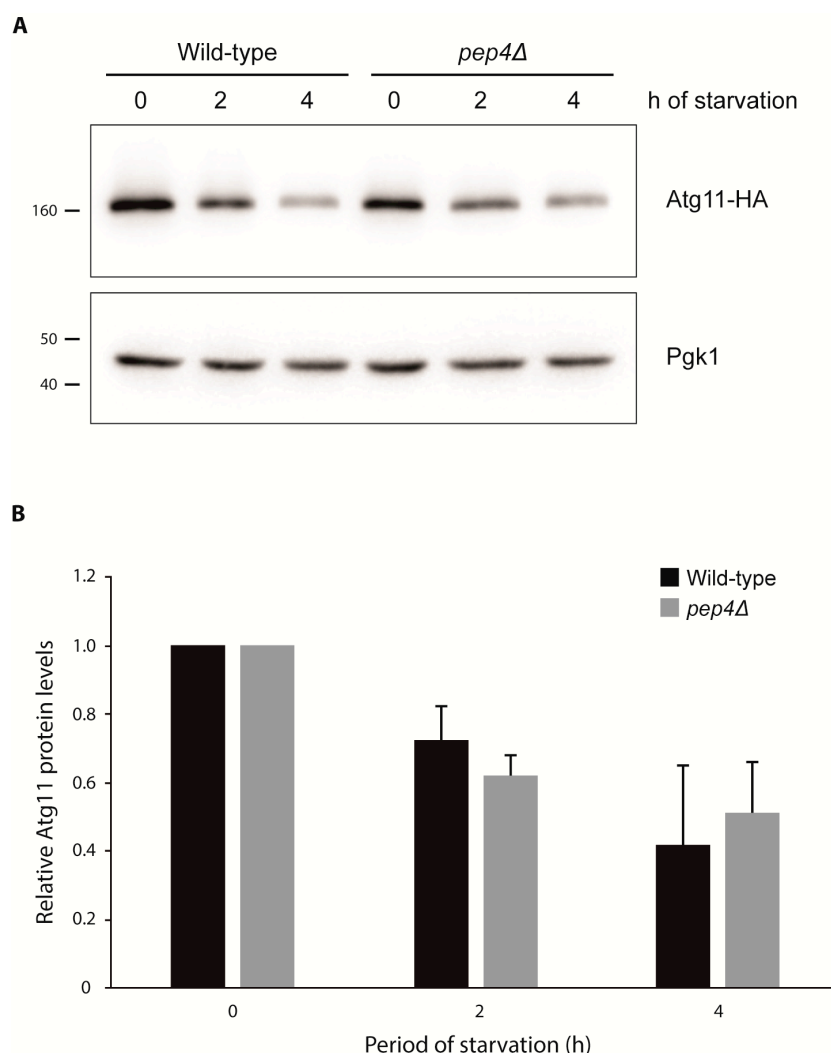


**Figure 30: Atg11 degradation in *pep4Δ* background.** (A) Western blot of cell lysates of wild-type and *pep4Δ* cells expressing HA-tagged Atg11. Staining against the HA-tag showed a decrease of Atg11 protein levels in both cases. As an internal loading control, the blot was stained against Pgc1. (B) Band intensities from anti-HA blots of four independent experiments were quantified and normalized against Pgc1. The graph displays Atg11 levels relative to non-starved cells without showing a significant difference between wild-type and mutant.

This mutant lacks the vacuolar protease Pep4 that is required for the maturation of other vacuolar hydrolases (Woolford et al., 1986). As shown in Figure 30A, Atg11 levels declined in both, wild-type and mutant cells. The quantification of band intensities confirmed that there was no significant difference between the two strains (Figure 30B). Thus, Atg11 is not degraded within the vacuole. To test whether the degradation is specific to Atg11, the protein levels of Atg17 during starvation were determined as well (Figure 31A). As shown in Figure 31B, Atg17 levels did not significantly decline during 6 h of starvation.

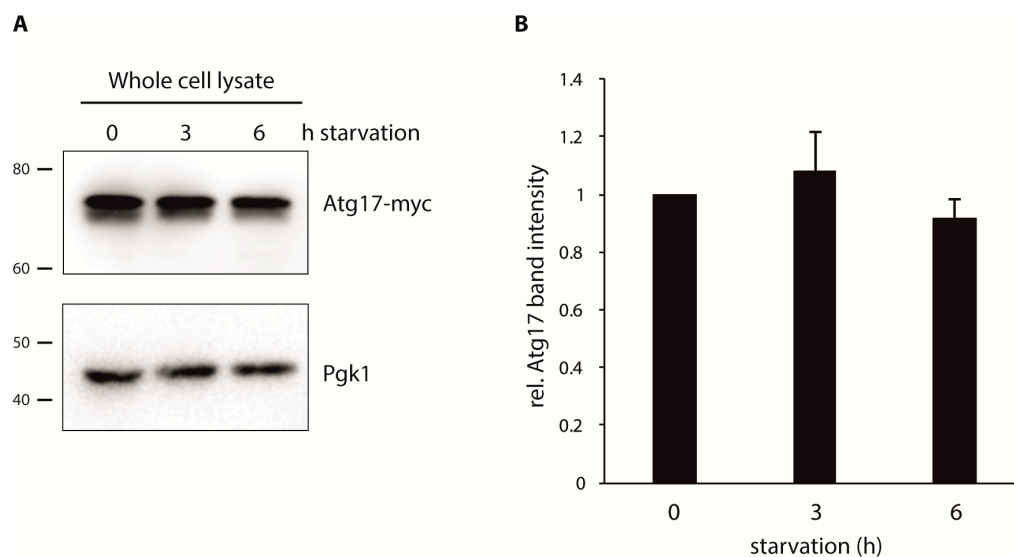


**Figure 31: Atg17 protein levels during starvation.** (A) Protein levels of myc-tagged Atg17 were assessed by Western blotting and anti-myc antibody staining. As a loading control, blots were stripped and stained with anti-pgk1 antibody. (B) Atg17 band intensities from three independent experiments were quantified and normalized against Pgk1 band intensities. The graph displays Atg17 levels relative to non-starved cells.

### 3.5.2 Proteasomal degradation of Atg11 during starvation

Atg11 degradation was found to be independent of autophagy and vacuolar proteases. Therefore, the observed decline in protein levels could be the result of degradation by the proteasome. To test this hypothesis, cells were treated with the selective proteasome inhibitor MG132 (Lee and Goldberg, 1996). To enhance the inhibitory effect, the intracellular concentration of this drug was increased by the deletion of the efflux pump Pdr5 (Fleming et al., 2002). As shown in Figure 32A, Atg11 degradation was blocked in cells treated with MG132 but not in presence of DMSO, which was used as a solvent for the drug and served as

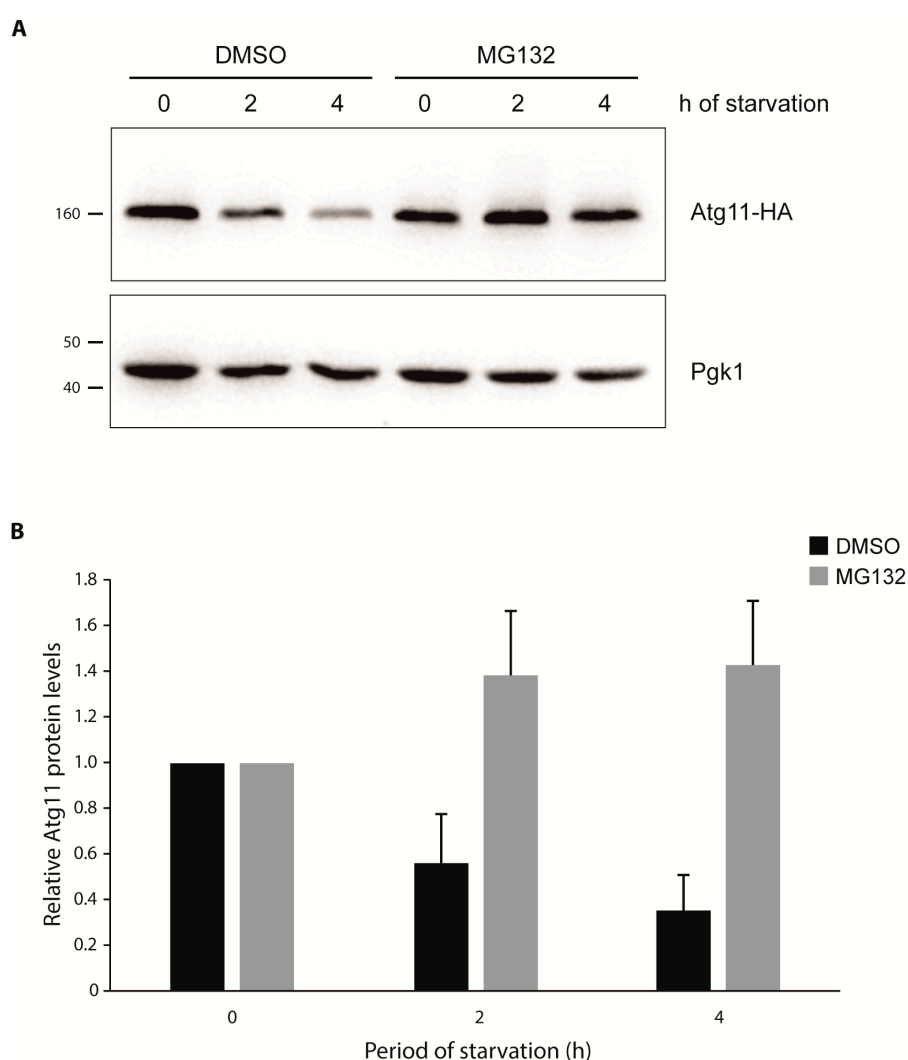


**Figure 32: Atg11 degradation is blocked by inhibition of the proteasome.** (A) Protein levels of HA-tagged Atg11 in non-starved and starved cells were determined by Western blots. Cells were either treated with the proteasome inhibitor MG132 or DMSO, which was used as a solvent for the drug. (B) Atg11 band intensities from four independent experiments were quantified and normalized against the band intensities of Pgk1. Intensities are given as relative values with non-starved samples set to 1.

a control. The inhibition of Atg11 degradation by MG132 was significant as determined by the quantification of band intensities (Figure 32B).

Proteasomal degradation requires the ubiquitination of the target protein. In order to further characterize the degradation of Atg11 by the proteasome, the levels of ubiquitinated Atg11 were examined. To ensure unchanged, native expression levels, Atg11 was genomically tagged with a myc-tag. Ubiquitinated proteins were immunoprecipitated from non-starved and starved cell lysates and Atg11 was detected by Western blotting using anti-myc antibodies. As shown in Figure 33A, Atg11 bands were observed in the immunoprecipitated fraction of non-starved and starved cells. Moreover, Atg11 specifically precipitated with the anti-ubiquitin antibody but not the Protein A resin itself (Figure 33A, last lane). While the overall level of Atg11 decreased upon starvation (compare input in Figure 33A), a strong increase in the amount of ubiquitinated Atg11 upon starvation was observed. A semi-quantitative analysis using the Atg11 band intensities normalized to the Atg11 levels in the input revealed a three-fold increase in Atg11 amounts precipitated from lysates of starved cells compared to non-starved cells (Figure 33B). In non-starved cells, on average  $0.019 \pm 0.008\%$  of the total amount of Atg11 was immunoprecipitated. After 2 h of starvation this value increased to  $0.051 \pm 0.010\%$ . This significant increase indicates that Atg11 is specifically ubiquitinated upon starvation. Considering the effect of MG132 on Atg11 degradation these results strongly suggest, that Atg11 is selectively targeted by the proteasome upon starvation.

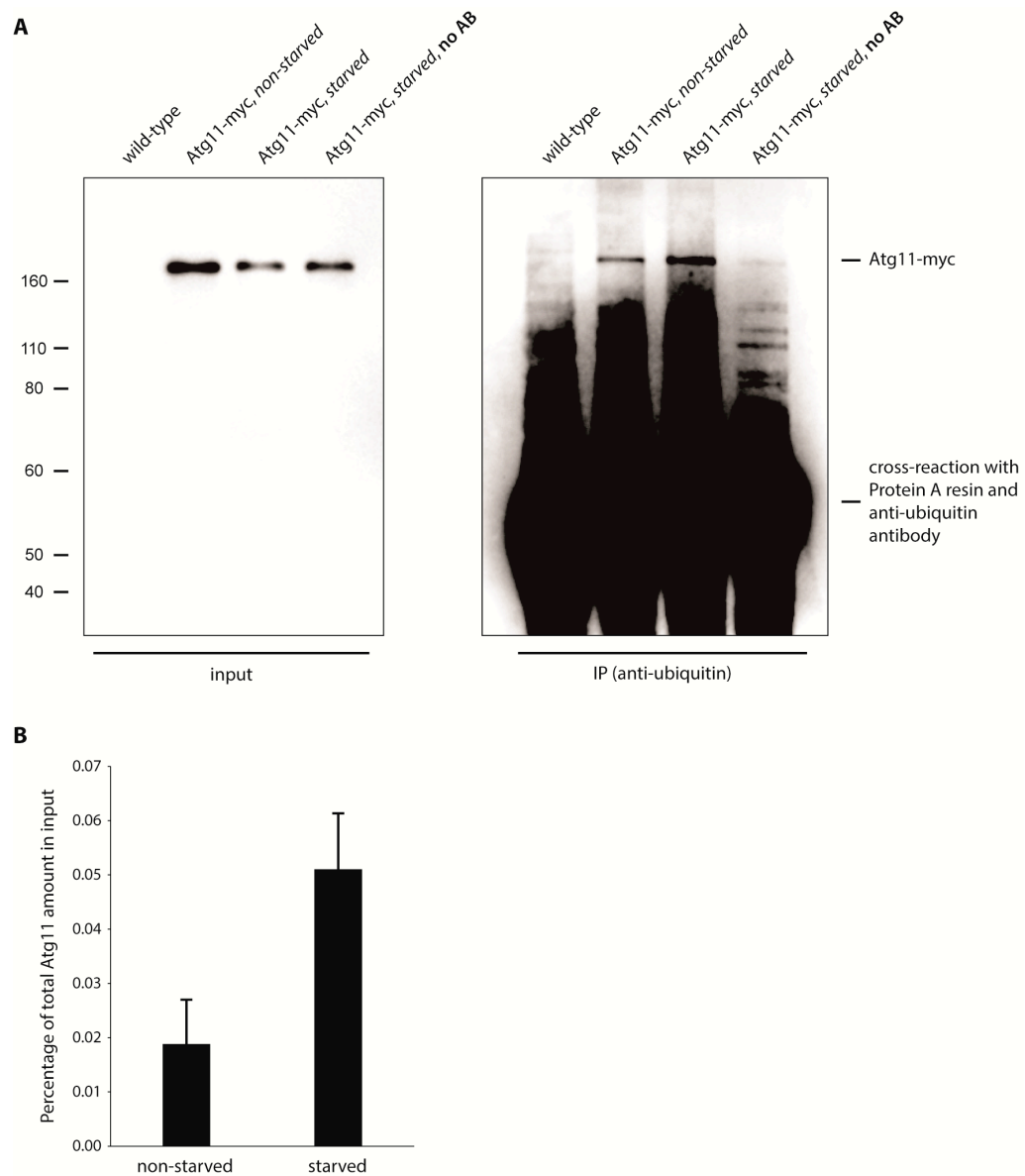


**Figure 33: Ubiquitination of Atg11 upon starvation.** (A) Proteins were immunoprecipitated using an anti-ubiquitin antibody bound to Protein A coupled magnetic beads. Samples were analyzed by Western blots stained against myc-tag. Atg11-myc was specifically precipitated. The amount of bound protein was higher in the starved sample despite the decreased amount in the input. (B) Bands from three independent experiments were quantified. The graph shows the amount of immunoprecipitated Atg11-myc as percentage of the total amount in the input.



## 4 Discussion

Autophagy is a highly conserved recycling pathway that engulfs cytoplasmic material in a newly formed double membrane vesicle and delivers it to the lysosome for degradation. While material is non-selectively captured as a response to nutrient deprivation, cargo is selectively degraded during nutrient-rich conditions to maintain cellular homeostasis. In yeast, a special set of vesicles containing the transmembrane protein Atg9 are required for autophagy. Upon starvation but not during nutrient-rich conditions, these Atg9 vesicles are tethered by Atg17, a subunit of the Atg1 kinase complex. Interestingly, Atg11, which has been described as a scaffolding protein, is specifically required for selective autophagy. However, the molecular function of this protein was unclear. In this thesis Atg11 was identified as a novel tethering factor for Atg9 vesicles, which substitutes for the function of Atg17 during nutrient-rich conditions. Furthermore, the regulation of this event by a cargo receptor could be revealed. Thus, the results presented in this thesis lead to a new model of autophagosome biogenesis, showing that a decision for either the selective or the non-selective pathway is already made during autophagy initiation. In humans, the selective removal of, for example, damaged organelles and protein aggregates serves as a protection against numerous pathologies, including cancer and neurodegenerative diseases. However, although many yeast autophagic proteins have human homologues, the initiation of autophagy in human cells is poorly understood. Thus, the mechanistic insights gained from the yeast model system might contribute to our understanding of selective autophagy in humans.

### 4.1 Atg11 directly interacts with Atg9 vesicles

Atg11 had been identified to be an essential protein for selective autophagy. It had been reported to bind the transmembrane protein Atg9 and subunits of the Atg1 kinase complex, as well as to cargo receptors *in vivo* (Chang et al., 2006; Yorimitsu and Klionsky, 2005). In order to investigate whether these are direct interactions, proteins were purified and reconstituted *in vitro*. These experiments confirmed that Atg11 binds specifically and efficiently to Atg9 proteoliposomes without the requirement for additional factors.

Atg11 had been reported previously to co-precipitate with Protein-A-tagged Atg9 from yeast cell lysates (Chang et al., 2006). In order to test this interaction *in vitro*, a truncated version of Atg9 comprising residues 281-779 was reconstituted into liposomes. Even though lacking large portions of the unstructured N- and C-terminal regions, this construct, termed the Atg9<sup>core</sup>, was shown to be sufficient to bind the Atg9 vesicle tether Atg17 (Rao et al., 2016). This interaction largely depended on the conserved N-terminal helix preceding the

transmembrane domain (residues 281-315) as well as the central cytosolic domain (residues 424-507). In vivo, deletion of only the N-terminal helix and the central cytosolic domain strongly reduced the amount of Atg17 co-precipitating with Atg9 from yeast cell lysates, which is thus in agreement with the in vitro data (Rao et al., 2016). Interestingly, Atg9<sup>core</sup> also interacted with Atg11. Recombinant Atg11 efficiently bound to Atg9 proteoliposomes in floatation assays. This interaction was even stronger than for Atg17. Although equal molar amounts of Atg11 and Atg17 were present in the input, the amount of Atg11 recovered from the floatation fraction was more than five times higher than that of Atg17. Furthermore, the binding of Atg11 to the proteoliposomes was specific to Atg9 as no Atg11 could be recovered with protein-free liposomes. This indicates a high similarity of Atg11 and Atg17 in respect to Atg9 interaction. This finding is also surprising as a requirement for Atg9 residues 154-201 for interaction with Atg11 in vivo had been reported previously (Chang et al., 2006). However, the results provided by Chang and colleagues were based on yeast two-hybrid screens and co-immunoprecipitation experiments. Thus, the observations made for the  $\Delta$ 154-201 variant could be an indirect effect, for example by affecting the proper maturation of Atg9 vesicles. Also, this domain could have a regulatory role in the recruitment of Atg11 to Atg9 vesicles in vivo, that is not required for the direct interaction between Atg11 and Atg9 in vitro.

Furthermore, the coiled-coil domains CC1 and CC2 of Atg11 were reported to be required for its interaction with Atg9 (Chang et al., 2006). As expected, the Atg11<sup>ΔC</sup> variant, which contains both coiled-coil domains, was efficiently binding to Atg9 proteoliposomes. Interestingly, also the Atg11<sup>Δdim</sup> variant could be recovered with Atg9 proteoliposomes in the floatation fraction even though it was lacking coiled-coil domain CC2. This suggests that the CC2 domain is not required for direct interaction between Atg11 and Atg9 in vitro.

Surprisingly, co-immunoprecipitation experiments conducted by Dr. Nena Matscheko showed, that the amounts of Atg9 co-precipitating with the Atg11<sup>ΔC</sup> and Atg11<sup>Δdim</sup> variants were strongly decreased compared to full-length Atg11. Both variants lack the C-terminal domain that contains coiled-coil domains CC3 and CC4. The latter had been reported to be the binding region for cargo receptors that activate cargo for degradation by autophagy (Yorimitsu and Klionsky, 2005). Thus, the interaction of Atg11 with Atg9 might require the activation of Atg11 by a cargo receptor. However, in vitro the binding of Atg11 to Atg9 proteoliposomes was independent of Atg32. Still, cargo receptors might facilitate the recruitment of Atg11 to the site of autophagosome biogenesis as a possible requirement for efficient interaction with Atg9 vesicles.

## 4.2 Atg11 dimerizes upon complex formation with Atg32

Previous studies reported that Atg11 can self-interact *in vivo*. However, recombinant Atg11 was monomeric in solution. In this thesis it could be shown that Atg11 directly interacts with the cargo receptor Atg32. This induces dimerization of Atg11, suggesting cargo-dependent activation of Atg11.

By utilizing yeast two-hybrid, fluorescence microscopy and co-immunoprecipitation assays the self-interaction region of Atg11 had been mapped to two of the four predicted the coiled-coil domains, CC2 and CC3 (Yorimitsu and Klionsky, 2005). Similar results were obtained from experiments conducted by Dr. Nena Matscheko utilizing co-expression of two differently tagged Atg11 copies. Self-interaction was assessed by the co-precipitation of different HA-tagged Atg11 variants with myc-tagged full-length Atg11. Interaction was observed with full-length Atg11 as well as with Atg11<sup>ΔC</sup>, which lacks the C-terminal domain containing CC3 and CC4. However, no co-precipitation was observed for Atg11<sup>Δdim</sup>, a N-terminal fragment that lacks all coiled-coil domains but CC1. This suggests that Atg11 self-interacts requires the CC2 domain but not CC3 and CC4. However, analytical ultracentrifugation revealed that recombinant Atg11 is monomeric in solution, indicating the requirement for additional factors to facilitate the direct or indirect interaction between two Atg11 molecules. Interestingly, in contrast to the full-length protein, recombinant Atg11<sup>ΔC</sup> is a dimer in solution. This suggested that there is indeed direct self-interaction, yet this interaction is inhibited by the Atg11 C-terminal domain. The most C-terminal coiled-coil domain of Atg11, CC4, had been reported to be the binding region for cargo receptors (Yorimitsu and Klionsky, 2005). This raised the question, whether the dimerization of Atg11 can be induced by the binding of a cargo receptor like the mitochondrial protein Atg32. However, it was not possible to observe complex formation by methods like size exclusion chromatography. This could be due to weak binding that results in the disassembly of the complex upon the separation from its subunits. When Atg11 was recruited to the membrane of giant unilamellar vesicles (GUVs), this was sufficient to specifically recruit Atg32 to the membrane as well (data not shown; experiment conducted by Dr. Nena Matscheko). Here, Atg11 was present in a very high local concentration, which might favor the interaction with Atg32. Moreover, subunits were not separated, which might have increased complex formation. *In vivo*, the recruitment of the different factors to the PAS would result in a high local concentration of proteins and thus might favor the interaction between Atg11 and Atg32 specifically at the site of autophagosome biogenesis.

In order to observe a direct interaction between Atg11 and Atg32 as well as possible changes in the oligomeric state of Atg11, crosslinking was used. This allowed to stabilize a complex in

solution and in absence of other factors and membranes and to determine its size by SDS-PAGE. However, commonly used crosslinkers like glutaraldehyde resulted in the formation of aggregates but not distinct complexes. This might have been caused by the tendency of Atg11 to aggregate over time in solution. This problem could be solved by the use of LC-SDA, a hetero-bifunctional crosslinker, that allows better control through a two-step process. First, the crosslinker was only added to Atg32 to allow the reaction of the NHS ester group with primary amines of the protein. Only then Atg11 was added and crosslinking was induced by activation of the diazirine group with UV light. This way, Atg32 could crosslink with proteins in close proximity while unspecific crosslinking between Atg11 molecules was prevented. With this crosslinker it was possible to detect the formation of a distinct complex by SDS-PAGE. The crosslinking of one Atg32 with one Atg11 molecule would result in a complex of 177 kDa. However, no band of such size was observed by SDS-PAGE. Instead, distinct bands of higher molecular weight were detected upon UV activation. The molecular weight of the stronger band was estimated to be about 340 kDa which corresponds to a complex of two Atg11 and two Atg32 molecules. Mass spectrometry analysis of this band revealed that both proteins were present. Thus, these results strongly suggest that Atg32 directly interacts with Atg11, thereby inducing the formation of Atg11 dimers. As Atg11 molecules should not have been able to crosslink each other, the detection of this high molecular weight band also indicated that Atg32 has crosslinked not only with the Atg11 molecule it was directly interacting with but also with the second Atg11 molecule. This might be an explanation for the presence of a second, weaker but again specific band in the acrylamide gel. Its molecular weight corresponds to approximately two Atg11 molecules and one Atg32 molecule. Presumably, Atg11 dimer formation was again induced by two Atg32 molecules but only one of them might have crosslinked with the Atg11 molecules.

### **4.3 Atg11 is a cargo-activated membrane tether**

Atg11 is a monomer in solution but dimerizes upon interaction with the cargo receptor Atg32. This indicated a specific function of the Atg11 dimer. Using *in vitro* assays, Atg11 was identified as a novel tethering factor for Atg9 vesicles in a cargo receptor-dependent manner. *In vitro* experiments strongly supported the model of Atg11 dimerization specifically upon activation by a cargo receptor. However, the function provided by the dimer formation remained unclear. Recently, a Atg17-like region was identified in the N-terminal domain of Atg11 (Li et al., 2014). Furthermore, both bind to Atg9 proteoliposomes and form homodimers. As the dimerization of Atg17 is crucial for the tethering of Atg9 proteoliposomes, it was tested whether Atg11 dimerization exhibits a similar function. The tethering of Atg17

had been previously characterized using dynamic light scattering of Atg9 proteoliposomes. As a consequence of tethering, the incubation with Atg17, which constitutively forms dimers, but not with a monomeric variant of Atg17 led to an increase of their hydrodynamic radius (Rao et al., 2016). The same approach was used for Atg11. Full-length Atg11 did not increase the hydrodynamic radius of Atg9 proteoliposomes, which is in agreement with its monomeric state. In contrast, Atg11<sup>ΔC</sup> increased the hydrodynamic radius of Atg9 proteoliposomes as observed previously for Atg17. This suggested that Atg11, like Atg17, tethers Atg9 proteoliposomes upon dimerization. When Atg32 was co-incubated with full-length Atg11 and Atg9 proteoliposomes, the hydrodynamic radius increased to a similar level as measured in presence of Atg11<sup>ΔC</sup>. This indicated that the cargo receptor-dependent dimerization of Atg11 leads to tethering of Atg9 vesicles.

Even though the similarities to Atg17 in the DLS measurements were striking, the increase in the hydrodynamic radius cannot only be explained by tethering but could as well be the result of, for example, fusion or the clustering of proteins to the liposome membrane. Therefore, Atg9 proteoliposomes were visualized by cryo-electron microscopy. When co-incubated with Atg11 in absence of Atg32, some liposomes were observed in close proximity but no specific tethering was visible. The liposomes contained phosphatidylserine, which is negatively charged at a neutral pH and would thus cause the liposomes to repulse each other. However, the self-interaction of Atg9 overcomes this repulsion and leads to the clustering of proteoliposomes. This was the reason for the high polydispersity of Atg9 proteoliposomes that interfered with the measurement of the hydrodynamic radius by DLS. This clustering could be prevented by the binding of Atg11 to Atg9 resulting in a monodisperse signal. Indeed, the liposomes visualized by cryo-EM were mostly dispersed and did not show any clustering. The observation that some liposomes were in close proximity to each other was presumably due to the binding of Atg11, which could shield the negative charges of the lipids. However, as suggested by the DLS measurements, this effect is not sufficient for stable tethering. This was further confirmed by cryo-EM of Atg9 proteoliposomes that were incubated with both, Atg11 and Atg32. Specifically in presence of Atg32 tight tethering could be detected. This was striking, as the tethering led to membrane deformations and the generation of large contact areas which does not happen spontaneously. Comparable observations had so far only been reported as an intermediate of SNARE-mediated membrane fusion. The use of mutant SNARE proteins, that allowed only incomplete zippering and were thus fusion incompetent, led to similar tight tethering events (Yavuz et al., 2018). This strongly suggests that the dimerization of Atg11 upon interaction with Atg32 specifically induces the tethering of Atg9 vesicles. Even though complex formation induced membrane deformations it was insufficient to drive fusion of the membranes. In all tight tethering events observed the two lipid bilayers were

intact and no hemifusion had occurred. Hemifusion would result in the fusion of the outer leaflets of the lipid bilayer while the inner leaflets remain intact. This had been reported as an intermediate step in SNARE-mediated fusion (Hernandez et al., 2012). The clear separation of the lipid bilayers of Atg9 proteoliposomes thus indicate a role of Atg11 in vesicle tethering but not fusion. Instead, fusion most probably requires the presence of SNAREs, as it had been proposed previously (Nair et al., 2011).

Generally, the finding that Atg17 and Atg11 are membrane tethers is highly interesting. Despite the different mode of regulation, their tethering function is very similar. Although they clearly differ from other known membrane tethers some similarities can be found, especially to multi-subunit tethering complexes like HOPS. HOPS contains two different subunits that bind either of the membranes, thus complex formation is required for tethering. Likewise, Atg11 and Atg17 only bind to one Atg9 vesicle and tether only upon dimer formation. HOPS tethers membranes by binding the membrane-anchored, active form of the Rab GTPase Ypt7. Rab GTPases are common regulators of membrane trafficking events throughout the cell. In contrast, Atg11 and Atg17 tether membranes by binding to the autophagy-specific membrane protein Atg9. Generally, the observed tethering function of Atg11 and Atg17 applies to the initiation of autophagosome biogenesis. Previous studies reported that Atg9 vesicles are not sufficient for autophagosome formation and additional membrane sources, most likely COPII vesicles derived from the ER, are presumably required (Yamamoto et al., 2012). Interestingly, even though a membrane tether itself, Atg17 was reported to interact with the COPII vesicle tether TRAPP3 and thus might indirectly aid in the tethering of vesicles other than Atg9 vesicles.

#### **4.4 Atg11 and Atg17 are mutually exclusive Atg9 vesicle tethers**

It could be shown that both, Atg11 and Atg17, share a highly similar function as they both tether Atg9 proteoliposomes *in vitro* upon dimer formation. However, they differ in the way they are regulated requiring either the interaction with a cargo receptor or the starvation-induced formation of the Atg1 kinase complex. *In vitro* assays revealed that Atg11 and Atg17 are competing for Atg9 binding sites, suggesting that both proteins tether Atg9 vesicles independently from each other to exclusively initiate selective or non-selective autophagy.

It had been reported previously that Atg11 interacts with Atg17 based on yeast two-hybrid screens (Yorimitsu and Klionsky, 2005). However, direct protein-protein interaction had not been confirmed. Using a defined *in vitro* system with recombinant Atg11 and Atg17 as well as Atg9 proteoliposomes revealed no physical interaction between the two tethers. Instead, both proteins were competing for the same or similar binding sites in Atg9. Atg11 was binding

to Atg9 proteoliposomes more efficiently than Atg17 but increasing amounts of Atg17 in the input could gradually replace Atg11 in the interaction with Atg9 proteoliposomes. The total amount of bound proteins remained constant in all tested conditions, indicating that both tethers bind to the same or overlapping binding sites of Atg9.

Even though Atg11 could be eventually outcompeted by Atg17, a 25-fold molar excess of Atg17 was necessary to substitute 50% of the Atg11 molecules bound to Atg9 proteoliposomes. However, similar expression levels had been reported in vivo under growing conditions (Kulak et al., 2014). Yet, when equal molar amounts of Atg11 and Atg17 were incubated with Atg9 proteoliposomes, Atg11 made up 85% of the total amount of bound proteins. This suggests that in vivo Atg9 vesicles might be largely sequestered by Atg11. During nutrient-rich conditions Atg17 forms a constitutive complex with Atg31-Atg29. This trimeric complex was shown to fully inhibit the tethering function of Atg17 and partly decrease the binding to Atg9 (Rao et al., 2016). Therefore, the stronger interaction of Atg11 with Atg9 might prevent the sequestering of a large portion of Atg9 vesicles during nutrient-rich conditions by inactive Atg17 molecules.

Upon induction of non-selective autophagy Atg11 needs to be replaced by Atg17. Fluorescence microscopy conducted by Dr. Nena Matscheko showed a decrease of Atg11 PAS localization upon starvation in wild-type but not in *atg17Δ* cells. Moreover, the amount of Atg9 that co-precipitated with Atg11 upon starvation was increased in *atg17Δ* cells, indicating that Atg17 replaces Atg11 in vivo as well. Upon starvation the assembly of the full Atg1 kinase complex activates the tethering activity of Atg17 and increases its interaction with Atg9 (Rao et al., 2016). However, as demonstrated by the in vitro assays even active Atg17, either Atg17 alone or the full Atg1 kinase complex, is not sufficient to outcompete Atg11 when present in equal amounts. Thus, additional regulatory mechanisms are required to remove Atg11 from Atg9 vesicles and facilitate Atg17 binding.

#### **4.5 A possible effect of protein phosphorylation on Atg11-Atg17 competition**

Atg11 and Atg17 function as tethers for Atg9 vesicles. While both competed for exclusive binding to Atg9 proteoliposomes the observed interaction of Atg9 with Atg11 was substantially stronger than that with Atg17. Therefore, additional mechanisms are required to facilitate the replacement of Atg11 by Atg17. Starvation induces the phosphorylation of Atg29 and the dephosphorylation of Atg13. However, these modifications were not sufficient to outcompete Atg11 by Atg17 in vitro.

It had been reported previously that Atg29 is specifically phosphorylated upon starvation, which induces its interaction with Atg11 (Mao et al., 2013). This indicated, that Atg11 might

recruit the Atg1 kinase complex upon starvation. In vivo experiments conducted by Dr. Nena Matscheko revealed that the phosphomimetic Atg29<sup>SD</sup> mutant decreased the amount of Atg9 co-precipitating with Atg11 under nutrient-rich conditions compared to wild-type Atg29. This observation led to the hypothesis that the recruitment of the Atg1 kinase complex via phosphorylated Atg29 could aid in the replacement of Atg11 by Atg17. However, in the reconstituted system no effect of the Atg29<sup>SD</sup> mutant on protein-protein interaction could be observed. Both subcomplexes, Atg31-Atg29 and Atg31-Atg29<sup>SD</sup>, were binding weakly to Atg9 proteoliposomes but binding was not increased for either of them in presence of Atg11. Thus, the phosphomimetic mutation of Atg29 did not induce interaction with Atg11. Also, no increased binding of Atg17 or decreased binding of Atg11 to Atg9 proteoliposomes was detectable when using the mutant trimeric complex Atg17-Atg31-Atg29<sup>SD</sup> or the mutant Atg1 kinase complex. Thus, a role of Atg29 phosphorylation in Atg17 recruitment and replacement of Atg11 through direct interactions could not be confirmed in vitro. The observations made in vivo might have therefore derived from indirect effects. However, the underlying mechanism remains unclear.

Another regulatory effect could be provided by the phosphorylation state of Atg13. Atg13 is phosphorylated during nutrient-rich conditions by the TOR kinase, which prevents the interaction of the Atg1-Atg13 subcomplex with the Atg17 trimeric complex. The dephosphorylation of Atg13 upon starvation facilitates the assembly of the full Atg1 kinase complex to enhance the binding of Atg17 to Atg9 vesicles and to activate its tethering function. Even though binding of the Atg1 kinase complex to Atg9 proteoliposomes was slightly increased in presence of Atg11, the complex formation was not sufficient to compete with the efficient binding of Atg11. It had been previously reported that Atg13 binds to Atg11 during nutrient-rich conditions (Kamber et al., 2015). To examine this interaction in the reconstituted system, Atg13 was phosphorylated in vitro by Atg1. Unphosphorylated Atg13 was found to interact very weakly with Atg9 proteoliposomes but was strongly recruited in presence of the trimeric complex due to the interaction with Atg17. However, no significant increase in Atg13 binding was detected in presence of Atg11. After phosphorylation, no Atg13 was co-floating with Atg9 proteoliposomes. As expected, Atg17 was not able to recruit phosphorylated Atg13 to the proteoliposomes, but surprisingly Atg11 was not either. It could possibly be that the reported interaction of phosphorylated Atg13 with Atg11 during vegetative conditions in vivo was only an indirect effect. On the other hand, Atg13 is phosphorylated by the TOR kinase and not by Atg1, which could result in different properties of native and recombinant Atg13.

#### 4.6 Atg11 degradation could aid in Atg17 recruitment

Atg11 binds Atg9 proteoliposomes stronger than Atg17 but neither the starvation-induced phosphorylation of Atg29 nor the formation of the Atg1 kinase complex were sufficient *in vitro* to increase recruitment of Atg17. However, it could be shown that Atg11 is degraded by the proteasome specifically upon starvation, which could free binding sites on Atg9 and consequently allow recruitment of Atg17.

In the search of another mechanism that explains the switch from Atg11 to Atg17 as membrane tethers, an interesting observation was made. In Western blots of *in vivo* studies the amount of Atg11 in cell lysates decreased upon starvation. Quantification of band intensities in Western blots revealed a strong and significant decline in Atg11 levels, whereas Atg17 protein levels remained constant. This indicated that Atg11 is degraded specifically upon starvation. Generally, the degradation of cytosolic proteins depends on one of two different pathways. Proteins can be either sequestered by autophagosomes and transported to the vacuole or ubiquitinated and subsequently degraded by the proteasome. Due to the localization of Atg11 to the site of autophagosome formation it was hypothesized that Atg11 might be captured non-selectively in autophagosomes along with other cytoplasmic material upon starvation. However, a block in autophagy by deletion of Atg7 did not inhibit the degradation of Atg11. To further confirm this finding, Atg11 levels in *pep4Δ* cells were determined. Pep4 is a vacuolar protease that activates other proteases and is thus essential for protein degradation within the vacuole (Woolford et al., 1986). As observed for *atg7Δ* cells, the deletion of Pep4 had no impact on the degradation of Atg11. Thus, Atg11 is most likely targeted by the proteasome pathway.

This hypothesis was investigated using the proteasome inhibitor MG132. Indeed, addition of this inhibitor blocked the degradation of Atg11 in starved cells. Quantification of band intensities even revealed a slight increase in Atg11 levels. This was not highly significant but could indicate that Atg11 expression continues during starvation and that protein levels are mostly regulated via its proteasomal degradation. To further investigate the proteasomal degradation of Atg11, ubiquitinated proteins were immunoprecipitated from non-starved and starved cell lysates. Atg11 could be specifically precipitated with an anti-ubiquitin antibody and the amount of immunoprecipitated Atg11 increased upon starvation. This indicates that Atg11 is specifically ubiquitinated upon starvation, which is consistent with the observed stabilization of Atg11 upon proteasome inhibition. However, only when a protein is modified with a special type of poly-ubiquitin chain, where the C-terminus of one ubiquitin is linked to lysine 48 of another ubiquitin, it is recognized by the proteasome (Thrower et al., 2000). Thus, increased ubiquitination is not a direct proof for proteasomal degradation but

could also have a regulatory effect (Ikeda and Dikic, 2008). To analyze the type of ubiquitination and map the ubiquitinated sites of Atg11 mass spectrometry was performed. However, the amount of protein extracted from an SDS-PAGE gel was not sufficient to identify the ubiquitination sites or the type of ubiquitin chains. Nevertheless, the observation that a proteasome inhibitor stabilized Atg11 levels but not a block in autophagy or vacuolar degradation strongly suggests the specific degradation of Atg11 by the proteasome upon starvation.

In vitro experiments showed that Atg11 binds more efficiently to Atg9 proteoliposomes than Atg17. Thus, Atg9 vesicles are likely sequestered by Atg11 and degradation of Atg11 could allow binding of Atg17 to Atg9. From this and the findings discussed before a model for a selectivity switch at the time of autophagy initiation can be proposed (see Figure 34). Under nutrient-rich conditions, Atg11 efficiently binds Atg9 vesicles but tethering is inhibited in absence of cargo, while Atg17 is inhibited by forming a constitutive complex with Atg31-Atg29. Selective autophagy is specifically initiated by the presence of a cargo receptor that induces Atg11 dimerization and thus Atg9 vesicle tethering. Upon starvation, Atg11 is degraded, which allows increased binding of Atg17 to Atg9 vesicles. Binding is further enhanced by the starvation-induced assembly of the Atg1 kinase complex, which also activates the tethering function of Atg17. This allows autophagy to switch from the selective formation of autophagosomes exclusively around specific cargo to a non-selective, cargo-independent pathway to ensure survival during nutrient deprivation.

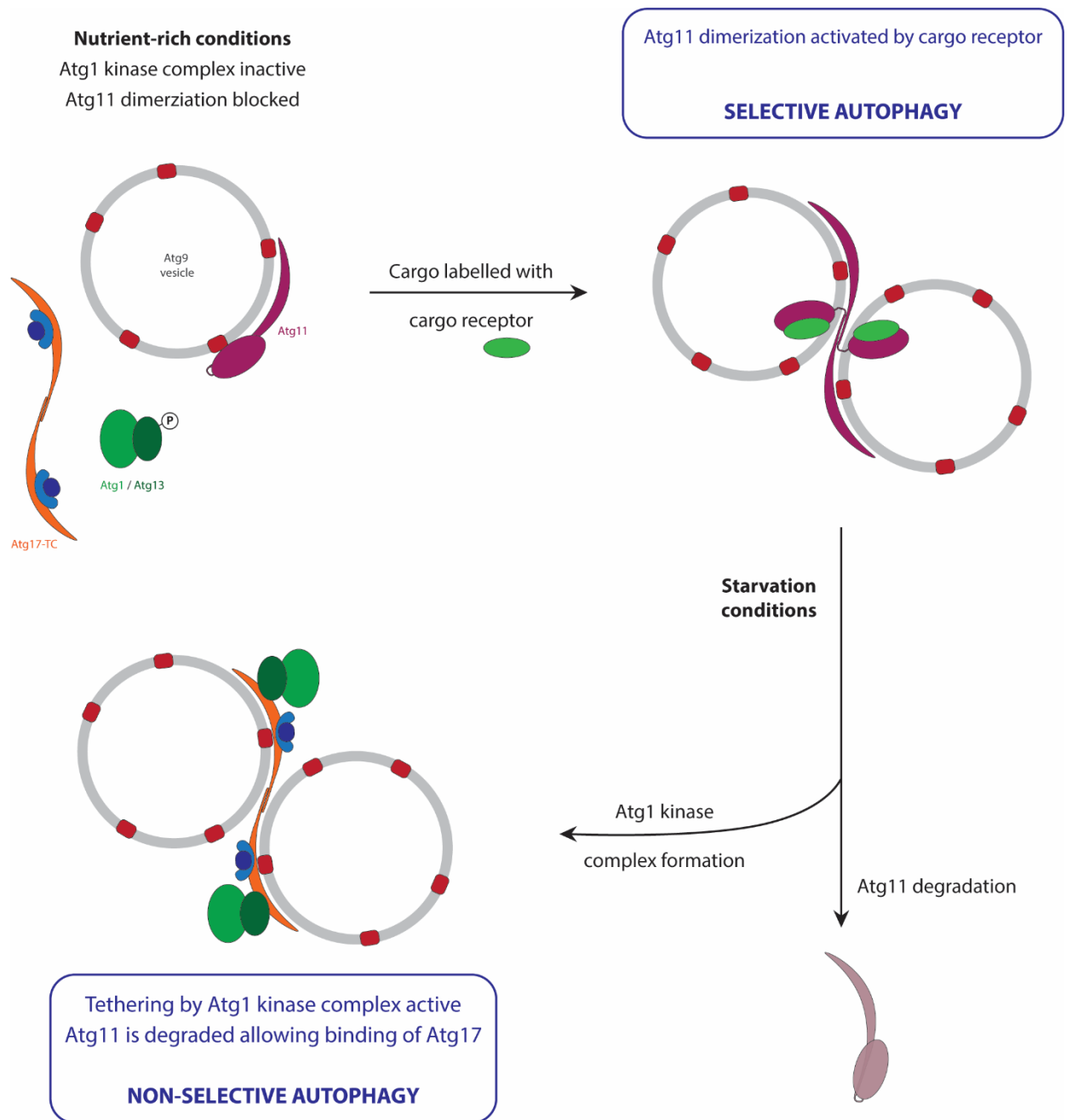


**Figure 34: Model for Atg9 vesicle tethering in autophagy initiation.** During nutrient-rich conditions binding and tethering of Atg17 is inhibited by Atg31-Atg29. Atg11 can bind Atg9 vesicles but dimerization is blocked by its C-terminal domain. Binding of a cargo receptor to that domain activates Atg11 dimerization and thereby leads to selective autophagy. Upon starvation, formation of the full Atg1 kinase complex allows Atg9 vesicle tethering without the requirement of a cargo receptor, thereby leading to non-selective autophagy. At the same time, Atg11 is degraded which can free binding places for an efficient binding of Atg17 to Atg9 vesicles.

## 4.7 Outlook

Atg11 had been reported previously to be an essential scaffolding protein in selective autophagy in yeast. However, molecular details of its function remained unclear. By employing an *in vitro* approach using recombinant proteins in a defined, reconstituted system, it could be shown that Atg11 functions as a tether for Atg9 vesicles upon cargo receptor-induced dimerization. Cryo-EM revealed that activated Atg11 leads to tight tethering and membrane deformations, but was not sufficient to drive fusion. This is similar to Atg17, which was also shown to tether but not fuse Atg9 proteoliposomes (Rao et al., 2016). Thus, the question remains which additional factors are required to facilitate membrane fusion. Most probably these are SNAREs, as this protein family is involved in membrane fusion events throughout the cell. Several SNAREs had been reported to be required during early stages of autophagosome biogenesis (Nair et al., 2011; Tan et al., 2013). However, it remains unclear whether they facilitate fusion specifically of Atg9 vesicles. SNAREs required for autophagy are known to play roles in other pathways as well, which makes it difficult to rule out indirect effects by perturbations of vesicular trafficking. This problem can be solved by using a reconstituted system. *In vitro* fusion assays are well established in the literature and had been used, for example, to investigate the acceleration of SNARE-mediated fusion by the HOPS tethering complex (Stroupe et al., 2009). This experimental setup allows to clearly decipher the correct SNARE combination as well as the regulatory factors required for efficient SNARE pairing. So far, it is still unclear whether Atg11 or the Atg1 kinase complex directly interact with SNARE proteins to mediate fusion. Recently, interaction of Atg11 and Atg17 with the vacuolar SNARE Vam7 had been reported (Liu et al., 2016). However, there is no indication that Atg11 and Atg17 play a direct role in fusion, as Vam7 is only required for the fusion of the completed autophagosome with the vacuole. It is also likely that Atg11 and Atg17 interact with additional factors that regulate SNARE complex formation as it has been reported for various multi-subunit tethering complexes.

*In vitro* experiments revealed a competition between Atg11 and Atg17 for binding to Atg9 vesicles, however a direct proof for this competition *in vivo* is still missing. The degradation of Atg11 upon starvation possibly facilitates the binding of Atg17 to Atg9 vesicles. To further support this model, the interaction of the two tethers with Atg9 vesicles could be determined depending on different expression levels or the stabilization of Atg11 levels by inhibition of the proteasome. Furthermore, it is still an open question how the degradation of Atg11 is regulated. It is unclear, which factor serves as the ubiquitin ligase for Atg11 and how it is activated in a starvation-dependent manner.

The results presented in this thesis support the model of two differently regulated tethers for Atg9 vesicles that allow the cell to switch between selective and non-selective autophagy. Also in human cells both pathways exist. Selective autophagy is particularly important as a protection against various diseases. Aggregates of misfolded proteins, for example, are ubiquitinated but cannot be degraded by the proteasome. The ubiquitin adapter protein p62 binds these proteins and links them to the autophagic machinery. The clearance of these aggregates by autophagy is an important mechanism in the protection against neurodegenerative diseases (Ross and Poirier, 2004). Mitophagy was also reported to depend on ubiquitination of outer mitochondrial membrane proteins in order for dysfunctional mitochondria to be recognized by p62 (Geisler et al., 2010). One key player in the ubiquitination of mitochondrial proteins is Parkin, which is frequently mutated in patients with Parkinson's disease (Narendra et al., 2008). These examples illustrate the importance of selective autophagy in health. Moreover, they show that the principle of adapters linking specific cargo to the autophagic machinery is highly conserved. However, initiation of autophagy in humans is poorly understood and it remains unclear whether the mechanisms observed in yeast applies to human cells as well. Ulk1 has been identified as a homologue of yeast Atg1. It forms a complex with Atg13, FIP200 and Atg101 to initiate autophagy (Zachari and Ganley, 2017). However, molecular details of the function of the Ulk1 complex are still unclear. FIP200 is suggested to be a homologue of yeast Atg17, despite its high molecular weight (183 kDa compared to 49 kDa of Atg17). Thus, FIP200 might include additional regulatory domains, for example to substitute the function of yeast Atg31-Atg29. For Atg11 it is unclear whether a human homologue exists. However, Huntingtin was recently discussed as a possible Atg11 homologue (Ochaba et al., 2014). While mutations in the Huntingtin gene are the major cause for Huntington's Disease, the normal function of this protein is poorly understood. Ochaba and colleagues reported that the C-terminal domain of Huntingtin co-precipitates subunits of the Ulk1 complex as well as the cargo receptor p62 and thus might act as a scaffolding protein similar to Atg11. Therefore, the principle of switching between non-selective and cargo-dependent autophagy initiation could be conserved in humans. However, to clearly decipher the molecular function of the human proteins a similar *in vitro* approach as presented for Atg17 and Atg11 would be required. This would allow to determine whether FIP200 and Huntingtin function as Atg9 vesicle tethers to initiate autophagy and how these processes are regulated. For a long time, yeast Atg8 was seen as the major link between cargo receptor and phagophore membrane. Similarly, links are found between cargo receptors and the human homologues of Atg8. However, considering the insights gained from the yeast system it would be interesting to see, whether there might be a mechanism in humans as well that specifically initiates autophagy at the appropriate place and time.



## References

- Aoki, Y., Kanki, T., Hirota, Y., Kurihara, Y., Saigusa, T., Uchiumi, T., Kang, D., and Subramani, S. (2011). Phosphorylation of Serine 114 on Atg32 mediates mitophagy. *MBoC* *22*, 3206–3217.
- Baker, R.W., Jeffrey, P.D., Zick, M., Phillips, B.P., Wickner, W.T., and Hughson, F.M. (2015). A direct role for the Sec1/Munc18-family protein Vps33 as a template for SNARE assembly. *Science* *349*, 1111–1114.
- Bas, L., Papinski, D., Licheva, M., Torggler, R., Rohringer, S., Schuschnig, M., and Kraft, C. (2018). Reconstitution reveals Ykt6 as the autophagosomal SNARE in autophagosome–vacuole fusion. *J Cell Biol* *217*, 3656–3669.
- Bröcker, C., Kuhlee, A., Gatsogiannis, C., Balderhaar, H.J. kleine, Hönscher, C., Engelbrecht-Vandré, S., Ungermann, C., and Raunser, S. (2012). Molecular architecture of the multisubunit homotypic fusion and vacuole protein sorting (HOPS) tethering complex. *PNAS* *109*, 1991–1996.
- Cai, H., Zhang, Y., Pypaert, M., Walker, L., and Ferro-Novick, S. (2005). Mutants in *trs120* disrupt traffic from the early endosome to the late Golgi. *The Journal of Cell Biology* *171*, 823–833.
- Cai, H., Yu, S., Menon, S., Cai, Y., Lazarova, D., Fu, C., Reinisch, K., Hay, J.C., and Ferro-Novick, S. (2007). TRAPPI tethers COPII vesicles by binding the coat subunit Sec23. *Nature* *445*, 941–944.
- Chang, C.-Y., Huang, W.-P., and Subramani, S. (2006). Atg19 Mediates a Dual Interaction Cargo Sorting Mechanism in Selective Autophagy. *MBoC* *18*, 919–929.
- Christoforidis, S., Miaczynska, M., Ashman, K., Wilm, M., Zhao, L., Yip, S.-C., Waterfield, M.D., Backer, J.M., and Zerial, M. (1999). Phosphatidylinositol-3-OH kinases are Rab5 effectors. *Nature Cell Biology* *1*, 249–252.
- Demircioglu, F.E., Burkhardt, P., and Fasshauer, D. (2014). The SM protein Sly1 accelerates assembly of the ER–Golgi SNARE complex. *PNAS* *111*, 13828–13833.
- Fitzgerald, D.J., Berger, P., Schaffitzel, C., Yamada, K., Richmond, T.J., and Berger, I. (2006). Protein complex expression by using multigene baculoviral vectors. *Nature Methods* *3*, 1021–1032.
- Fleming, J.A., Lightcap, E.S., Sadis, S., Thoroddsen, V., Bulawa, C.E., and Blackman, R.K. (2002). Complementary whole-genome technologies reveal the cellular response to proteasome inhibition by PS-341. *PNAS* *99*, 1461–1466.
- Gao, J., Langemeyer, L., Kümmel, D., Reggiori, F., and Ungermann, C. (2018). Molecular mechanism to target the endosomal Mon1-Ccz1 GEF complex to the pre-autophagosomal structure. *ELife*.
- Geisler, S., Holmström, K.M., Skujat, D., Fiesel, F.C., Rothfuss, O.C., Kahle, P.J., and Springer, W. (2010). PINK1/Parkin-mediated mitophagy is dependent on VDAC1 and p62/SQSTM1. *Nature Cell Biology* *12*, 119–131.
- Graef, M., Friedman, J.R., Graham, C., Babu, M., Nunnari, J., and Hegde, R.S. (2013). ER exit sites are physical and functional core autophagosome biogenesis components. *MBoC* *24*, 2918–2931.
- Guo, W., Roth, D., Walch-Solimena, C., and Novick, P. (1999). The exocyst is an effector for Sec4p, targeting secretory vesicles to sites of exocytosis. *The EMBO Journal* *18*, 1071–1080.
- Hanada, T., Noda, N.N., Satomi, Y., Ichimura, Y., Fujioka, Y., Takao, T., Inagaki, F., and Ohsumi, Y. (2007). The Atg12-Atg5 Conjugate Has a Novel E3-like Activity for Protein Lipidation in Autophagy. *J. Biol. Chem.* *282*, 37298–37302.

- Hernandez, J.M., Stein, A., Behrmann, E., Riedel, D., Cypionka, A., Farsi, Z., Walla, P.J., Raunser, S., and Jahn, R. (2012). Membrane Fusion Intermediates via Directional and Full Assembly of the SNARE Complex. *Science* 336, 1581–1584.
- Hershko, A., and Ciechanover, A. (1998). The ubiquitin system. *Annu. Rev. Biochem.* 67, 425–479.
- Huang, W.-P., Scott, S.V., Kim, J., and Klionsky, D.J. (2000). The Itinerary of a Vesicle Component, Aut7p/Cvt5p, Terminates in the Yeast Vacuole via the Autophagy/Cvt Pathways. *J. Biol. Chem.* 275, 5845–5851.
- Hyttinen, J.M.T., Amadio, M., Viiri, J., Pascale, A., Salminen, A., and Kaarniranta, K. (2014). Clearance of misfolded and aggregated proteins by autophagy and implications for aggregation diseases. *Ageing Research Reviews* 18, 16–28.
- Ikeda, F., and Dikic, I. (2008). Atypical ubiquitin chains: new molecular signals. *EMBO Reports* 9, 536–542.
- Imai, K., Hao, F., Fujita, N., Tsuji, Y., Oe, Y., Araki, Y., Hamasaki, M., Noda, T., and Yoshimori, T. (2016). Atg9A trafficking through the recycling endosomes is required for autophagosome formation. *J Cell Sci* 129, 3781–3791.
- Inoue, H., Nojima, H., and Okayama, H. (1990). High efficiency transformation of *Escherichia coli* with plasmids. *Gene* 96, 23–28.
- Itakura, E., Kishi, C., Inoue, K., Mizushima, N., and Subramani, S. (2008). Beclin 1 Forms Two Distinct Phosphatidylinositol 3-Kinase Complexes with Mammalian Atg14 and UVRAG. *MBoC* 19, 5360–5372.
- Janke, Magiera, Maria M., Rathfelder, Nicole, Taxis, Christof, Reber Simone, Maekawa, Hiromi, Moreno-Borchart, Alexandra, Doenges, Georg, Schwob, Etienne, Schiebel, Elmar, et al. (2004). A versatile toolbox for PCR-based tagging of yeast genes: new fluorescent proteins, more markers and promoter substitution cassettes. *Yeast* 21, 947–962.
- Jao, C.C., Ragusa, M.J., Stanley, R.E., and Hurley, J.H. (2013). A HORMA domain in Atg13 mediates PI 3-kinase recruitment in autophagy. *PNAS* 110, 5486–5491.
- Kabeya, Y., Noda, N.N., Fujioka, Y., Suzuki, K., Inagaki, F., and Ohsumi, Y. (2009). Characterization of the Atg17–Atg29–Atg31 complex specifically required for starvation-induced autophagy in *Saccharomyces cerevisiae*. *Biochemical and Biophysical Research Communications* 389, 612–615.
- Kamada, Y., Funakoshi, T., Shintani, T., Nagano, K., Ohsumi, M., and Ohsumi, Y. (2000). Tor-Mediated Induction of Autophagy via an Apg1 Protein Kinase Complex. *The Journal of Cell Biology* 150, 1507–1513.
- Kamber, R.A., Shoemaker, C.J., and Denic, V. (2015). Receptor-Bound Targets of Selective Autophagy Use a Scaffold Protein to Activate the Atg1 Kinase. *Molecular Cell* 59, 372–381.
- Kaufmann, A., Beier, V., Franquelim, H.G., and Wollert, T. (2014). Molecular Mechanism of Autophagic Membrane-Scaffold Assembly and Disassembly. *Cell* 156, 469–481.
- Kawamata, T., Kamada, Y., Kabeya, Y., Sekito, T., and Ohsumi, Y. (2008). Organization of the Pre-autophagosomal Structure Responsible for Autophagosome Formation. *Mol Biol Cell* 19, 2039–2050.
- Kihara, A., Noda, T., Ishihara, N., and Ohsumi, Y. (2001). Two Distinct Vps34 Phosphatidylinositol 3-Kinase Complexes Function in Autophagy and Carboxypeptidase Y Sorting in *Saccharomyces cerevisiae*. *The Journal of Cell Biology* 152, 519–530.
- Kirisako, T., Ichimura, Y., Okada, H., Kabeya, Y., Mizushima, N., Yoshimori, T., Ohsumi, M., Takao, T., Noda, T., and Ohsumi, Y. (2000). The Reversible Modification Regulates the Membrane-Binding State of Apg8/Aut7 Essential for Autophagy and the Cytoplasm to Vacuole Targeting Pathway. *The Journal of Cell Biology* 151, 263–276.

- Klopper, T.H., Kienle, C.N., Fasshauer, D., and Munro, S. (2007). An Elaborate Classification of SNARE Proteins Sheds Light on the Conservation of the Eukaryotic Endomembrane System. *MBoC* 18, 3463–3471.
- Kondo-Okamoto, N., Noda, N.N., Suzuki, S.W., Nakatogawa, H., Takahashi, I., Matsunami, M., Hashimoto, A., Inagaki, F., Ohsumi, Y., and Okamoto, K. (2012). Autophagy-related protein 32 acts as an autophagic degron and directly initiates mitophagy. *J. Biol. Chem.* jbc.M111.299917.
- Kraft, C., Kijanska, M., Kalie, E., Siergiejuk, E., Lee, S.S., Semplicio, G., Stoffel, I., Brezovich, A., Verma, M., Hansmann, I., et al. (2012). Binding of the Atg1/ULK1 kinase to the ubiquitin-like protein Atg8 regulates autophagy. *The EMBO Journal* 31, 3691–3703.
- Krämer, L., Ungermann, C., and Barr, F.A. (2011). HOPS drives vacuole fusion by binding the vacuolar SNARE complex and the Vam7 PX domain via two distinct sites. *MBoC* 22, 2601–2611.
- Krick, R., Tolstrup, J., Appelles, A., Henke, S., and Thumm, M. (2006). The relevance of the phosphatidylinositolphosphat-binding motif FRRGT of Atg18 and Atg21 for the Cvt pathway and autophagy. *FEBS Letters* 580, 4632–4638.
- Kuhlee, A., Raunser, S., and Ungermann, C. (2015). Functional homologies in vesicle tethering. *FEBS Letters* 589, 2487–2497.
- Kulak, N.A., Pichler, G., Paron, I., Nagaraj, N., and Mann, M. (2014). Minimal, encapsulated proteomic-sample processing applied to copy-number estimation in eukaryotic cells. *Nature Methods* 11, 319–324.
- Kuma, A., Mizushima, N., Ishihara, N., and Ohsumi, Y. (2002). Formation of the ~350-kDa Apg12-Apg5-Apg16 Multimeric Complex, Mediated by Apg16 Oligomerization, Is Essential for Autophagy in Yeast. *J. Biol. Chem.* 277, 18619–18625.
- Lee, D.H., and Goldberg, A.L. (1996). Selective Inhibitors of the Proteasome-dependent and Vacuolar Pathways of Protein Degradation in *Saccharomyces cerevisiae*. *J. Biol. Chem.* 271, 27280–27284.
- Li, F., Pincet, F., Perez, E., Eng, W.S., Melia, T.J., Rothman, J.E., and Tareste, D. (2007). Energetics and dynamics of SNAREpin folding across lipid bilayers. *Nature Structural & Molecular Biology* 14, 890–896.
- Li, F., Chung, T., and Vierstra, R.D. (2014). AUTOPHAGY-RELATED11 Plays a Critical Role in General Autophagy- and Senescence-Induced Mitophagy in Arabidopsis. *The Plant Cell* 26, 788–807.
- Liu, X., Mao, K., Yu, A.Y.H., Omairi-Nasser, A., Austin, J., Glick, B.S., Yip, C.K., and Klionsky, D.J. (2016). The Atg17-Atg31-Atg29 Complex Coordinates with Atg11 to Recruit the Vam7 SNARE and Mediate Autophagosome-Vacuole Fusion. *Current Biology* 26, 150–160.
- Lu, K., Psakhye, I., and Jentsch, S. (2014). Autophagic Clearance of PolyQ Proteins Mediated by Ubiquitin-Atg8 Adaptors of the Conserved CUET Protein Family. *Cell* 158, 549–563.
- Lynch-Day, M.A., Bhandari, D., Menon, S., Huang, J., Cai, H., Bartholomew, C.R., Brumell, J.H., Ferro-Novick, S., and Klionsky, D.J. (2010). Trs85 directs a Ypt1 GEF, TRAPPIII, to the phagophore to promote autophagy. *PNAS* 107, 7811–7816.
- Mao, K., Chew, L.H., Inoue-Aono, Y., Cheong, H., Nair, U., Popelka, H., Yip, C.K., and Klionsky, D.J. (2013). Atg29 phosphorylation regulates coordination of the Atg17-Atg31-Atg29 complex with the Atg11 scaffold during autophagy initiation. *PNAS* 110, E2875–E2884.
- Mari, M., Griffith, J., Rieter, E., Krishnappa, L., Klionsky, D.J., and Reggiori, F. (2010). An Atg9-containing compartment that functions in the early steps of autophagosome biogenesis. *The Journal of Cell Biology* 190, 1005–1022.
- Matsuura, A., Tsukada, M., Wada, Y., and Ohsumi, Y. (1997). Apg1p, a novel protein kinase required for the autophagic process in *Saccharomyces cerevisiae*. *Gene* 192, 245–250.
- Mayer, A., Wickner, W., and Haas, A. (1996). Sec18p (NSF)-Driven Release of Sec17p ( $\alpha$ -SNAP) Can Precede Docking and Fusion of Yeast Vacuoles. *Cell* 85, 83–94.

- McNew, J.A., Parlati, F., Fukuda, R., Johnston, R.J., Paz, K., Paumet, F., Söllner, T.H., and Rothman, J.E. (2000). Compartmental specificity of cellular membrane fusion encoded in SNARE proteins. *Nature* *407*, 153–159.
- Mizushima, N., Noda, T., Yoshimori, T., Tanaka, Y., Ishii, T., George, M.D., Klionsky, D.J., Ohsumi, M., and Ohsumi, Y. (1998). A protein conjugation system essential for autophagy. *Nature* *395*, 395–398.
- Morsomme, P., and Riezman, H. (2002). The Rab GTPase Ypt1p and Tethering Factors Couple Protein Sorting at the ER to Vesicle Targeting to the Golgi Apparatus. *Developmental Cell* *2*, 307–317.
- Motley, A.M., Nuttall, J.M., and Hettema, E.H. (2012). Pex3-anchored Atg36 tags peroxisomes for degradation in *Saccharomyces cerevisiae*. *The EMBO Journal* *31*, 2852–2868.
- Nair, U., Cao, Y., Xie, Z., and Klionsky, D.J. (2010). Roles of the Lipid-binding Motifs of Atg18 and Atg21 in the Cytoplasm to Vacuole Targeting Pathway and Autophagy. *J. Biol. Chem.* *285*, 11476–11488.
- Nair, U., Jotwani, A., Geng, J., Gammoh, N., Richerson, D., Yen, W.-L., Griffith, J., Nag, S., Wang, K., Moss, T., et al. (2011). SNARE Proteins Are Required for Macroautophagy. *Cell* *146*, 290–302.
- Nair, U., Yen, W.-L., Mari, M., Cao, Y., Xie, Z., Baba, M., Reggiori, F., and Klionsky, D.J. (2012). A role for Atg8-PE deconjugation in autophagosome biogenesis. *Autophagy* *8*, 780–793.
- Narendra, D., Tanaka, A., Suen, D.-F., and Youle, R.J. (2008). Parkin is recruited selectively to impaired mitochondria and promotes their autophagy. *The Journal of Cell Biology* *183*, 795–803.
- Noda, N.N., and Fujioka, Y. (2015). Atg1 family kinases in autophagy initiation. *Cell. Mol. Life Sci.* *72*, 3083–3096.
- Noda, N.N., Kumeta, H., Nakatogawa, H., Satoo, K., Adachi, W., Ishii, J., Fujioka, Y., Ohsumi, Y., and Inagaki, F. (2008). Structural basis of target recognition by Atg8/LC3 during selective autophagy. *Genes to Cells* *13*, 1211–1218.
- Noda, T., Kim, J., Huang, W.-P., Baba, M., Tokunaga, C., Ohsumi, Y., and Klionsky, D.J. (2000). Apg9p/Cvt7p Is an Integral Membrane Protein Required for Transport Vesicle Formation in the Cvt and Autophagy Pathways. *The Journal of Cell Biology* *148*, 465–480.
- Obara, K., Sekito, T., and Ohsumi, Y. (2006). Assortment of Phosphatidylinositol 3-Kinase Complexes—Atg14p Directs Association of Complex I to the Pre-autophagosomal Structure in *Saccharomyces cerevisiae*. *MBoC* *17*, 1527–1539.
- Ochaba, J., Lukacsovich, T., Csikos, G., Zheng, S., Margulis, J., Salazar, L., Mao, K., Lau, A.L., Yeung, S.Y., Humbert, S., et al. (2014). Potential function for the Huntingtin protein as a scaffold for selective autophagy. *PNAS* *111*, 16889–16894.
- Okamoto, K., Kondo-Okamoto, N., and Ohsumi, Y. (2009). Mitochondria-Anchored Receptor Atg32 Mediates Degradation of Mitochondria via Selective Autophagy. *Developmental Cell* *17*, 87–97.
- Pankiv, S., Clausen, T.H., Lamark, T., Brech, A., Bruun, J.-A., Outzen, H., Øvervatn, A., Bjørkøy, G., and Johansen, T. (2007). p62/SQSTM1 Binds Directly to Atg8/LC3 to Facilitate Degradation of Ubiquitinated Protein Aggregates by Autophagy. *J. Biol. Chem.* *282*, 24131–24145.
- Parlati, F., McNew, J.A., Fukuda, R., Miller, R., Söllner, T.H., and Rothman, J.E. (2000). Topological restriction of SNARE-dependent membrane fusion. *Nature* *407*, 194–198.
- Pfaffenwimmer, T., Reiter, W., Brach, T., Nogellova, V., Papinski, D., Schuschnig, M., Abert, C., Ammerer, G., Martens, S., and Kraft, C. (2014). Hrr25 kinase promotes selective autophagy by phosphorylating the cargo receptor Atg19. *EMBO Reports* *15*, 862–870.
- Ragusa, M.J., Stanley, R.E., and Hurley, J.H. (2012). Architecture of the Atg17 Complex as a Scaffold for Autophagosome Biogenesis. *Cell* *151*, 1501–1512.

- Rao, Y., Perna, M.G., Hofmann, B., Beier, V., and Wollert, T. (2016). The Atg1-kinase complex tethers Atg9-vesicles to initiate autophagy. *Nature Communications* 7, 10338.
- Ross, C.A., and Poirier, M.A. (2004). Protein aggregation and neurodegenerative disease. *Nature Medicine* 10, S10-S17.
- Salminen, A., and Novick, P.J. (1987). A ras-like protein is required for a post-Golgi event in yeast secretion. *Cell* 49, 527-538.
- Scholz, J., Besir, H., Strasser, C., and Suppmann, S. (2013). A new method to customize protein expression vectors for fast, efficient and background free parallel cloning. *BMC Biotechnology* 13, 12.
- Stenmark, H. (2009). Rab GTPases as coordinators of vesicle traffic. *Nature Reviews Molecular Cell Biology* 10, 513-525.
- Stroupe, C., Hickey, C.M., Mima, J., Burfeind, A.S., and Wickner, W. (2009). Minimal membrane docking requirements revealed by reconstitution of Rab GTPase-dependent membrane fusion from purified components. *PNAS* 106, 17626-17633.
- Su, M.-Y., Peng, W.-H., Ho, M.-R., Su, S.-C., Chang, Y.-C., Chen, G.-C., and Chang, C.-I. (2015). Structure of yeast Ape1 and its role in autophagic vesicle formation. *Autophagy* 11, 1580-1593.
- Südhof, T.C., and Rothman, J.E. (2009). Membrane Fusion: Grappling with SNARE and SM Proteins. *Science* 323, 474-477.
- Sutton, R.B., Fasshauer, D., Jahn, R., and Brunger, A.T. (1998). Crystal structure of a SNARE complex involved in synaptic exocytosis at 2.4 Å resolution. *Nature* 395, 347-353.
- Tan, D., Cai, Y., Wang, J., Zhang, J., Menon, S., Chou, H.-T., Ferro-Novick, S., Reinisch, K.M., and Walz, T. (2013). The EM structure of the TRAPP3 complex leads to the identification of a requirement for COPII vesicles on the macroautophagy pathway. *PNAS* 110, 19432-19437.
- Tanaka, C., Tan, L.-J., Mochida, K., Kirisako, H., Koizumi, M., Asai, E., Sakoh-Nakatogawa, M., Ohsumi, Y., and Nakatogawa, H. (2014). Hrr25 triggers selective autophagy-related pathways by phosphorylating receptor proteins. *J Cell Biol* 207, 91-105.
- Thrower, J.S., Hoffman, L., Rechsteiner, M., and Pickart, C.M. (2000). Recognition of the polyubiquitin proteolytic signal. *The EMBO Journal* 19, 94-102.
- Ungermann, C., Sato, K., and Wickner, W. (1998). Defining the functions of *trans*-SNARE pairs. *Nature* 396, 543-548.
- Wang, J., Menon, S., Yamasaki, A., Chou, H.-T., Walz, T., Jiang, Y., and Ferro-Novick, S. (2013a). Ypt1 recruits the Atg1 kinase to the preautophagosomal structure. *PNAS* 110, 9800-9805.
- Wang, K., Jin, M., Liu, X., and Klionsky, D.J. (2013b). Proteolytic processing of Atg32 by the mitochondrial i-AAA protease Yme1 regulates mitophagy. *Autophagy* 9, 1828-1836.
- Wasilko, D.J., Edward Lee, S., Stutzman-Engwall, K.J., Reitz, B.A., Emmons, T.L., Mathis, K.J., Bienkowski, M.J., Tomasselli, A.G., and David Fischer, H. (2009). The titerless infected-cells preservation and scale-up (TIPS) method for large-scale production of NO-sensitive human soluble guanylate cyclase (sGC) from insect cells infected with recombinant baculovirus. *Protein Expression and Purification* 65, 122-132.
- Weidberg, H., Shvets, E., Shpilka, T., Shimron, F., Shinder, V., and Elazar, Z. (2010). LC3 and GATE-16/GABARAP subfamilies are both essential yet act differently in autophagosome biogenesis. *The EMBO Journal* 29, 1792-1802.
- Wilson, M.I., Dooley, H.C., and Tooze, S.A. (2014). WIPI2b and Atg16L1: setting the stage for autophagosome formation. *Biochemical Society Transactions* 42, 1327-1334.
- Woolford, C.A., Daniels, L.B., Park, F.J., Jones, E.W., Van Arsdell, J.N., and Innis, M.A. (1986). The PEP4 gene encodes an aspartyl protease implicated in the posttranslational regulation of *Saccharomyces cerevisiae* vacuolar hydrolases. *Mol Cell Biol* 6, 2500-2510.

- Yamamoto, H., Kakuta, S., Watanabe, T.M., Kitamura, A., Sekito, T., Kondo-Kakuta, C., Ichikawa, R., Kinjo, M., and Ohsumi, Y. (2012). Atg9 vesicles are an important membrane source during early steps of autophagosome formation. *J Cell Biol* 198, 219–233.
- Yamasaki, A., and Noda, N.N. (2017). Structural Biology of the Cvt Pathway. *J. Mol. Biol.* 429, 531–542.
- Yamasaki, A., Watanabe, Y., Adachi, W., Suzuki, K., Matoba, K., Kirisako, H., Kumeta, H., Nakatogawa, H., Ohsumi, Y., Inagaki, F., et al. (2016). Structural Basis for Receptor-Mediated Selective Autophagy of Aminopeptidase I Aggregates. *Cell Rep* 16, 19–27.
- Yavuz, H., Kattan, I., Hernandez, J.M., Hofnagel, O., Witkowska, A., Raunser, S., Walla, P.J., and Jahn, R. (2018). Arrest of trans-SNARE zippering uncovers loosely and tightly docked intermediates in membrane fusion. *J. Biol. Chem.* 293, 8645–8655.
- Yen, W.-L., and Klionsky, D.J. (2008). How to Live Long and Prosper: Autophagy, Mitochondria, and Aging. *Physiology* 23, 248–262.
- Yorimitsu, T., and Klionsky, D.J. (2005). Atg11 Links Cargo to the Vesicle-forming Machinery in the Cytoplasm to Vacuole Targeting Pathway. *MBoC* 16, 1593–1605.
- Yu, I.-M., and Hughson, F.M. (2010). Tethering Factors as Organizers of Intracellular Vesicular Traffic. *Annu. Rev. Cell Dev. Biol.* 26, 137–156.
- Zachari, M., and Ganley, I.G. (2017). The mammalian ULK1 complex and autophagy initiation. *Essays In Biochemistry* 61, 585–596.
- Zhang, T., Lei, J., Yang, H., Xu, K., Wang, R., and Zhang, Z. (2011). An improved method for whole protein extraction from yeast *Saccharomyces cerevisiae*. *Yeast* 28, 795–798.

# Appendix

## List of Figures

Figure 1: Autophagosome biogenesis.....	15
Figure 2: Activation of the Atg1 kinase complex.....	17
Figure 3: Interactions with Atg11.....	23
Figure 4: Expression conditions for Atg11 fusion protein.....	43
Figure 5: Schematic of the Atg11 fusion protein for improved binding to the HisTrap.....	44
Figure 6: HisTrap purification of Atg11.....	45
Figure 7: Size exclusion chromatography of Atg11.....	46
Figure 8: Purification of Atg11 variants.....	47
Figure 9: Purification of trimeric complex components.....	49
Figure 10: Purification of Atg32 <sup>SE</sup> .....	50
Figure 11: Purification of Atg9 <sup>core</sup> .....	51
Figure 12: Purification of Atg13.....	51
Figure 13: Purification of Atg1.....	52
Figure 14: Illustration of a floatation assay.....	53
Figure 15: Interaction of Atg11 variants and Atg32 with Atg9 proteoliposomes.....	54
Figure 16: Crosslinking of Atg11 <sup>ΔC</sup> .....	55
Figure 17: Glutaraldehyde crosslinking of full-length Atg11.....	56
Figure 18: Crosslinking of Atg11 and Atg32.....	57
Figure 19: Size estimation of crosslinked complexes.....	57
Figure 20: Results of mass spectrometry analysis of crosslinking experiment.....	59
Figure 21: Dynamic light scattering to determine tethering.....	60
Figure 22: Cryo-electron microscopy imaging of Atg9 proteoliposome tethering.....	61
Figure 23: Competition for Atg9 proteoliposome binding.....	63
Figure 24: Stability of the trimeric complex in respect of Atg29 phosphorylation.....	65
Figure 25: Effects of Atg29 phosphorylation on protein-protein interactions.....	67
Figure 26: Recruitment of the Atg17 trimeric complex to Atg9 proteoliposomes.....	68

Figure 27: Flootation assay to determine binding of the Atg1 kinase complex (pentameric complex) to Atg9 proteoliposomes..... 69

Figure 28: Interaction of Atg13 with Atg9 proteoliposomes..... 71

Figure 29: Atg11 degradation upon starvation in vivo. .... 72

Figure 30: Atg11 degradation in *pep4Δ* background..... 73

Figure 31: Atg17 protein levels during starvation..... 74

Figure 32: Atg11 degradation is blocked by inhibition of the proteasome. .... 75

Figure 33: Ubiquitylation of Atg11 upon starvation. .... 77

Figure 34: Model for Atg9 vesicle tethering in autophagy initiation..... 89

**List of Tables**

Table 1: Human orthologues of yeast ATGs. .... 24

Table 2: List of *E. coli* strains. .... 27

Table 3: List of plasmids for bacterial and yeast expression..... 28

Table 4: List of yeast strains. .... 29

Table 5: List of antibodies..... 29

Table 6: Size estimation of crosslinked complexes..... 58

## Acknowledgements

I want to thank my supervisor Dr. Thomas Wollert for the opportunity to work on this challenging and exciting project, for his input and the constructive scientific discussions.

I want to thank my former lab members at the Max-Planck-Institute for Biochemistry in Munich for their support during the first two years of my PhD. Special thanks goes to Dr. Nena Matscheko and Dr. Yijian Rao for the productive collaboration on autophagy initiation in yeast.

I want to thank all my current lab members at the Institut Pasteur in Paris for their support and I am thankful that we became such a great team. Especially I want to thank Satish Moparthi, I am deeply grateful to have found a true friend in you.

I am also deeply thankful to my family and friends. I am grateful for the incredible support I got from my family that made all of this possible and I want to especially thank my grandmother who could not share this moment with us anymore.

I am also deeply grateful to Giovanni and to have him in my life. Thank you for your continuous support, even in our times of separation, and the great time we spent together in all these years.